Sensitivity of snow models in the semi-arid Andes of Chile

A comparison between SNOWPACK and SnowModel

A.B. Voordendag

TU Delft

Sensitivity of snow models in the semi-arid Andes of Chile

A comparison between SNOWPACK and SnowModel

by

A.B. Voordendag

to obtain the degree of Master of Science
at the Delft University of Technology,
to be defended publicly on Monday 17 December 2018 at 11:00 AM.

Student number:	4223691	
Project duration:	1 February 2018 – 17 December 2018	
Thesis committee:	Dr. S.L.M. Lhermitte	TU Delft
	Dr. R.C. Lindenbergh	TU Delft
	Prof.dr.ir. B.J.H. van de Wiel	TU Delft
	Dr. M. Réveillet	CEAZA
	Dr. S. MacDonell	CEAZA

An electronic version of this thesis is available at `http://repository.tudelft.nl/`.

TU Delft

Abstract

Melting snow in the Andes is a main water resource for the population of Chile. Snow models are used to increase the knowledge about the amount of snow in the mountains. These physically-based models use the energy balance equation to model sublimation and melt correctly. This study is the first comparison between snow models in the semi-arid Andes and focusses on the sensitivity of the models SNOWPACK and SnowModel to its input parameters and parametrizations. SNOWPACK is especially designed for forecasting avalanches in the Alps and SnowModel is often used to model wind transport of snow. The models are evaluated on a point scale with data from the Automatic Weather Station Tapado (-30°S, 69°W, 4306 m.a.s.l.) in the year 2017.

Firstly, the forcing data of the models (air temperature, relative humidity, precipitation, air pressure, incoming shortwave and longwave radiation and wind direction and velocity) are complemented and their uncertainties are assessed. The temperature and relative humidity data are interpolated with data from nearby stations according to a linear gradient depending on the altitude during the five months that the sensor was not working. The accumulated precipitation has been corrected with the wind velocity by the empirical, exponential formula by MacDonald and Pomeroy (2007). The uncertainty of the precipitation measurement is assessed by the proposal of two types of distributions between the measured data from the precipitation gauge and the precipitation derived from the snow water equivalent (SWE) measurements.

Secondly, the models are calibrated with the focus on the parametrizations of the snow albedo and fresh snow density and on different roughness lengths. The snow albedo is a good measure for snow melt, because a high albedo leads to a higher amount of reflected shortwave radiation and eventually less available energy for melt. The snow density provides the conversion between the SWE and the snow depth and controls the way of compaction of the snowpack. The roughness value influences the sublimation rate of the snowpack.

After the models have been calibrated, a Monte Carlo approach has been applied to assess the influence of variations in the forcing data on the output of the models. A normally distributed random number based on the measurement uncertainties has been added to the hourly forcing data. The models are run 1000 times with this variable forcing.

Results show that the models are predominantly sensitive to the input of precipitation. The measured precipitation is very uncertain and the actual fallen amount of precipitation at the position of the SWE sensor is estimated to be twice as large as the measured amount at the precipitation gauge. The simulated SWE is the amount of precipitation minus melt, sublimation and eventually wind transport and as the precipitation is very uncertain, so is the output of the models. The evolution of the SWE is simulated similarly for both models if the snowpack is only influenced by sublimation. The simulation of melt is done differently in the models, where SNOWPACK models a more gradual melt, because the refreezing of melt water within in the snowpack is simulated more correctly, whereas the melt simulated by SnowModel is dominantly influenced by air temperatures above 0°C. Furthermore, the models are significantly sensitive to the forced relative humidity and air temperature. This influences the melt, acceptance of precipitation events (SNOWPACK) and the snow density (SnowModel). The influence of air pressure, incoming longwave and shortwave radiation and wind velocity and direction is inconsiderable. The most appropriate model for understanding snowpack processes and model snow depth evolution in the semi-arid Andes is SNOWPACK, because it models the start of the melting period at the right moment, evaluates the internal evolution of the snowpack and parametrizes the albedo better than SnowModel.

This thesis demonstrates the importance of good forcing data, especially considering the precipitation and is the first to assess the sensitivity of two snow models in the semi-arid Andes. The empirical parameters in SNOWPACK and SnowModels are not yet adapted to this region and improvements can be made to these parameters, but the physical processes in SNOWPACK are better applicable to this region than the approaches by SnowModel.

Preface

Graduating sometimes feels like climbing a mountain, where the degree of Master of Science is obtained at the top. Anybody who knows me a little better, knows that I especially like mountains and the challenges that we face when climbing high mountains. The writing of this master thesis also had some practical and mental challenges, such as literally climbing mountains (with altitude sickness as result), the occupation of the university of La Serena, adapting to the Chilean culture, learning Spanish, but also being far away from family and friends and frustration that came from the code of the models and data.

The top of this mountain could not have been reached without the guidance of several persons. I am very grateful to Stef Lhermitte, who gave me the opportunity to go to La Serena in Chile and who always was available for good advice. In one of our first meetings, he told me that at the end of your thesis it feels like you could have done the work in just a few months, whereas it took a lot longer. I always kept this in mind when I was a bit frustrated and Stef was absolutely right.

I want to thank Marion Réveillet and Shelley MacDonell for guiding me when I was in Chile. Marion changed my view on science and on what it is like to do research and she was always willing to help me. Shelley made science a lot of fun and creates a very nice atmosphere within her glaciology group at CEAZA. Furthermore, the people at the glaciology group made my stay in La Serena a lot more pleasant. Muchas gracias!

Additionally, I am very thankful for the funding I was granted from the Lamminga fonds. This financial support made it possible to do fieldwork trips and to fly to Chile.

Glen Liston and the WSL Institute for Snow and Avalanche Research SLF are acknowledged for their models, SnowModel and SNOWPACK respectively, which I have used in my study. Most of the time it was a pleasure to work with them.

The support of friends and family in the Netherlands was also indispensable. Maaike Izeboud helped me to get started with SNOWPACK. Dirk and Coco gave me useful advice on how to survive Chile. Last but not least, the friends and family that were available for endless phone calls on Sundays and Skype-calls were very important to me. They really made Europe feel less far away.

Let's hope that the views from the top of my graduation mountain is comparable to the climate in the semi-arid Andes, because it would be nice to have a cloudless sky and a good outlook on a possible future in research.

A.B. Voordendag
Delft, November 2018

Contents

List of Figures

List of Tables

1 Introduction

1.1. Background

Human beings are highly dependent on water for their everyday life. Whereas a lot of people are accustomed that water just flows out of the tap when opening it, this is not so self-evident in the semi-arid Andes of Chile (26–32°S). This region has to deal with small amounts of precipitation and the precipitation that falls, mainly falls into the mountains, whereas most people do not live in the mountains, but closer to the sea (Favier et al., 2009). Hence, snow and glaciers are the main reservoirs of water in the Andes. Run-off from the Andes during winter rainstorms and snow melt during spring and early summer are the most important resources of water in the region (Favier et al., 2009). The precipitation mainly falls during the winter period and thus events of snowfall are of main interest.

The region of interest of this study covers the Chilean regions Atacama and Coquimbo. The region has a population of more than a million inhabitants (Instituto Nacional de Estadísticas - Chile, 2014) and hosts a considerable amount of economic activity, especially agricultural and mining activity (Hublart et al., 2016). The mining is mainly open pit gold mining, which is also known for the high water consumption and acidification of water (Urkidi, 2010).

A semi-arid climate is characterized by small amounts of precipitation. For example, the capital of the Coquimbo region, La Serena, has a mean annual precipitation of 113.7 mm from the period between 1869 and 2004 (Vuille and Milana, 2007). This amount of precipitation declines even further, because of climate change (Vuille and Milana, 2007). According to the study of Squeo et al. (1999), the mean annual precipitation has decreased with a factor of two in La Serena over the twentieth century. It is therefore inevitable to have good information about the amount of water available in the Andes to supply the local agriculture and the Chileans with enough water for there quotidian needs now and in the future.

The knowledge about precipitation and discharge is limited by the amount of data available in the Andes, especially at high elevations which are often inaccessible and covered by snow during winter (Favier et al., 2009). The spatial distribution of hydrological measurements is insufficient to correctly interpolate the spatial distribution of water production (Favier et al., 2009), because the topography of the region causes orographic effects (Scaff et al., 2017). Therefore it is necessary to properly evaluate snow coverage and its evolution and to quantify the water available from the snow melt.

A possible way to expand the knowledge of the amount of snow in the mountains, along with taking in situ measurements, is with snow models. Snow models simulate the amount of snow and the corresponding water equivalent. Physically based snow models use input parameters such as precipitation, air temperature, relative humidity and radiation terms to do so and the snow depth, snow surface temperature and snow water equivalent are generated as output. This forcing data and physical parameters to validate the output of the models can be obtained from automatic weather stations or weather models, but both measurements and models have uncertainties. Chapter 2 of this thesis gives a revision on how snow modelling works.

Along with the uncertainties in forcing data, the quantification of the snow is strongly influenced by two complex physical processes. The first process is sublimation, which is the transition of snow directly to gas. If the snow is in a gas state it is not in the water reservoir anymore. Sublimation is increased by an arid atmosphere, high wind speeds, high solar radiation and low air temperatures and as the region meets these requirements, sublimation plays a big role (MacDonell et al., 2013a). Sublimation can be measured with an

eddy covariance sensor, but these measurements are uncommon in complex mountainous environments and thus sublimation is evaluated by a modelling approach. Ginot et al. (2001) has found a sublimation rate of 1.9 mm/day for the Tapado glacier, which is close to the exact study area (Section 3.1) of this thesis. The second process that influences the area are strong winds. The average wind speed measured close to the Tapado glacier are 4.2 m/s in 2017 and reaches peaks of more than 15 m/s. The wind effects consist of snow drift (suspension and saltation) and blowing snow sublimation (Gascoin et al., 2013).

1.2. Problem definition

During the last couple of years, studies have been performed to model snowpack evolution in different catchments in the semi-arid Andes of Chile. Most of which have been driven by current or former members of CEAZA (*Spanish: Centro de Estudios Avanzados en Zonas Áridas*, Center for Advanced Studies in Arid Zones). These studies have used different models, such as SnowModel (Gascoin et al., 2013), SNOWPACK (Mengual Henríquez, 2017) and the Mass Balance model (MacDonell et al., 2013a). Nevertheless no comparisons have been made between these models. The uncertainties caused by variations in forcing and model parametrizations of each of those models are not properly quantified to evaluate the most adequate one for this environment. This master thesis compares different modelling approaches to evaluate the model performances and to quantify the uncertainties to identify the most appropriate one to simulate snowpack evolution at point scale in semi-arid conditions. Two models are compared in this study: SnowModel, the spatially distributed snow evolution model developed by (Liston and Elder, 2006b) and SNOWPACK developed by the WSL Institute for Snow and Avalanche Research SLF from Switzerland (Bartelt and Lehning, 2002; Lehning et al., 2002a,b).

1.3. Research objectives

Main question:

What is the sensitivity of the snow models SNOWPACK and SnowModel to its input parameters and parametrizations?

Five subquestions are needed to answer this main question:

1. What data handling and processing steps are necessary to constitute a consistent set of forcing data for the models?
2. What is the effect of different parametrizations on the snow depth, snow water equivalent and snow surface temperature of each model? Which parametrization is the most appropriate one?
3. What is the influence of variations in the input parameters on the output of each of the models?
4. What are the physical differences between simulations of snow depth, snow water equivalent and surface temperature on a point scale of SNOWPACK and SnowModel?
5. Which model is the most appropriate for understanding snowpack processes, and model snow depth evolution in arid settings?

1.4. Thesis outline

Several steps are needed to answer the research questions. First of all, the study area and available data are outlined in Chapter 3. The available data is used as input data for the snow models, but also as calibration and validation data of the snow depth, snow water equivalent and surface temperature (Section 3.2). Sections 3.3.1 and 3.3.2 describes the models SNOWPACK and SnowModel respectively. The measured temperature and relative humidity data are incomplete and the accumulated amount of precipitation is influenced by the wind and spatial effects. The interpolation and correction respectively of these data are done in Section 4.1. Two types of simulations are done and described in Section 4.2. Firstly, different calibrations of the two snow models are tested to find the most optimal set of parameters. Secondly, variations are applied to the forcing data and run with a Monte Carlo approach. The individual results of SNOWPACK and SnowModel are given in Section 5.2 and 5.3 and those results are compared to derive the most appropriate snow model for this region in Section 5.4. The thesis is continued with a discussion of the possible reasons for the results in the previous sections and an elaboration of the input parameters and parametrizations in Chapter 6. The study is ended with the conclusion in Chapter 7.

2

Snow modelling

2.1. Energy balance equation

An approach to quantify the amount of snow is surface energy balance modelling. The advantage of simulating the snow depth evolution with this physically-based method is that it can quantify the proportion of sublimation and melt and that it can be extended spatially and temporally, especially when measurements are not available. A physical approach (e.g. Lehning et al. (2002b); Liston and Elder (2006b); Brun et al. (1989); Mölg (2004))is often needed due to the sublimation and which is not account for in less extensive empirical methods such as a degree-day approach (Rango and Martinec, 1995).

The surface energy balance equation (Equation 2.1) takes the influence of incoming and outgoing fluxes into account (Oke, 1988), where Q_{LW} symbolizes the net energy flux from longwave radiation, Q_{SW} is the net energy flux form shortwave radiation, Q_S and Q_L symbolize the turbulent sensible heat flux and the turbulent latent heat flux, respectively, Q_P symbolizes the heat flux supplied by precipitation, and Q_G symbolizes the total energy flux in the subsurface. The resulting energy flux at the surface is denoted by F. Fluxes towards the surface are defined as positive, and those away from the surface are defined as negative. If the surface temperature is at 0°C and the right-hand side of Equation 2.1 is positive, F represents the latent energy flux for melting, Q_M.

$$Q_{LW} + Q_{SW} + Q_S + Q_L + Q_P + Q_G = F \tag{2.1}$$

The incoming longwave radiation ($L_\downarrow$ in $\mathrm{W\,m^{-2}}$) is parametrized with Equation 2.2, which depends on the air temperature T_a and the effective atmospheric emissivity ϵ_a. σ is the Stefan–Boltzmann constant ($5.670367 \times 10^{-8}\,\mathrm{W\,m^{-2}\,K^{-4}}$). The atmospheric emissivity depends on the humidity and air temperature (e.q. Brutsaert (1975); Brunt (1932); Dilley and O'Brien (1998); MacDonell et al. (2013b)) and is generally a value between 0.5 and 0.95, depending on the cloudiness of the sky. The outgoing longwave radiation ($L_\uparrow$ in $\mathrm{W\,m^{-2}}$) is calculated with Equation 2.3. T_s is the surface temperature and ϵ_s is the emissivity. This emissivity for snow is close to 1 (Cuffey and Paterson, 2010, Chapter 5) and an often-used value for snow is 0.98 by for example Liston and Hall (1995) and Shea and Jamieson (2011).

$$L_\downarrow = \epsilon_a \sigma T_a^4 \tag{2.2}$$

$$L_\uparrow = \epsilon_s \sigma T_s^4 \tag{2.3}$$

The incoming shortwave radiation ($S_\downarrow$ in $\mathrm{W\,m^{-2}}$) is calculated with Equation 2.4, the solar constant G_{SC} (1367 $\mathrm{W\,m^{-2}}$), the atmospheric transmissivity ψ and the position on Earth Z (Cuffey and Paterson, 2010, Chapter 5).

$$S_\downarrow = G_{SC} \cos Z \psi \tag{2.4}$$

The reflected shortwave radiation ($S_\uparrow$ in $\mathrm{W\,m^{-2}}$) is calculated with the albedo α. Equation 2.5 results into daily albedo α, because the sum of the RSWR and the sum of the ISWR are used. The albedo depends on the type of surface and is high for fresh snow and lower for older snow and soil. Snow models have different methods to calculate the albedo. More straightforward approaches use the snow depth and moment and amount of fresh precipitation (e.q. Strack et al. (2004)) and more extensive methods use the air temperature,

snow density, surface temperature, wind speed, longwave radiation and different characteristics of the grains in the snowpack (Brock et al., 2000; Klok and Oerlemans, 2004; Lehning et al., 2002a).

$$\alpha = \frac{\sum_{k=1}^{24} S_{\uparrow}}{\sum_{k=1}^{24} S_{\downarrow}} \tag{2.5}$$

Turbulent eddies vertically mix the air above the snow surface. If the air layer above the snow surface is warmer than the surface, the mixing transfers sensible heat to the surface. This is the turbulent sensible heat flux. A similar process happens with the moisture content of the air. If the overlying air is drier, mixing transfers moisture away from the surface. Evaporation or sublimation takes place at the surface to maintain the saturation of the air adjacent to it. This uses latent heat and is thus the turbulent latent heat flux (Cuffey and Paterson, 2010, Chapter 5). In models, those fluxes are always computed by using the bulk aerodynamic approach (Cuffey and Paterson, 2010, Chapter 5). The turbulent sensible heat flux Q_S (Equation 2.6) depends on the density of air ρ_a, the specific heat capacity at constant pressure c_a, the difference between the air temperature T_a and surface temperature T_s, the wind velocity u and the bulk exchange parameter for heat C_H (Cuffey and Paterson, 2010, Chapter 5).

$$Q_S = \rho_a c_a C_H u(T_{air} - T_s) \tag{2.6}$$

The turbulent latent heat flux Q_L (Equation 2.7) also depends on the air density and the wind speed, but uses absolute humidity of the lower boundary layer q_a and surface q_s, the latent heat of sublimation L_s and the bulk exchange parameter for moisture C_E (Cuffey and Paterson, 2010, Chapter 5).

$$Q_L = \rho_a L_s C_E u(q_a - q_s) \tag{2.7}$$

Equations 2.6 and 2.7 are referred to as the bulk aerodynamic method, because T_a, q_a and u are considered as representative values for the lower boundary layer as it is assumed that this layer is completely mixed. These parameters actually vary with height, so the the exchange parameters must be adapted to the height of the temperature, relative humidity and wind sensors (Cuffey and Paterson, 2010, Chapter 5).

Equation 2.6 can be rewritten as vertical flux proportional to the vertical temperature gradient $\delta T/\delta z$ (Equation 2.8), where K_h is the eddy diffusivity for heat, an coefficient specifying the transfer process of the vertical flux of heat (Cuffey and Paterson, 2010, Chapter 5).

$$Q_S = K_h \rho_a c_a \frac{\delta T}{\delta z} \tag{2.8}$$

The vertical flux of vapour can also be written in terms of K_w, the eddy diffusivity for water vapour. First of all, the amount of heat per unit volume $\rho_a c_a T$ is replaced by the humidity q, the mass of water vapour per unit volume and K_w is the eddy diffusivity for water vapour. If q is replaced with the gas law, expressed in terms of water vapour pressure e, this leads to Equation 2.9 (Cuffey and Paterson, 2010, Chapter 5).

$$Q_L = \rho_a K_w L_s \frac{0.622}{P} \frac{\delta q}{\delta z} \tag{2.9}$$

The third type of eddy viscosity that is introduced is K_m for the turbulence of air. This is defined by Equation 2.10, where τ stands for the shear stress acting on the surface and in the air above and u is the wind speed at height z. Theoretical and experimental results have shown that τ does not vary with the height, at least at a few meters above the horizontal surface and thus it can be written as in Equation 2.11 (Cuffey and Paterson, 2010, Chapter 5).

$$\tau = \rho_a K_m \frac{\delta u}{\delta z} \tag{2.10}$$

$$K_m \frac{\delta u}{\delta z} = \frac{\tau}{\rho_a} = \text{constant} \tag{2.11}$$

$(\tau/\rho_a)^{1/2}$ is also known as the friction velocity u_*. According to measurements, the wind speed u has a logarithmic relation to the height, scales with u_* and depends on the dimensionless von Kármán's constant k_0 (0.4) and the roughness length z_0 (Equation 2.12) (Cuffey and Paterson, 2010, Chapter 5).

$$u(z) = \frac{1}{k_0} u_* \ln\left(\frac{z}{z_0}\right) \tag{2.12}$$

The three eddy viscosities K_m, K_h and K_w are approximately equal in a neutral atmosphere, where the temperature gradient equals the dry adiabatic lapse rate. If this is assumed, it is easy to replace K_w and K_h in Equations 2.9 and 2.8 respectively with K_m from Equation 2.11 and thereupon the eddy viscosities only depend on the wind speed and roughness length (Cuffey and Paterson, 2010, Chapter 5).

Nevertheless, the assumption that the atmosphere has a neutral stability and that the wind profile is perfectly logarithmic not always holds and thus it is sometimes necessary to correct for this with atmospheric stability corrections. Two methods of correction are very common. The first method is based on the theory of Monin and Obukhov (1954) and the second correction is based on the Richardson number (Liston and Hall, 1995; Essery, 2015).

Q_P can be calculated with Equation 2.13 which uses the specific heat of water c_p (4190joule/kg/K) and the rain rate ($\mathrm{kg s^{-1}}$). Lehning et al. (2002a) uses this equation, but as the value is generally rather small, because most precipitation falls as snow in winter and the intensity of the precipitation is weak, this term is cancelled out of the energy balance equationin in most cases (e.q. Liston and Elder (2006b) and Cuffey and Paterson (2010)).

$$Q_P = r_r C_p (T_a - T_s) \tag{2.13}$$

The energy flux in the subsurface Q_G depends on the amount of layers in the snowpack, the refreezing and the thermal conductivity in the snowpack. Bartelt and Lehning (2002) offer an extensive way to calculate this, whereas Liston and Hall (1995) comes up with a more simplistic approach. As the approach of this energy flux strongly differs per model, no general equation is given for the flux.

If F from Equation 2.1 is positive, it represents the latent energy flux for melting Q_M. If the surface temperature is below 0°C and F is negative, energy Q_f is available to refreeze the snowpack. The potential snow melt rate $\dot{m}_s$ ($\mathrm{m s^{-1}}$ water equivalent) is calculated with the density of water ρ_w (1000 kilogram/$\mathrm{m^3}$, the time step dt and the latent heat of fusion of ice L_f ($3.34 \times 10^5\,\mathrm{J kg^{-1}}$) (Cuffey and Paterson, 2010, Chapter 5).

$$\rho_w L_f \dot{m}_s (1 - f_r) + \int_0^{\Delta z} \rho c \frac{\delta T}{\delta t}\, \mathrm{d}z = F \tag{2.14}$$

The parameter f_r is a value between zero and one and indicates the fraction of melt that refreezes within the layer. The second term of the left-hand side denotes the rate of gain of sensible heat in a vertical column through the layer with density ρ, specific heat capacity c, temperature T and time t.

The equations above do not implement the snow depth *SD*, but only the water equivalent *SWE*. This can be converted to snow depth if the snow density ρ_s and water density ρ_w are known (Equation 2.15). The snow density can be parametrized (Lehning et al., 2002a; Anderson, 1976), taken from in situ measurements or values from literature can be used (Cuffey and Paterson, 2010, Chapter 2). Often the rule of thumb is used that 1 meter of fresh snow is equal to 10 cm of water (Judson and Doesken, 2000).

$$SD = SWE \frac{\rho_w}{\rho_s} \tag{2.15}$$

2.2. Snow model parameters

Several parameters are needed to force, calibrate and validate snow models. Figure 2.1 gives a general visualisation of the process of snow modelling. The parameters in blue indicate forcing data and can be measured with sensors at an Automatic Weather Stations (AWS) or simulated with weather models. The figure gives four yellow blocks that are used to calibrate the snow model. Albedo can be measured (Equation 2.5), but if measurements are unavailable parametrizations are used. The same accounts for the snow density. The model can be forced with in situ measurements, but as these are generally unavailable, the model parametrizes the density. Furthermore, a roughness value and an atmospheric stability correction need to be implemented. The roughness length generally comes from literature. Ultimately, the red blocks are the output of the model, but also parameters that can be measured with sensors at an AWS and used as validation data. The validation parameters are the surface temperature, which is calculated with the outgoing longwave radiation (Equation 2.3), snow depth and snow water equivalent.

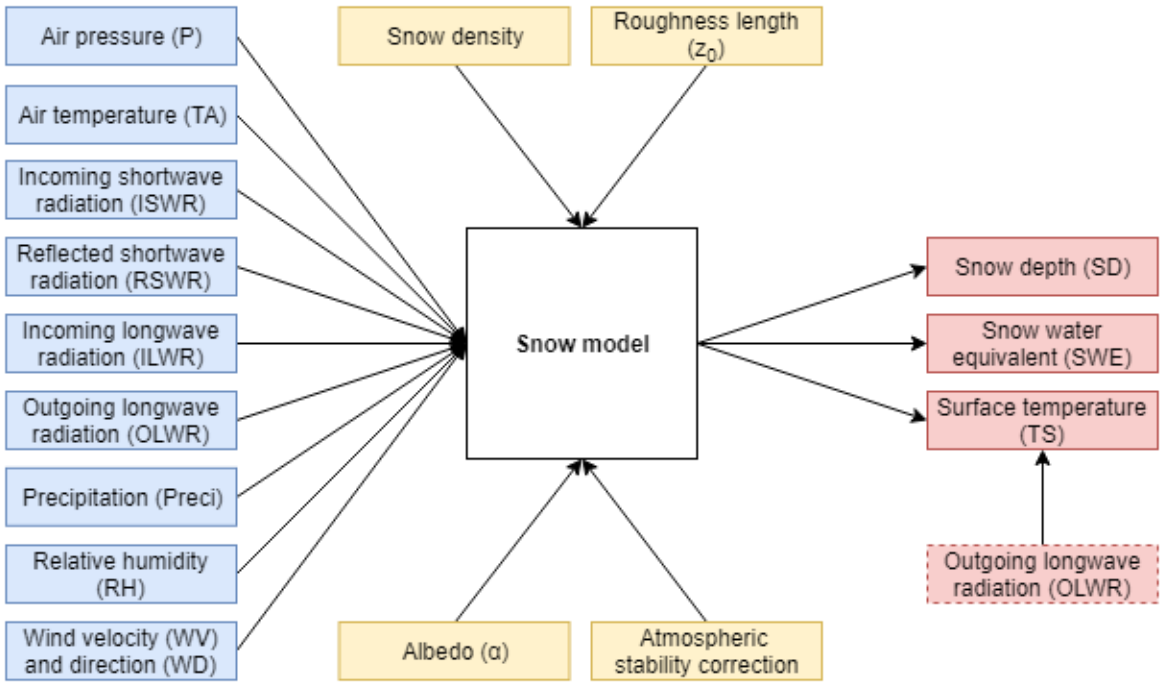

Figure 2.1: Visualisation of the process of snow modelling. The parameters in blue indicate forcing data, the yellow blocks are model calibration parameters and red blocks are parameters to validate the output of the model.

3

Study area, data and used models

3.1. Study area

The study region is located between the latitudes 26 and 32°S, the Pacific Ocean and the high Andes. The topography impacts the climate of this part of the semi-arid Andes. The area close to the coast is often covered by clouds due to a very stable lower troposphere and relatively cold sea surface temperature (Garreaud et al., 2002), but more inland, the air is extremely dry and cloud free (Kull et al., 2002). This causes shortwave radiation to be particularly strong in the Andes (MacDonell et al., 2013b).

This thesis focusses only on a part of the semi-arid Andes, namely on the La Laguna catchment (Figure 3.1). Different Automatic Weather Stations (AWSs) are located in this catchment (e.g. Tapado, Paso Agua Negra, La Laguna and Llano de Las Liebres, see Figure 3.1). The study is performed at local point using data from AWS Tapado for the year 2017 as it offers the most complete dataset.

AWS Tapado is located at -30° 9' 29.88", -69° 54' 29.44" at an altitude of 4306 m above sea level. It is named after the Tapado glacier whose terminus is about 1.7 km away from the weather station (CEAZAmet). Furthermore, the border with Argentina called Paso Agua Negra can be reached after about 8.5 km from the weather station (CEAZAmet) and La Laguna is 13.3 km away.

3.2. Available data

AWS Tapado is a weather station maintained by CEAZAmet, an unit within CEAZA (*Spanish: Centro de Estudios Avanzados en Zonas Áridas*, Center for Advanced Studies in Arid Zones) dedicated to monitor and study climate and meteorology. AWS Tapado, hereinafter referred to as Tapado, is an extensive station and provides data from sensors that are needed to model snow depth evolution at high altitude. It is the only station in the region provided with a snow water equivalent (SWE) sensor. The meteorological measurements that are relevant for this study are the temperature (TA), relative humidity (RH), air pressure (P), wind direction and velocity (WD, WV), precipitation (Preci), incoming shortwave radiation (ISWR), reflected shortwave radiation (RSWR), incoming longwave radiation (ILWR), outgoing longwave radiation (OLWR), snow depth (SD) and SWE sensors. The measurement and the corresponding manufacturers of the sensors are listed in Table 3.1. All sensors provide hourly measurements in 2017, except the SWE sensor, which gives an average SWE every six hours. Furthermore, the station is provided with a solar panel of 30W and a satellite antenna to transmit the data to CEAZAmet. This makes it possible to obtain the real-time data from the CEAZAmet-website.

Tapado has been installed in November 2009 and re-installed on 7 April 2017, but the wind sensors have been installed a month later on the 4th of May. The re-installation changed the location of the main tower of the station. The main tower with temperature, relative humidity and wind sensors is approximately 6 meters high and about 25 meters away from the precipitation gauge. The location of the tower can be described as in a small bowl, just a few meters lower as the surrounding area. Furthermore, the tower is placed behind a small hill of about 5 meters high. The area between the precipitation sensor and main tower is rather flat. Figure 3.2 is a photo made during the fieldwork in April 2018 of the precipitation sensor on the left and the main tower on the right. The soil type is representative for the location, because the surrounding area has the same type of soil. On the contrary, the small hill behind the station functions as a kind of snow fence (Antonissen, 2017). This might lead to unrepresentative amounts of snow for the location and more SWE than what is comparable to the amount of water collected at the precipitation gauge.

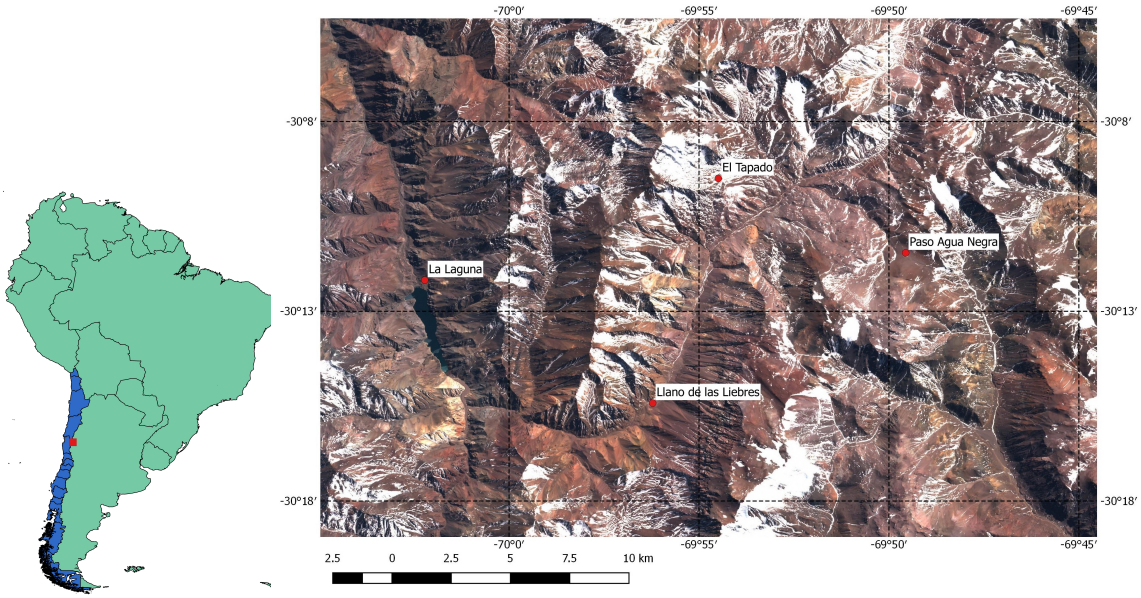

Figure 3.1: Chile is the country in blue in the map of South-America and the study area is marked with a red square. The right side shows the La Laguna catchment with the AWSs Tapado, Paso Agua Negra, La Laguna and Llano de Las Liebres (red points). The background map is constructed from Sentinel 2 images.

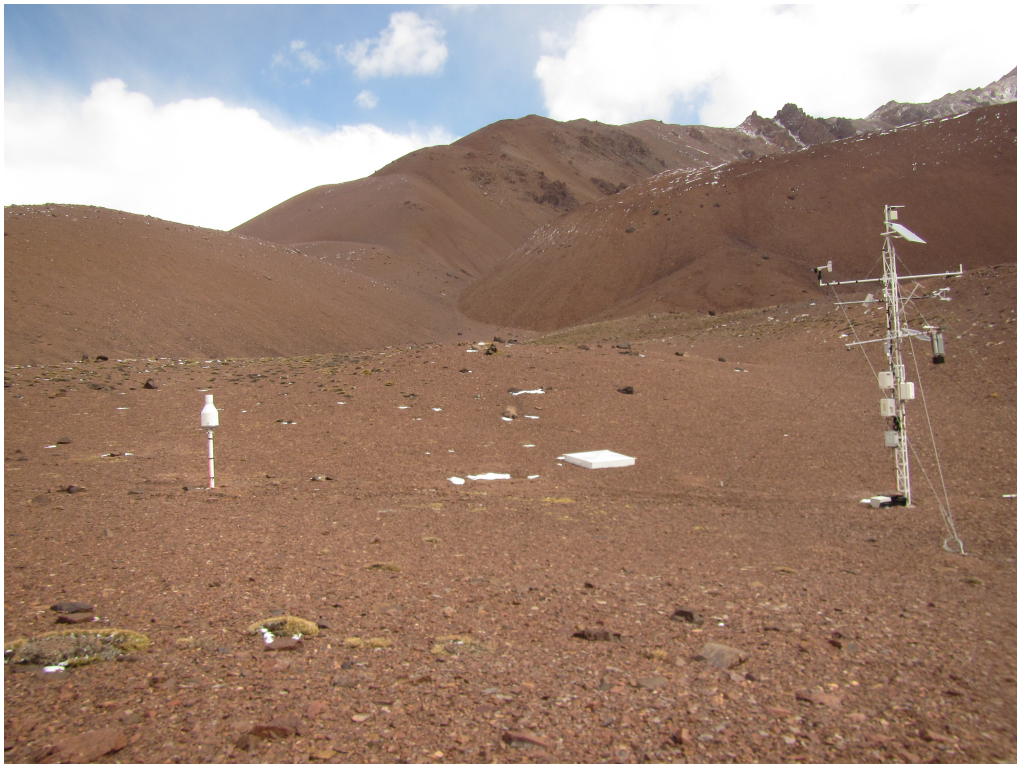

Figure 3.2: Photo of AWS Tapado taken on 26 April 2018 by Annelies Voordendag. At the left side of the picture the precipitation gauge is visible and the station with the other sensors is on the right.

Table 3.1: Available measurements, sensor height from the ground and the manufacturers of the corresponding sensor at AWS Tapado.

Measurement	Unit	Height (m)	Brand/type
Accumulated precipitation	mm	1.5	Geonor/T-200B 1000mm
Air pressure	hPa	3.5	Vaisala/PTB110
Air temperature	°C	3.5	Vaisala/HMP45C
Incoming longwave radiation	W/m^2	3.5	Kipp and Zonen/CNR4
Incoming shortwave radiation	W/m^2	3.5	Kipp and Zonen/CNR4
Outgoing longwave radiation	W/m^2	3.5	Kipp and Zonen/CNR4
Reflected shortwave radiation	W/m^2	3.5	Kipp and Zonen/CNR4
Relative Humidity	%	3.5	Vaisala/HMP45C
Wind velocity	m/s	5.4	RM Young/5103
Wind direction	°	5.4	RM Young/5103
Snow depth	m	3.5	Campbell/SR50A
Water equivalent (thallium, Tl)	mm	3.5	Campbell/CS725
Water equivalent (potassium, K)	mm	3.5	Campbell/CS725

An AWS at such an altitude needs maintenance. This is not always possible, as the road to the border crossing and thus to the AWS is closed in the winter period. The sensors sometimes malfunction during short time slots or longer periods of time. The available data for Tapado is shown in Figure 3.3.

The period where the models are run, starts at 4 May 2017 15:00. This is done, because at this point, the snow depth is zero and initially all sensors are working and thus data is available from all sensors. At 4 May 2017 11:00:00, a small peak of precipitation and change in snow depth is visible, but this is not clearly registered by the SWE sensor. The first registration of the SWE sensor was at 14:00 that day, but as the event of precipitation was very short and the SWE sensor measures an average over 6 hours, this measurement is not taken into account. The model is run until 1 December 2017. The snow is gone at this date.

The models used in this study can work with different kinds of input data and in this study the same data set has been composed for both models with air temperature, relative humidity, wind direction and velocity, air pressure, incoming shortwave radiation, incoming longwave radiation and hourly precipitation rates as input. The reflected shortwave radiation is used to calculate the albedo (Equation 2.5) and the outgoing longwave radiation to calculate the snow surface temperature (Equation 2.3). The next paragraphs show and describe the wind, air pressure and radiation data and the validation parameters. The temperature and relative humidity sensor at Tapado were not working from 23 June 11:00 until 31 October 10:00. The temperature and relative sensor are mounted in the same device, so they are both not working at the same periods. The reconstruction of this missing data is given in Section 4.1, using available temperature and relative humidity data of Laguna, Llano de Las Liebres and Paso Agua Negra (Figure 3.4). The other available sensors at Laguna, Llano de Las Liebres and Paso Agua Negra are given in Tables A.1, A.2 and A.3 in Appendix A respectively and the locations of these stations are found in Table 3.1. The precipitation measurement also needs some corrections, because of its location relative to the main tower of the weather station. The precipitation gauge and the corresponding raw data is discussed in Section 3.2.1 and the methods the correct the data are given in Section 4.1.

Table 3.2: Locations, elevations of the used AWSs and altitudinal differences between the stations and Tapado station.

AWS name	Latitude (WGS-84)	Longitude (WGS-84)	Elevation (m.a.s.l.)	Altitudinal difference with Tapado (m)
Tapado	-30° 09' 29.88"	-69° 54' 29.44"	4306	0
Laguna	-30° 12' 11.20"	-70° 02' 14.01"	3209	-1097
Llano de las Liebres	-30° 15' 26.66"	-69° 56' 13.15"	3565	741
Paso Agua Negra	-30° 11' 26.53"	-69° 49' 31.91"	4774	-468

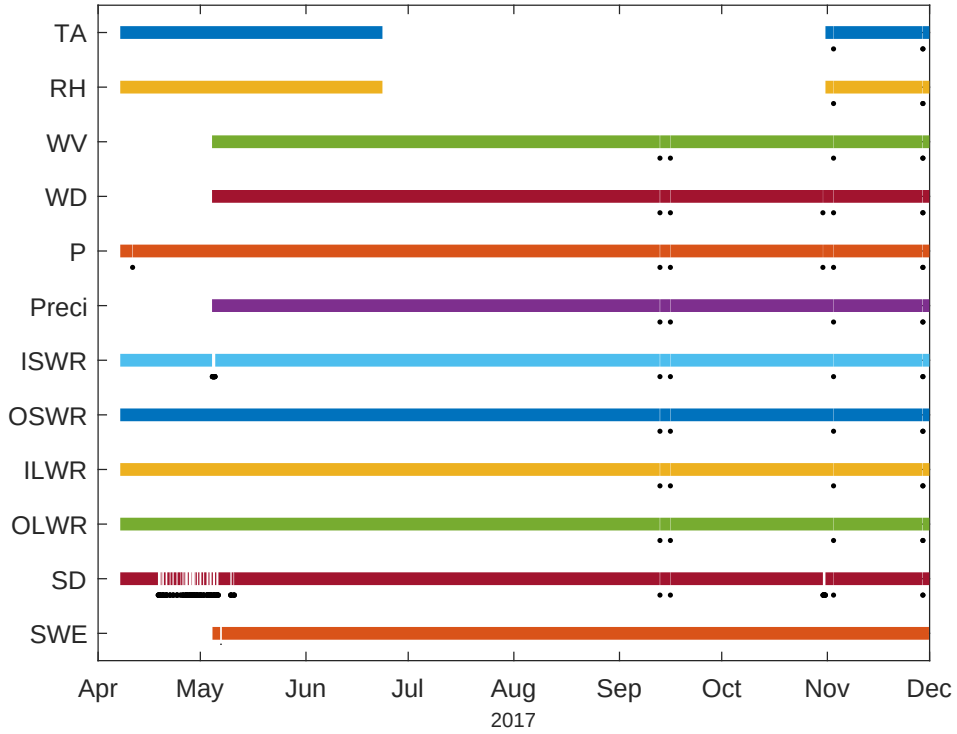

Figure 3.3: Gantt plot of available data used in this study at Tapado. The color bars represent the moment that sensors were working. Malfunctioning of sensors during only one or a few hours are highlighted with dots underneath the bar.

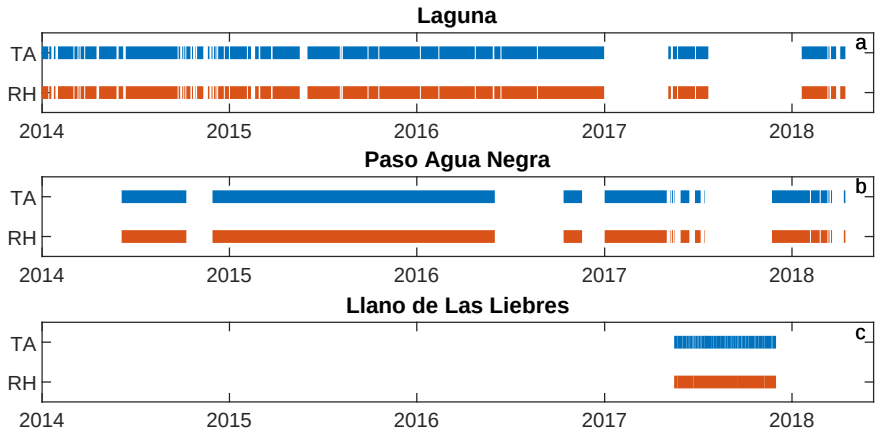

Figure 3.4: Gantt plot of available temperature and relative humidity data at a) Laguna, b) Paso Agua Negra and c) Llano de Las Liebres between 2014 and 2018. The bars display the availability of daily data.

Table 3.3: Specification of the Geonor T-200B precipitation gauge.

Geonor T-200B	
Capacity (including antifreeze)	1000 mm
Collecting area	200 cm^2
Sensitivity	0.075 mm
Accuracy:	0.1% full scale
Repeatability	0.1 mm
Temperature range	Sensor: -40°C to 60°C
Temperature drift	0.001% FS/°C
Materials	Aluminium alloy
Size	∅ = 390 mm, H = 800 mm
Mounting	Universal 3-point with leveling system incorporated in base

3.2.1. Precipitation

The sensor that has been used to measure cumulative precipitation is the Geonor/T-200B 1000mm. This sensor collects water in the container which is weighed with a vibrating wire load sensor and this gives a frequency output. The frequency is a function of the applied tension on the wire and from this, the amount of precipitation can be computed. The frequency is recorded as a square-shaped 0-5 V signal (Geonor, 2010). Further specifications of this sensor are given in Table 3.3. As the sensor measures only accumulated precipitation, the signal should only increase, but some noise is visible on the signal (Figure 3.5, black line). Negative peaks are repeatedly visible in the precipitation data. Correlation has been found with the power of the battery, because during the hours of the day where the voltage from the battery is the highest because of stronger solar radiation, those negative peaks are visible. This problem has not been investigated more, but nonetheless those negative peaks need to be filtered. A filter has been applied where the next value of the precipitation data is set to the previous one if it is lower than the previous one and remained the same if it is higher than the previous one as well as the median of the 60 next measurements is also higher than the previous value. This last step is done to filter out some noise in the data later in the season.

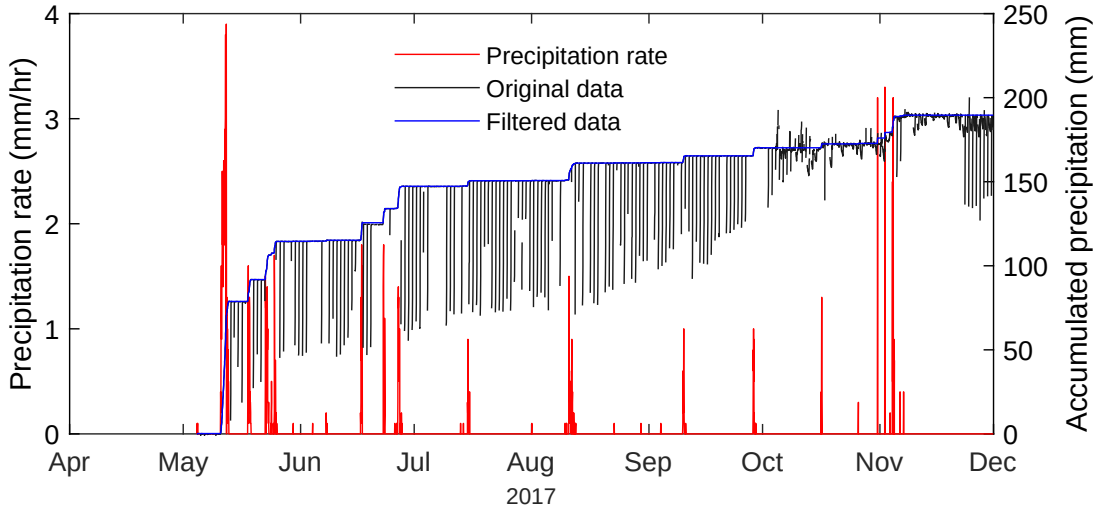

Figure 3.5: The raw data of precipitation (black), the filtered precipitation data (blue) and the precipitation rates (red).

3.2.2. Wind direction and velocity

The 5 missing measurements of wind direction and 6 missing measurements of velocity (Figure 3.3) have been interpolated by taking the mean over the two hours before and two hours after the measurement is missing. The height of the wind sensor has been measured by Robinson Godoy in May 2018 and set to 5.4 meters. As the surface below the station is covered with rocks and pebbles, the height of the sensor has an

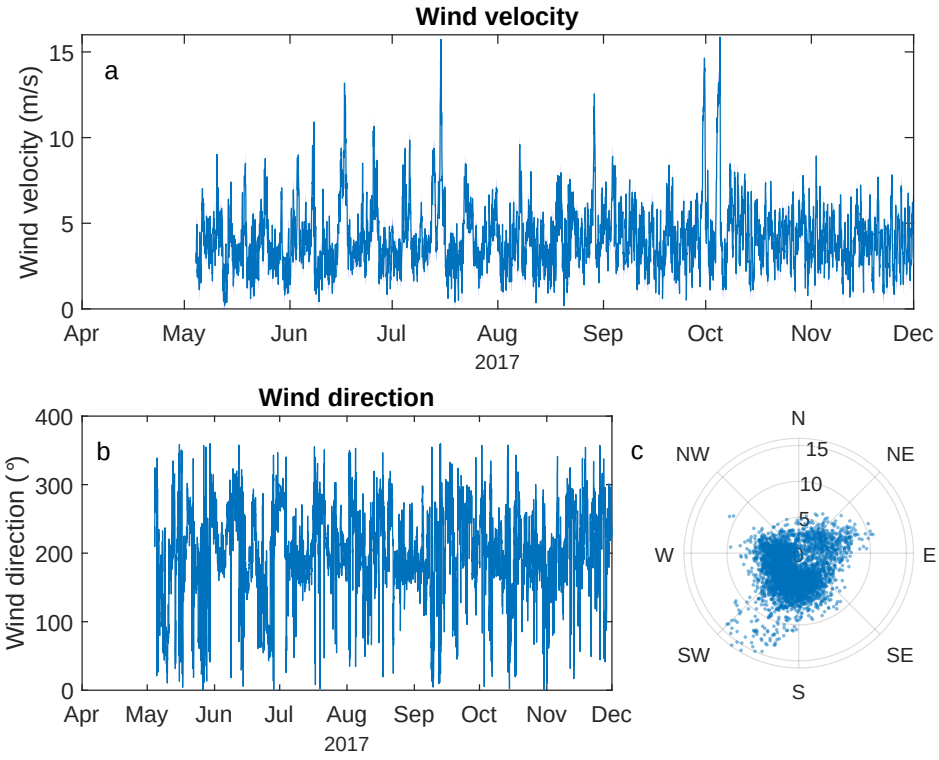

Figure 3.6: The a) wind velocity and b) direction and c) the combined wind rose. The 95% interval of confidence has been plotted in a) and b), but hardly visible as the uncertainties of the wind sensor are small. The wind rose gives the direction (angle) and velocity (radius) of individual measurements.

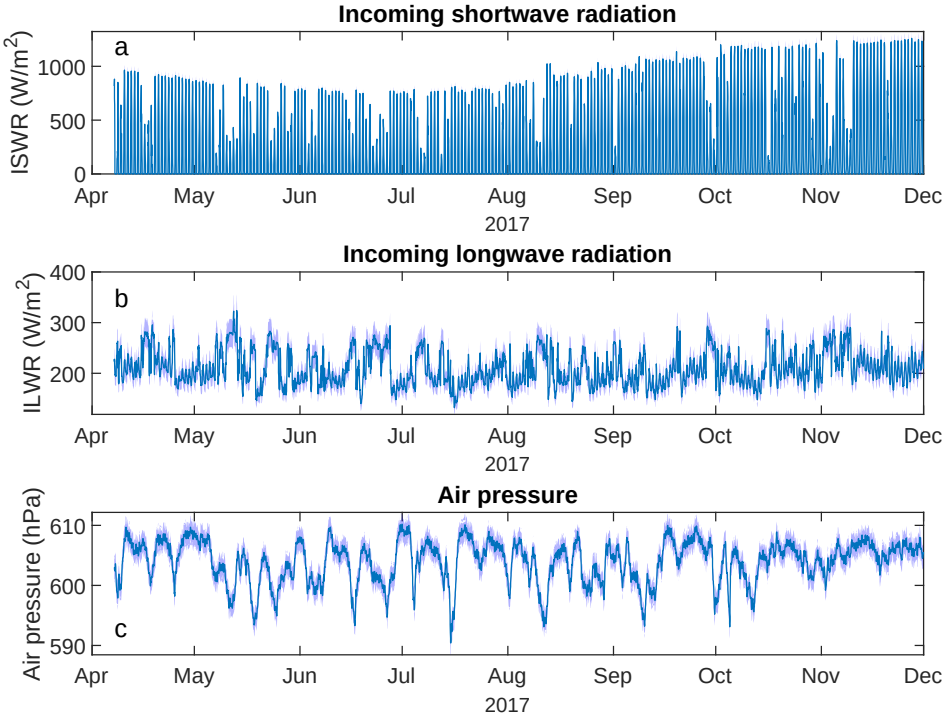

Figure 3.7: a) ISWR, b) ILWR and c) air pressure. The 95% interval of confidence has been plotted, but hardly visible as the uncertainties of the sensors are small.

estimated uncertainty of ±0.1 m. The accuracy of the wind sensor given by R.M. Young Company is ±0.3 m/s or 1% of the reading for the wind velocity and ±3° for the wind direction. The maximum measured wind velocity is 15.86 m/s. 1% of this reading is 0.16 m/s. It is chosen to use 0.3 m/s for the wind velocity and ±3° for the direction as these are the maxima of the stated uncertainties.

The wind data is displayed in Figure 3.6. The interval where it is confident to have 95% of the measurements is calculated as 1.96σ where σ is 0.3 m/s and 3° for the velocity and direction respectively. This interval has been plotted in Figure 3.6, but this is hardly visible. The median of the wind direction is 205° and thus the predominant wind direction is south west. Furthermore, it is visible that if there are high wind velocities (>10 m/s), the wind always comes from the south-southwest.

3.2.3. Radiation

The radiation sensor is a CNR 4 from Kipp & Zonen. This is a 4 component net radiometer which consists of a pyranometer pair and a pyrgeometer pair. The pyranometer measures the shortwave radiation with one sensor faced upward and the other one downward. The pyrgeometer measures longwave radiation also with a upward and downward-facing sensor. The pyrgeometer misses 25 measurements irregularly spaced over the measurement period. 23 measurements are missed for the incoming shortwave radiation and 44 measurements for the reflected shortwave radiation (Figure 3.3). As the sensors are generally only missing a few hours and no large time slots, these points have been interpolated by taking the average value between the measurement 24 hours before and 24 hours after the missing value. This is done to simulate the diurnal and seasonal cycles of radiation terms. The incoming shortwave radiation is plotted in Figure 3.7a and clearly shows a seasonal dependence. The ISWR is stronger during the summer months. The incoming longwave radiation (Figure 3.7b) is stronger at the moments that the ISWR is smaller during the daytime. This indicates that the air is cloudy.

The pyranometer has an uncertainty in the daily total of less than 5% (95% confidence level) and the pyrgeometer has an uncertainty in the daily total of less than 10% (95% confidence level, indoor calibration) (Kipp and Zonen, 2014). Figure 3.7 also shows the radiation uncertainty, but this is hardly visible as the uncertainty of the radiation is so small.

3.2.4. Air pressure

The air pressure sensor has been operational during the winter of 2017 without any problems. The six missing measurements have been supplemented by taking the mean over the two hours before and two hours after the measurement is missing. Vaisala lists the accuracy of the sensor as ±0.3 hPa at +20°C and ±1.0 hPa in the temperature range between -20 and +45°C. Thus, the considered uncertainty is ±1.0 hPa. The air pressure and the 95% interval of confidence is displayed in Figure 3.7c. As expected at these altitudes, the air pressure is rather low, compared to the air pressure of 1013 hPa at reference sea level (Liston and Elder, 2006a).

3.2.5. Albedo

The albedo is used to calibrate the model. Equation 2.5 gives the albedo calculation. A daily albedo is used, because this is the most representative albedo during the day. Measurements errors caused by a low sun angle (van den Broeke et al., 2004) are moderated with this method. The daily albedo is displayed in Figure 3.8a. Albedo values above 1 are noticed. This is probably caused by a small inclination of the sensor (van den Broeke et al., 2004), which causes the ISWR measurement to be smaller than the RSWR measurement. At the start of October a rapid decrease of the albedo is visible. This can be correlated to a strong wind event at the same moment. During a field trip in August 2018, it was visible that the snow in the region sometimes gets covered with dust. It is assumed that this has also happened at the start of October 2017, because the weather station is located in a small bowl (Section 3.2) and that makes the snow prone to events where it can get covered by dust.

3.2.6. Surface temperature

The surface temperature is used as validation data and is calculated with Equation 2.3 (Figure 3.8). The emissivity is 0.98 according to Liston and Hall (1995) and the used value in both SNOWPACK and SnowModel. The surface temperatures are above 0° at the moments that no snow has been measured and during certain periods. Furthermore, daily variations are visible in the surface temperature. The surface temperature is higher during the day than in the night. At the end of the season, but while there is snow, the surface temperature gets more often above 0°. There are two snow events in October and November and an decrease in the surface

temperature is visible at these time slots.

3.2.7. Snow depth

Hourly snow depth data is measured by the SR50A sensor from Campbell Scientific. The acoustic sensor measures the distance from the sensor to the snowpack. The sensor can be used for other purposes as well, but it is typically used for snow depth or water depth measurements (Campbell Scientific, 2018). The accuracy of the snow depth is ±1 cm (Campbell Scientific, 2018).

The snow depth with the interval of confidence of 95% is plotted in Figure 3.9a. The measurements of the SR50A show 62 data gaps during strong snowfall events. This is caused by the fact that the sensor uses acoustic waves and those waves are disturbed by snow during a snowfall event. The sensor is programmed to take a measurement every 10 seconds. The SR50A rejects a reading if the target distance changes at a rate of 4 cm/s or more. The velocity of falling snow is generally faster than 4 cm/s (Magono and Nakamura, 1965), so it is likely that measurements are discarded during snowfall. These data gaps are not interpolated, as snow depth data is only used for validation. In the beginning of the season the snow depth decreases rapidly. This is due to compaction of the snow pack and thus the change of the snow density. Later in the season, the change of snow depth after a snowfall event is less rapidly. Big decreases in the snow depth are visible at 15 July and 29 August. This can be correlated to strong winds at these dates.

3.2.8. Snow Water Equivalent (SWE)

The CS725 sensor by Campbell Scientific measures the SWE by passively detecting the change in naturally emitted terrestrial gamma radiation from the ground after it passes through snow cover. It detects potassium and thallium gamma rays and allows two measurements (Wright, 2011). CEAZAmet delivers the results of both measurements and the measurement of the potassium rays is higher. According to people of CEAZAmet and the manufacturer, the starting point signal without snow for potassium was a lot higher than the signal for thallium. This shows that potassium is the stronger signal and the one that should be used to calculate SWE (Randall, 2018). The signal of the potassium rays is also less noisy and hence the measurement of SWE with potassium has been used to make an artificial data set of precipitation in Section 4.1.3. The accuracy according to the manufacturer is ±15 mm, but the maximum difference between the SWE from thallium and potassium gamma rays is 82 mm. It is therefore chosen to always plot both measurements, although the measurement for potassium is considered more reliable. The SWE measurements are plotted in Figure 3.9b. The SWE data follows the similar pattern as the snow depth data. The two events that are correlated with the strong wind events that are visible in the snow depth, are also visible in the SWE data.

3.3. Model descriptions

The aim of this thesis is to compare snow models, but as there are hundreds of snow models available, this study is restricted to two physically based snow models: SNOWPACK and SnowModel. These two models have been chosen as they are both models that use the energy balance equation, have a lot of literature available and are especially designed to model snow packs.

3.3.1. Description of SNOWPACK

The snowcover model SNOWPACK is developed by the Swiss Federal Institute for Snow and Avalanche Research (SLF) (Bartelt and Lehning, 2002; Lehning et al., 2002b,a). The SLF is part of the Swiss Federal Research Institute WSL. It has especially been designed for snow cover forecasting and its associated avalanche danger in the Swiss Alps. SNOWPACK is distributed as an application that assigns most of the work to a C++ library, called libsnowpack (SLF, 2017b). The model is a one-dimensional model, but can be implemented in the spatially distributed, three-dimensional snow cover and earth surface model Alpine3D, also developed by SLF. SNOWPACK must be installed together with SLF's MeteoIO plugin, which is a pre-processing library for meteorological data. Missing data is interpolated and atmospheric parameters, such as albedo are calculated with this tool.

SNOWPACK has especially been designed for avalanche forecasting in the Swiss Alps (Lehning et al., 1999). Other regions where it has been applied, are Japan, where the snow is predominantly wet, because of formation and percolation of meltwater throughout the entire winter (Yamaguchi et al., 2004), a glacier at Svalbard (Norway) to simulate snow and superimposed ice (Obleitner and Lehning, 2004) and to the Greenland ice sheet (Bellaire et al., 2017; Steger et al., 2017). The model has mainly been used for research purposes, but in Switzerland it is used in operational mode to help with the avalanche forecasting. The model has been

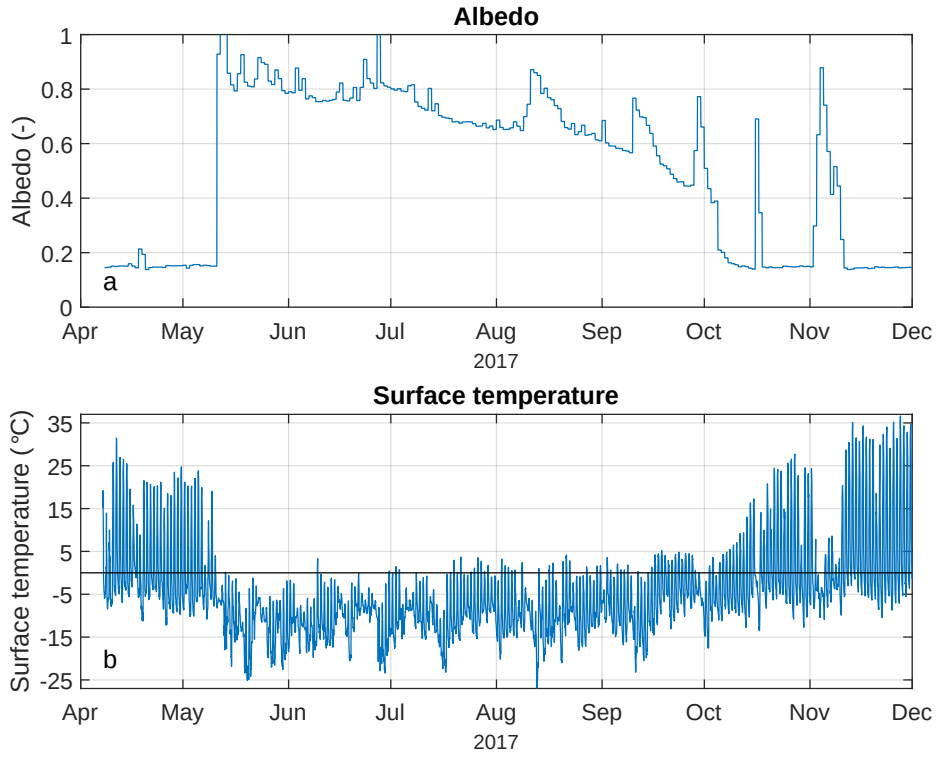

Figure 3.8: a) Albedo and b) surface temperature.

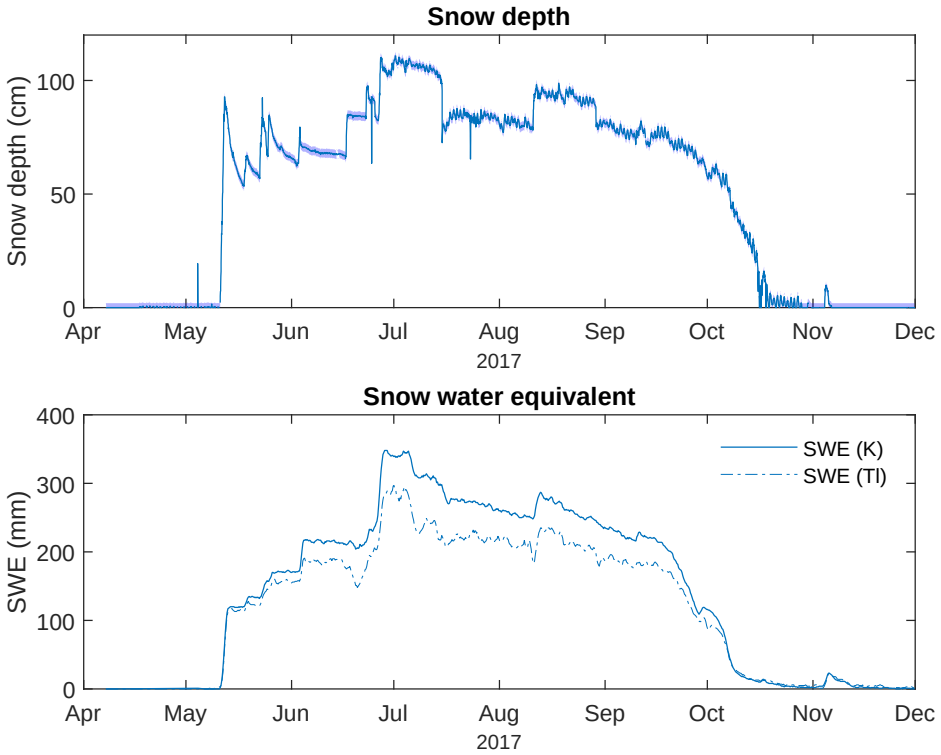

Figure 3.9: a) Snow depth and b) snow water equivalent. The 95% confidence interval is plotted for the snow depth. The snow water equivalent detected from potassium (K) and thallium (Tl) gamma rays are both plotted.

applied all over the world, but it has only been used once in the dry Andes for the undergraduate thesis of Mengual Henríquez (2017).

3.3.2. Description of SnowModel

SnowModel is a spatially distributed snow-evolution modelling system, developed by Glen Liston from the Cooperative Institute for Research in the Atmosphere, Colorado State University, Colorado. The SnowModel code is written in FORTRAN and provided with a lot of useful notes and references to literature. The model consists of the submodels MicroMet, EnBal, SnowPack and SnowTran3D.

MicroMet distributes the measurements of the weather stations over a larger area (Liston and Elder, 2006a). The MicroMet preprocessor interpolates missing data from weather stations (Liston and Elder, 2006a). The measurements are interpolated according to the topography of the region of interest with a Barnes objective analysis scheme (Barnes, 1964, 1973; Koch et al., 1983).

EnBal calculates surface energy exchanges with the equations given in Liston and Hall (1995). The albedo is also calculated in this subsection. SnowPack simulates snow depth and water-equivalent evolution and SnowTran3D accounts for snow redistribution by wind (Liston and Elder, 2006a).

The model has mainly been used in windy environments, for example in Alaska (Liston and Sturm, 2002), South East Greenland (Hasholt et al., 2003; Mernild et al., 2006) and Svalbard, Norway (Bruland et al., 2004). The model also has been used in the semi-arid Andes by Gascoin et al. (2013), where the focus was also on the redistribution of snow by wind. Those examples applied SnowModel to larger areas, but this thesis only evaluates one grid cell of the entire grid.

4

Methodology

This chapter consists of a description of the method of the interpolation and correction of the temperature, relative humidity and precipitation data. The way the model simulations are done, is visualised and given in Section 4.2. Lastly, the set up of the two models, SNOWPACK and SnowModel, are respectively given in Section 4.3 and Section 4.4.

4.1. Preparation of forcing data

4.1.1. Temperature

The temperature and relative humidity at the period where the sensor was not working, are computed using measurements from nearby stations Paso Agua Negra, Llano de Las Liebres and Laguna (Figure 3.1). The interpolation of the temperature data consists of three steps, namely the temperature calculation, its validation and evaluation of the uncertainties that arise from this calculation.

Temperature calculation

It has been chosen to calculate a temperature gradient between the AWSs Paso Agua Negra and La Laguna (Rolland, 2003). These stations are chosen, because they are the only two nearby stations that have long-term measurements. Measurements are available starting from 2014 and it was therefore possible to calculate a daily lapse rate with data over four years (Figure 3.4).

The temperature gradient Γ between the two stations is calculated for the time slots m where data is available with Equation 4.1.

$$\vec{\Gamma_m} = \frac{\Delta T_m}{\Delta z} = \frac{T_{Laguna_m} - T_{Paso_m}}{z_{Laguna} - z_{Paso}} \tag{4.1}$$

T_{Laguna} and T_{Paso} are daily mean temperatures and z_{Laguna} and z_{Paso} are the elevations of Laguna and Paso Agua Negra respectively (Table 3.2). No lapse rate is obtained during the entire period in 2017 (Figure 3.4), where the interpolated temperature is needed, so a fit is calculated through the data. It is assumed that the temperature gradient varies over the seasons (Rolland, 2003) and thus a sinusoidal least-squares fit has been calculated. The fit of the daily lapse rate $\hat{\Gamma}$ between the two stations is calculated with Equation 4.2-4.4.

$$\hat{\Gamma} = \begin{bmatrix} \Gamma_1 \\ \Gamma_2 \\ \vdots \\ \Gamma_n \end{bmatrix} = A\hat{x} \tag{4.2}$$

$$\hat{x} = \begin{bmatrix} a \\ b \\ c \end{bmatrix} = (A^T A)^{-1} A^T \vec{\Gamma} \tag{4.3}$$

$$A = \begin{bmatrix} 1 & cos(\frac{2\pi}{365} t_1) & sin(\frac{2\pi}{365} t_1) \\ 1 & cos(\frac{2\pi}{365} t_2) & sin(\frac{2\pi}{365} t_2) \\ \vdots & \vdots & \vdots \\ 1 & cos(\frac{2\pi}{365} t_n) & sin(\frac{2\pi}{365} t_n) \end{bmatrix} \tag{4.4}$$

A depends on the day of the year t_n. These fitted daily gradients are used to calculate the temperatures at Tapado $T_{Tapado,n}$ in the missing time slots with Equation 4.5.

$$T_{Tapado,n} = \Gamma_n \Delta z + T_{Llano} \tag{4.5}$$

n is the day number of the year, Δz is the altitude difference between Llano de Las Liebres and Tapado from Table 3.2 and T_{Llano} is the temperature at Llano de Las Liebres. If measurements at Tapado were available this data are used. Llano the las Liebres is the only station that provides data during the entire missing period. Figure 4.1 visualises the measurements at Tapado. The missing time slot is filled with the data in blue form Llano de Las Liebres. If the calculation with Paso Agua Negra was used, it was only possible to interpolate 390 of in total 3123 missing time slots.

Validation of the temperature calculation

The temperature at Tapado is also calculated with data from Llano de Las Liebres and Paso Agua Negra while the sensor at Tapado was working. With this data, the root mean square error *RMSE*) and the coefficient of determination (R^2) of the interpolation method are calculate to validate the use of the calculation of the temperature. The root mean square error is computed with Equation 4.6 and R^2 is computed with Equation 4.7.

$$RMSE = \sqrt{\frac{1}{n} \sum_{i=1}^{n} (T_{station,i} - T_{Tapado,i})^2} \tag{4.6}$$

$$R^2 = [\frac{\sum_{i=1}^{n} (T_{Tapado,i} - \bar{T_{Tapado}})(T_{station,i} - \bar{T_{station}})}{\sum_{i=1}^{n} (T_{Tapado,i} - \bar{T_{Tapado}})^2 \sum_{i=1}^{n} (T_{station,i} - \bar{T_{station}})^2}]^2 \tag{4.7}$$

n is the number of time slots that the sensor at Tapado and at the significant other station was working. T_{Tapado} is the temperature at Tapado and $T_{station}$ is the temperature calculated at Tapado with Llano de Las Liebres or Paso Agua Negra.

Furthermore, the mean and standard deviation of the difference between the measured temperature at Tapado and the calculated temperature at Tapado is calculated. The mean of this difference is supposed to be close to 0, because otherwise the interpolation is biased. The standard deviation is the assumed uncertainty in the measurements that has been introduced because of the interpolations.

Uncertainty of the temperature data

According to the manual provided by Campbell Scientific (1998), who cabled and modified the sensor made by Vaisala, the accuracy is ±0.4°C at -20°C, ±0.3°C at 0°C and ±0.2°C at 20°C. The value of ±0.3°C at 0°C is used as the uncertainty of the sensor σ_{sensor}, as the range of the temperatures is closest to 0°C. In addition, an uncertainty $\sigma_{calculation}$ is introduced, because of the interpolation of the data. This is the standard deviation that is calculated from the temperatures at Tapado and at Tapado, but calculated with data from Llano de Las Liebres. The final uncertainty σ_T of the temperature is calculated with Equation 4.8.

$$\sigma_T = \sqrt{{\sigma_{sensor}}^2 + {\sigma_{calculation}}^2} \tag{4.8}$$

4.1.2. Relative humidity

Relative humidity calculation and validation

The missing RH data is calculated with a similar approach as used for the temperature data, because the same period of RH data as for the temperature data is unavailable at Tapado. Thus, Equations 4.1-4.5 are used, but instead of the temperature measurements, the RH measurements are used. Furthermore, the calculation with Paso Agua Negra has been used if this was available to interpolate the data instead of only the data from Llano de Las Liebres. In Figure 4.2, it is visible that this mainly accounts for some time slots in the end of June

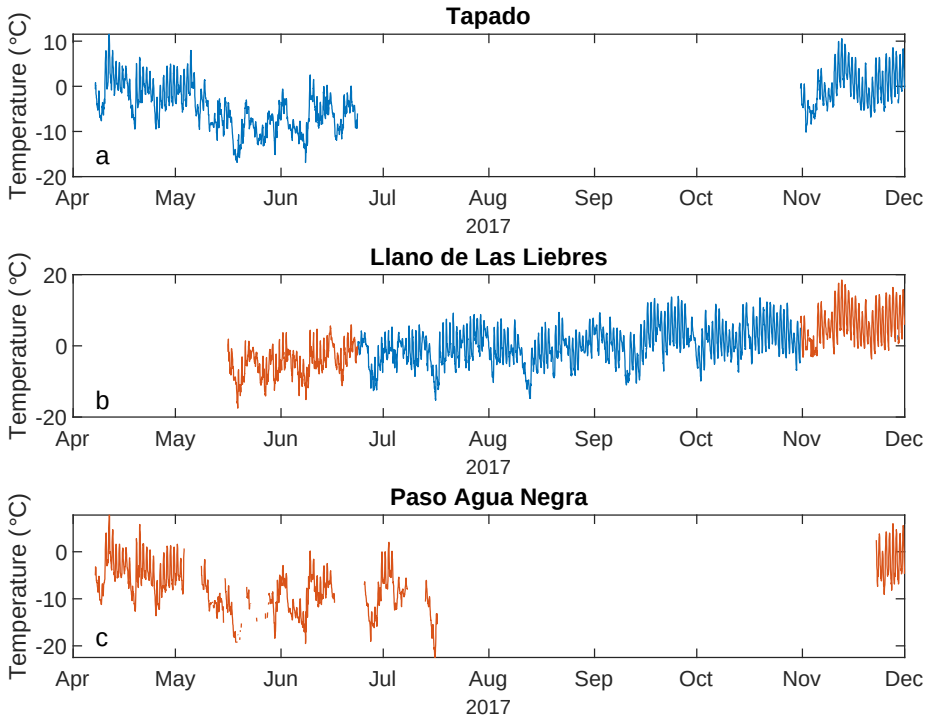

Figure 4.1: The available temperature measurements at a) Tapado, b) Llano de Las Liebres and c) Paso Agua Negra in 2017. The data in blue of Llano de Las Liebres is used to interpolate the missing time slot at Tapado.

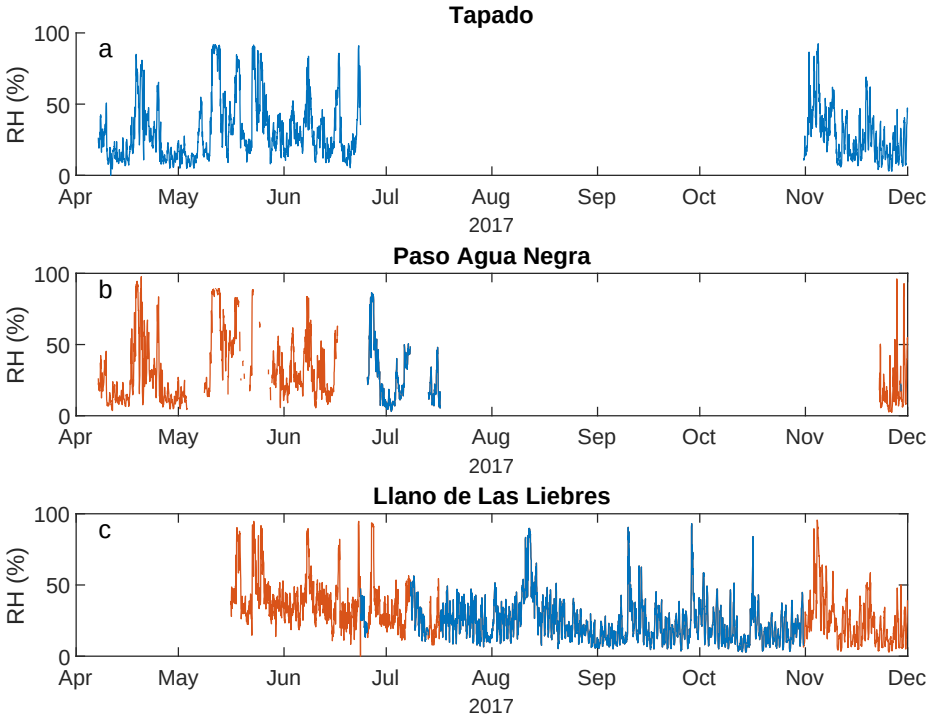

Figure 4.2: The available relative humidity measurements at a) Tapado, b) Paso Agua Negra and c) Llano de Las Liebres in 2017. The data in blue of Paso Agua Negra and Llano de Las Liebres is used to interpolate the missing time slot at Tapado.

and beginning of July. Lawrence (2005) tells us that the relationship between RH and altitude is not a linear gradient and that the relative humidity increases if the temperature decreases. An approach with Equations (4)-(7) of Liston and Elder (2006a) could have been used, but for simplicity reasons a linear gradient between AWSs has been assumed.

The validation of the relative humidity calculation is also done by calculating the mean and standard deviation between the differences of the RH at Tapado when measurements were available with the RH at Tapado calculated with data from Llano de Las Liebres or Paso Agua Negra. Equations 4.6 and 4.7 are used to calculate the root mean square error and the coefficient of determination.

Uncertainty of the relative humidity data

The accuracy of the sensor is ±1% RH at 20°C against factory reference, but when calibrated in the field its accuracy is ±2% (0% to 90% RH) and ±3% (90% to 100% RH) at 20°C. Furthermore the sensor has a temperature dependence of ±0.05% RH/°C (Campbell Scientific, 1998). There are only 39 data points with a relative humidity above 90% which is 0.68% of all data. Hence the accuracy σ_{sensor} of 2% is used in the calculation of the total uncertainty.

The final uncertainty of the RH is calculated with Equation 4.9. The $\sigma_{T_{dependence}}$ is the uncertainty that comes from the temperature dependence and is calculated with the mean temperature μ_T and the reference temperature of 20°C (Equation 4.10).

$$\sigma_{RH} = \sqrt{{\sigma_{sensor}}^2 + {\sigma_{T_{dependence}}}^2 + {\sigma_{calculation}}^2} \tag{4.9}$$

$$\sigma_{T_{dependence}} = 0.05(20 - \mu_T) \tag{4.10}$$

4.1.3. Precipitation

According to MacDonald and Pomeroy (2007), Smith (2007) and Wolff et al. (2015), it is known that the Geonor precipitation gauge deals with some undercatch in the sensor, especially if it is windy. This under-estimation is probably true at AWS Tapado, because strong winds are observed in the region and when comparing the accumulated precipitation with SWE measurements, results indicated a negative bias for the first peak of precipitation. Actually, immediately after the first snow fall event, the amount of snow water equivalent only depends on what has fallen and not on processes like melt and sublimation.

MacDonald and Pomeroy (2007), Smith (2007) and Wolff et al. (2015) have derived empirical formulas to correct the undercatch in the Geonor T-200B. An intercomparison of the models by MacDonald and Pomeroy (2007) and Smith (2007) has been done by Zhang et al. (2015). This study describes the general formula for the catch efficiency CE_{Geonor}, which is an exponential function that depends on the wind velocity and two parameters a and b that differ per author (Equation 4.11).

$$CE_{Geonor} = a\exp(bWV) \tag{4.11}$$

The corrections by MacDonald and Pomeroy (2007), Smith (2007) and Wolff et al. (2015) are applied to the filtered precipitation data. The corrected precipitation data that corresponds the best to the first peak in SWE is chosen as the precipitation to use in the models.

Additionally, another precipitation data set has been computed with the SWE measurement. The precipitation can only increase, as it is cumulative, but the SWE decreases due to sublimation, melt and wind events and increases due to snow events and snow deposition, because of the wind. The SWE has been filtered in such a way that only positive values while any precipitation has been registered at the Geonor T-200B have been added as precipitation, assuming that the wind has no influence at that moment. This dataset of precipitation calculated from SWE is used to quantify the uncertainties of the precipitation.

Uncertainty of the precipitation data

Table 3.3 lists the uncertainties for the precipitation sensor. The SWE measurement and the precipitation measurement differ a lot, so the uncertainty is higher than what has been stated by the manufacturer. Hence, two methods are proposed to assess the uncertainty of the precipitation. Both methods assume that the precipitation must be somewhere between the measurement and the precipitation dataset derived from the SWE data.

The first method calculates the middle point between the precipitation measurements and the precipitation derived from SWE. Precipitation rates are derived from this middle line and for every time slot the

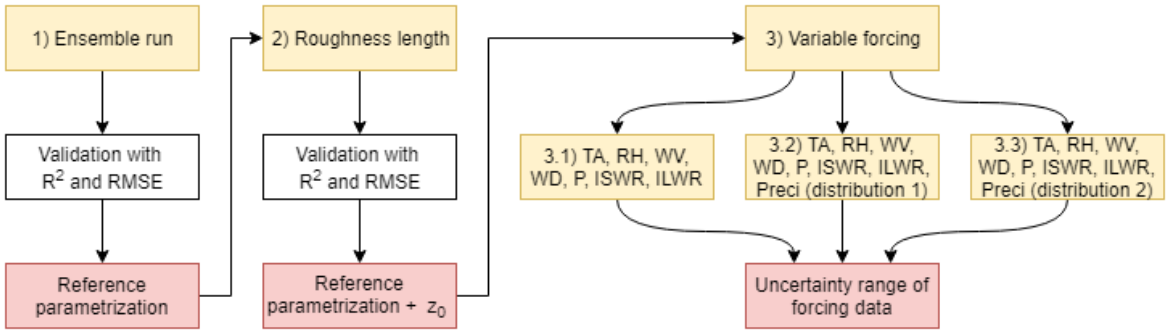

Figure 4.3: Flow chart of the three step approach to calibrate and evaluate SNOWPACK and SnowModel.

maximum and minimum precipitation rate is distracted. It is assumed that the difference between this minimum and maximum rate is the 99.7% interval of confidence. One σ is half of the difference between this maximum and minimum precipitation rate divided by 3. This is namely the standard deviation that assumes that 99.7% of the data is between the maximum and minimum precipitation rate. This standard deviation is multiplied by a normally distributed random number and added to the precipitation rate at the middle line precipitation. The random number remains the same for all the data points. The precipitation curves that result into an higher cumulative precipitation than the precipitation derived from SWE data or lower than the measurements at the end of the season are removed.

The second method assumes that the amount of precipitation per precipitation event is different. For every precipitation event a different random number has been taken, but this is kept constant during the event. Once more, it has been assumed that 99.7% of the calculated precipitation rates fall within the borders of the measured and estimated precipitation.

4.2. Simulations

A three step approach has been used to do the simulations with SNOWPACK and SnowModel. These steps are visualised in Figure 4.3. The method to validate these steps, is always the same. The validation of a model run is done by calculating the RMSE and the R^2 between the simulated and the measured snow depth and snow water equivalent (Equations 4.6 and 4.7). The model run with the lowest RMSE and highest R^2 is considered the 'most optimal' run.

The first step is to do an ensemble approach with all the possible combinations of parametrizations of the model. A parametrization is way to express a physical parameter such as albedo, snow density or atmospheric stability correction with equations. A combination of parametrizations of the different physical parameters is a calibration of the model. An ensemble approach runs all possible calibrations. This step is denoted as *Ensemble run* in Figure 4.3. The validation of the ensemble run is done with the RMSE and R^2. The best calibration is the reference run of the model.

The goal of the second step is to select the most optimal roughness length for the models. MacDonell et al. (2013a) and Pellicciotti et al. (2005) describe typical roughness lengths of 0.1 mm for fresh snow and an order-of-magnitude higher value for aged snow. The study of MacDonell et al. (2013a) has been done in the semi-arid Andes and increased the value linearly up to 4 mm. Andreas et al. (2004) describe similar ranges for the roughness lengths. There is more aged snow than fresh snow during the season and it is therefore chosen to use 1 mm as initial value for the roughness length. The reference calibration is run 100 times with different roughness lengths in the range between 0.1 and 10 mm on a logarithmic scale. The validation of this run is once more done with the RMSE and R^2. The most optimal roughness length is added to the set of reference parameters of the model.

The third step is the quantification of the model uncertainties with a Monte Carlo approach. This step is divided in three sub steps, as visualised in Figure 4.3.

Monte Carlo is a statistical simulation method that is used for the simulation of random processes. The distribution of the random input variables is assumed to be known. It has extensively been used a hydrology (e.q. Kuczera and Parent (1998), Khu and Werner (2003)), but also in snow modelling there are several uses (e.q. Conway and Cullen (2013), Sauter and Obleitner (2015)). The uncertainties of the models are quantified by running the model 1000 times with different forcing data. In Section 3.2 the uncertainties σ for the param-

eters VW, DW, P, ISWR and ILWR are discussed. The uncertainties of TA, RH, and precipitation follow from their interpolations. The TA, RH, VW, DW, P, ISWR and ILWR measurements are considered to be normally distributed and thus the forcing data is adjusted by adding hourly variations to the data according to $x\sigma$. x is a normally distributed random number generated with the Matlab-function *randn* and σ is the standard deviation of the different forcing parameters as discussed in Section 3.2. For the precipitation, two methods are proposed and these were discussed in Section 4.1.3.

Step 3.1 is a Monte Carlo runs with 1000 simulations each that only takes the variables TA, RH, VW, DW, P, ISWR and ILWR into account. The precipitation data is the same as for the reference run. Steps 3.2 and 3.3 consist of 1000 simulations with variable TA, RH, VW, DW, P, ISWR and ILWR and with the distributions of the precipitation according to the results of the two methods of Section 4.1.3. The runs with variable distribution of precipitation are separated from the run with the other variable input, because the precipitation input is very uncertain. The influence of the other forcing data has thus been tested separately as well.

The results of these Monte Carlo runs are ranges of possible outcomes. The 2.5 and 97.5% quantile is calculated from these results. This gives the 95% confidence interval, which is plotted together with the reference calibration, which resulted from step 2.

The ultimate step in this research is to compare SNOWPACK and SnowModel. The first step to compare the models, is to compare the results of the reference runs. The RMSE and R^2 are discussed to indicate which model performs better.

It is supposed that the reference run is the most optimal calibration of the separate models without considering uncertainties in the forcing data. The next step in comparing the results, is to plot the uncertainty ranges of the models acquired from the Monte Carlo runs.

4.3. Model set up of SNOWPACK

SNOWPACK needs three different input files to run the model, namely one with information about the initial snow profiles, one with forcing data and a simulation configuration file (Figure 4.4).

The file with the initial snow profile has been made with Matlab and is in the so-called .sno-format. The ascii-type file has the same header for every simulation and contains no data as there is no initial snow profile. The file is nevertheless needed to run the program correctly. The header contains information about the station, such as location and time zone. The soil albedo (SoilAlbedo) is set to 0.15, as this is the calculated average albedo at the moment when there is no snow (Figure 3.8). The roughness value of the bare soil (BareSoil_z0) is set to 0.020. The soil at Tapado is covered with pebbles and rocks and as no measurement are available of the true soil roughness value, the same default value is used as the default value of SnowModel.

The input file for the forcing data is provided in the SMET-format and has been made with a script in Matlab. The guideline provided by Bavay (2017) has been used to get a correct SMET-file. This file also contains a header and data. The header consists of the information of the station and specifies which measurements are provided. The data section of the SMET-file contains columns with the timestamp and measurements of P, TA, RH, WV, WD, ISWR, ILWR, precipitiation rate and surface ground temperature (TSG). The TSG has not been measured but needs to be provided and is therefore set to -1°C. This is the value for the surface ground temperature in SnowModel and ensures that the first snow stays and does not immediately melt away.

The last file needed to run the model is a simulation configuration file. This .ini-file can be made with the provided Java user interface INIshell. This tool is useful to get familiar with all the options possible for the model, but it is more efficient to make the files with a Matlab-script. The configuration file is divided in the subsections General, Input, Output, Snowpack, Snowpackadvanced, Filters, Interpolations1d and Generators. There are more than 100 parameters that can be changed in these sections, but most of them are kept to the default value.

Variables that are of main interest for SNOWPACK in this study are the snow albedo α, fresh snow density ρ, roughness length z_0 and atmospheric stability correction model. SNOWPACK has 6 different models to correct for atmospheric stability. The different options are given in the block *Atmospheric stability* in Figure 4.4. The atmospheric stability correction model *Richardson* is the default setting and is a simplified Richardson number stability correction. *Neutral* assumes neutral stratification, which means that the wind profile is logaritmic. The atmospheric stability correction models starting with *MO* are based on the Monin-Obukhov Similarity Theory (van den Broeke et al., 2005) and modified by different researchers.

It is chosen to use *Richardson* as reference parametrization, because this is the default setting. Furthermore, it is already known that SnowModel only uses an atmospheric stability correction based on the Richardson number and that makes it easier to compare the models. A correction based on the Richardson number

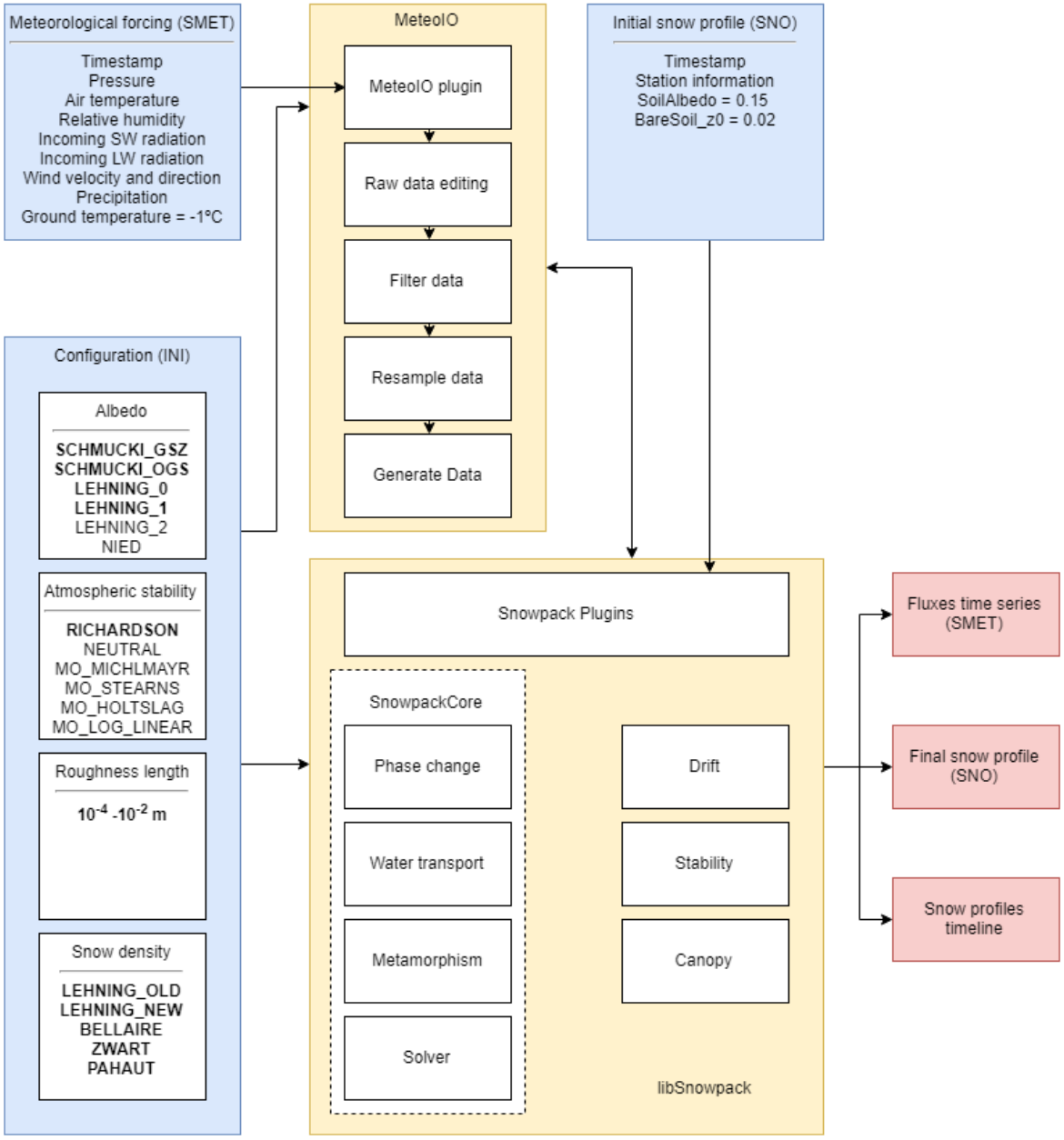

Figure 4.4: Flow chart of input files and output of SNOWPACK. The blue blocks in the diagram are the input files. The yellow blocks are the models MeteoIO and SNOWPACK. The red blocks are the output of the model.

is also used in other models (Wagnon, 2003; Mölg et al., 2008).

For the parameterization of the snow albedo, it is possible to set the albedo to a fixed value or to choose between one out of six parameterizations. The possible parameterizations are given in the block *Albedo* in Figure 4.4. *Lehning_1* is the parameterization according to equation 18 in Lehning et al. (2002a) and depends on the wind velocity, air temperature, surface temperature, reflected shortwave radiation, the fractional water content, bond radius, dendricity and sphericity of the snow grains and a categorical variable indicating previous melt and refreeze. There is no literature available that describes *Lehning_0* and *Lehning_2*, but according to the code they are statistical models based on measurements from the Weissfluhjoch study site. This is a mountain summit in the Swiss Alps. The two Schmucki-variants are statistical models by Edgar Schmucki based on measurements of incoming and reflected shortwave radiation at 4 stations in Switserland. *Schmucki_GSZ* considers grain size as a parameter, while *Schmucki_OGS* replaces grain size with optical equivalent grain size. The *NIED*-option is the Japanese version of *Lehning_2* (SLF, 2017a). The adjustments that had been made to *Lehning_2* are described by Yamaguchi et al. (2004). It is chosen to exclude the Japanese version *Nied* and *Lehning_2* from the ensemble runs. A provisional run where the measured albedo are compared with the albedo of the six different parametrizations, shows that those two parametrizations do not correspond to the measured albedo. *Nied* is not suitable, as it was designed for wet regions (Yamaguchi et al., 2004). *Lehning_2* overestimates the albedo significantly. The parametrized albedo stays above 0.7 until November and this is in strong contradiction with what the measurements reveal (Figure 3.8).

The fresh snow density can be chosen to be fixed, measured, as an event or parametrized. It is not realistic to keep this value fixed, because the factors that influence the fresh snow density, such as temperature, relative humidity and wind velocity are different for every precipitation event. There are no measurements of snow density available at Tapado for the winter of 2017 and the event option is a wind driven deposition of snow on Antarctica. Thus, the five density parametrizations remain. A decision can be made between the five options in the block *Snow density* in Figure 4.4. *Lehning_old* depends on the air temperature, surface temperature, relative humidity and wind velocity. *Lehning_new* is the parametrization described in (Lehning et al., 2002a), is the default parametrization and uses the same forcing data as*Lehning_old*, but takes ad-hoc wind and temperature effects with different empirical parameters into account. *Zwart* is a logarithmic parametrization using air temperature, relative humidity and wind velocity by Costijn Zwart.*Bellaire* has been made by Sascha Bellaire and is also a logarithmic function depending on air temperature, wind velocity and the altitude of the region of interest. *Pahaut* is a model by Edmond Pahaut which was introduced in September 1995 in *Crocus* by G. Giraud. The parametrizations only uses air temperature and wind velocity as parameters. It is chosen to keep all the density parametrizations for the ensemble run, because provisional runs do not show big differences between the runs or a run that is a clear outlier. Furthermore, it is also more difficult to validate snow density data, because measurements are not available at Tapado for the winter of 2017.

This set up leads to 20 different combinations, because 4 albedo and 5 snow density parametrizations are used. The selected parametrizations are in bold in Figure 4.4.

The ultimate parameter to consider is the roughness length. A roughness length of 1 mm is chosen as reference according to MacDonell et al. (2013a) and Pellicciotti et al. (2005). This deviates from the model's default roughness value of 2 mm.

4.4. Model set up of SnowModel

SnowModel needs at least three different input files, namely a configuration file, a file with information about the topography and file with forcing data. The flow chart with these files are visualised in Figure 4.5. It is optional to provide a file with information about the vegetation, but that is not needed in this study, because the model is analysed at point scale.

The minimum forcing data in SnowModel consists of a file with the timestamp, station ID, the coordinates and altitude of the AWS, TA, RH, Preci, WV and WD. The air pressure, incoming longwave radiation and incoming shortwave radiation can be implemented as well, but should be provided in separate files.

The file with topographic information is a digital elevation model (DEM). This DEM was constructed from SRTM data and resampled to a 100 meter resolution by Simon Gascoin. The focus of this thesis is to assess the sensitivity of the snow models at point scale. It is therefore chosen to use a DEM of 3 by 3 pixels and only analyse the centre pixel. Furthermore, MicroMet is disabled to distribute the wind over the topography and for this reason the wind has spatially constant wind velocities.

The parameters to configure the model are given in a third file. The subsections and different subrou-

tines are enabled or disabled in this file. The aim of this study is to compare two models with comparable calibrations. SNOWPACK is able to calculate wind erosion, but only if the height of snow is defined. As the snow depth is a validation parameter in this thesis, the wind erosion is not implemented in SNOWPACK. The conditions of both models should be kept constant and it is therefore chosen to disable the SnowTran3D subsection of SnowModel.

SnowModel can be run in a single layer set up, but in this case it is chosen to use the multilayer subroutine of the model, as been used by Liston and Mernild (2012). This subroutine takes the thermal conductivity of the snowpack into account and is more similar to the approach by SNOWPACK than the single layer configuration.

The albedo parametrization has two options. The first option assumes three possibilities for the albedo. The albedo is equal to the soil albedo if there is no snow, the albedo is a maximum albedo with temperatures below 0°C and the albedo is an intermediate value with temperatures above 0∘C. The second option takes the time evolution of albedo into account. This approach has been used in SnowModel by Strack et al. (2004) and uses Equation 4.12 with temperatures below 0°C and Equation 4.13 with temperatures above 0°C. α_s is the snow albedo, τ_a the linear gradient of 0.008, δt is 3600 s and τ_1 is 86400 s. The minimum albedo α_{min}, while there is snow is 0.5 by default and τ_f is 0.24. This approach resets the snow albedo to the maximum albedo if 3 mm of precipitation has fallen.

$$\alpha_s(t+\delta t) = \alpha_s(t) - \tau_a \frac{\delta t}{\tau_1} \tag{4.12}$$

$$\alpha_s(t+\delta t) = [\alpha_s(t) - \alpha_{min}] \exp\left(\tau_f \frac{\delta t}{\tau_1}\right) + \alpha_{min} \tag{4.13}$$

The albedo of fresh snow is set to 0.9 as this is the often used value in literature (e.q. Klok and Oerlemans (2004)) and the maximum value of albedo in SNOWPACK. The intermediate albedo at times when there is older snow is set to 0.6 (Cuffey and Paterson, 2010, Chapter 5) and the soil albedo is 0.15 according to the measurements.

SnowModel provides only one parametrization for the snow density (Liston and Hall, 1995), which depends on the ground and snow temperature and some empirical parameters according to Anderson (1976). The atmospheric stability correction is based on the Richardson number and is described in detail in Liston and Hall (1995). The model uses two different roughness values. The roughness value of soil is used if there is no snow and the roughness value defined by the user for snow does not change any more during the season. The default roughness length of soil is set to 0.02 m. For the roughness value of the snow the same value has been used as for SNOWPACK, which was 1 mm. The best albedo model is selected and used as reference run. It is possible to change the gradients of albedo change during cold and melt conditions, but as the aim of this thesis is to compare the base of two models, it is chosen not to change empirical parameters.

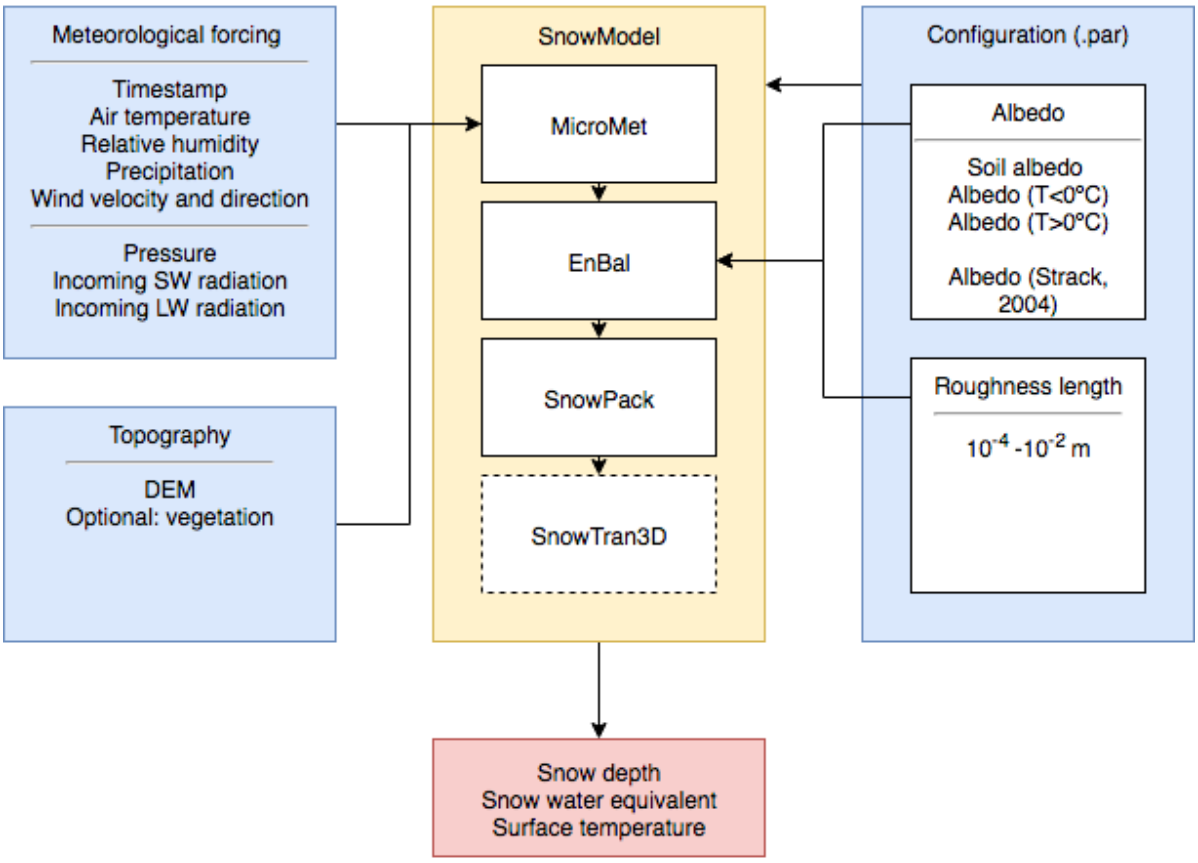

Figure 4.5: Flow chart of input files and output of SnowModel. The blue blocks in the diagram are the input files. The yellow block is SnowModel with the subsections MicroMet, EnBal, SnowPack and SnowTran3D. The red block is the output of the model.

5

Results

5.1. Forcing data

5.1.1. Temperature data

Figure 5.1a displays the daily lapse rates and the fit of this data. The fitted daily gradients have a maximum of -6.9°C/km in the winter and a minimum of -8.0°C/km in the summer. The temperature gradient is negative, which means that an increase in elevation decreases the temperature. The lapse rate agrees with general lapse rate changes of -9.8°C/km for dry air to about -4°C/km for saturated air (Rolland, 2003).

Figure 5.1b shows the final temperature calculations. The blue line in this plot indicates the temperature measured at Tapado and the red line is interpolated data. The mean and standard deviation of the differences between the calculated and available data from Tapado are listed in Table 5.1. The standard deviation of 2.78°C is the $\sigma_{calculation}$ in Equation 4.8. The final uncertainty of the temperature σ_T is 2.80°C. The 95% interval of confidence is $1.96\sigma_T$ and has also been displayed.

The statistics of Paso Agua Negra are better with a mean closer to 0, a higher R^2 and a smaller standard deviation and RMSE (Table 5.1), but nevertheless the data of Llano de Las Liebres has been used to interpolate the temperature data. Lastly, the linear regression analysis of the data from Llano de Las Liebres is given in Figure 5.1c. The interpolated temperatures with Llano de Las Liebres are plotted against the measurements at Tapado and a linear trend is fitted through the data. The calculated trend is $y = 1.13x - 0.45$.

Table 5.1: Statistics of the temperature calculations at Tapado with data from Paso Agua Negra and Llano de Las Liebres. The mean and standard deviation are calculated between the difference of the calculated temperature and the measured temperature at Tapado. The RMSE and R^2 are calculated with the interpolated temperature and the temperature at Tapado, if this was available. The number of observations where data of both Tapado and the significant other station is also given.

TA calculated with:	Llano de Las Liebres	Paso Agua Negra
# of observations	1638	1578
Mean	1.01	-0.07
Standard deviation	2.78	1.29
RMSE	2.68	1.28
R^2	0.84	0.94

5.1.2. Relative humidity

The calculated RH gradient between La Laguna and Paso Agua Negra varies between 3.33%/km in summer and 5.24%/km in winter (Figure 5.2a). These gradients are between 3.3 and 5.2%/km and the assumption that the relative humidity increases if the temperature decreases is satisfied. The final RH calculations are given in Figure 5.2b. The blue line in this plot indicate the RH measured at Tapado and the red line is interpolated data.

The uncertainty caused by the temperature dependence $\sigma_{T_{dependence}}$ is 1.22% with the average air temperature of -4.4°C (Equation 4.10). The standard deviation of the calculation with Llano de Las Liebres $\sigma_{calculation}$ is 12.81% (Table 5.2) and 47.95% of the total relative humidity data is calculated with Llano de Las Liebres. This is also the biggest uncertainty and as a simplistic assumption has been made for the interpolation of

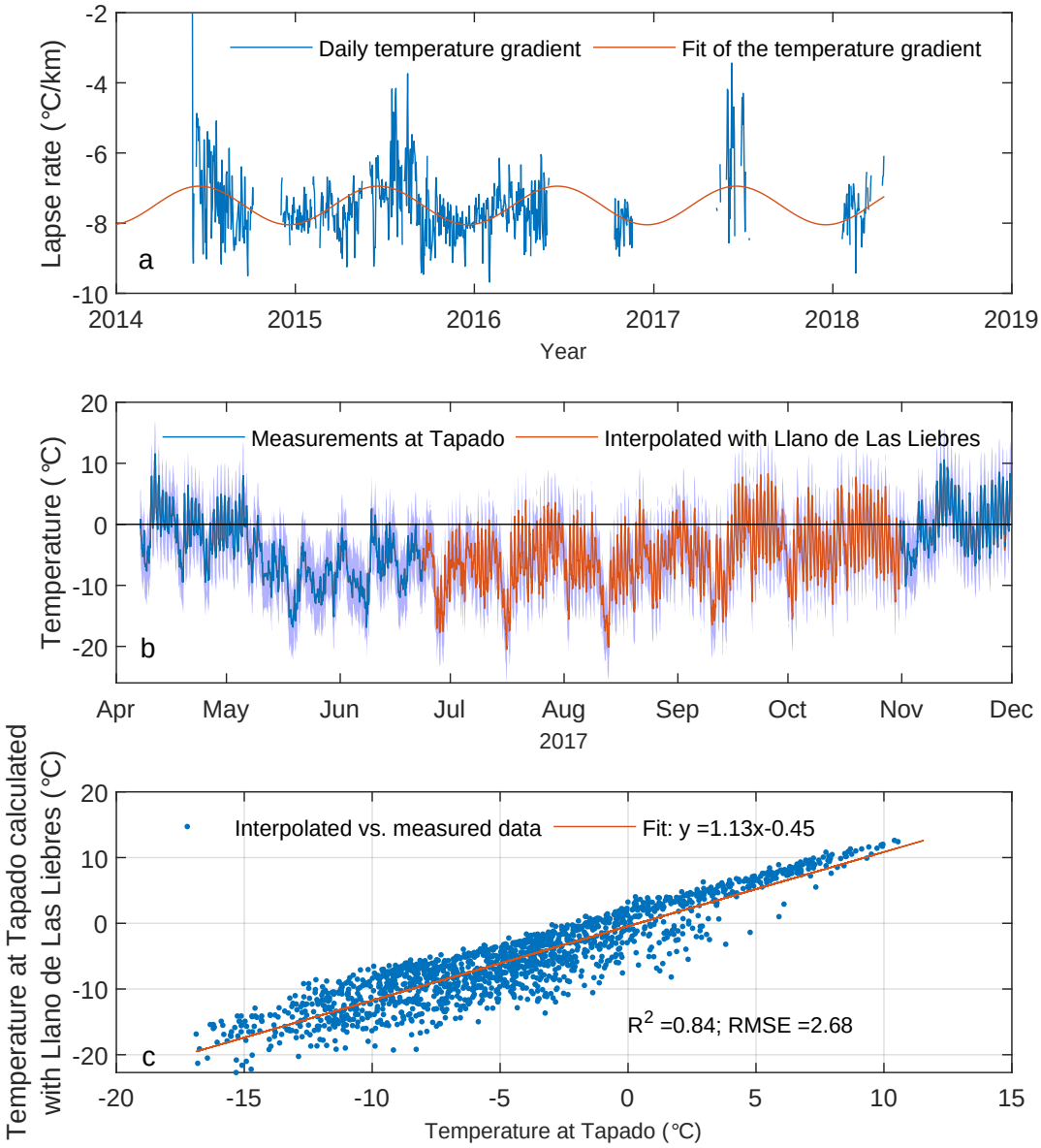

Figure 5.1: a) The daily lapse rate between AWS Paso Agua Negra and La Laguna (blue) and the seasonal fit of this daily temperature gradient (red) and b) the temperature at Tapado that is calculated with data from Llano de Las Liebres (red) and the measurements at Tapado (dark blue). The light blue area around the line represents the 95% interval of confidence. c) The regression analysis of the temperatures calculated with Llano de Las Liebres (blue) and its fit (red).

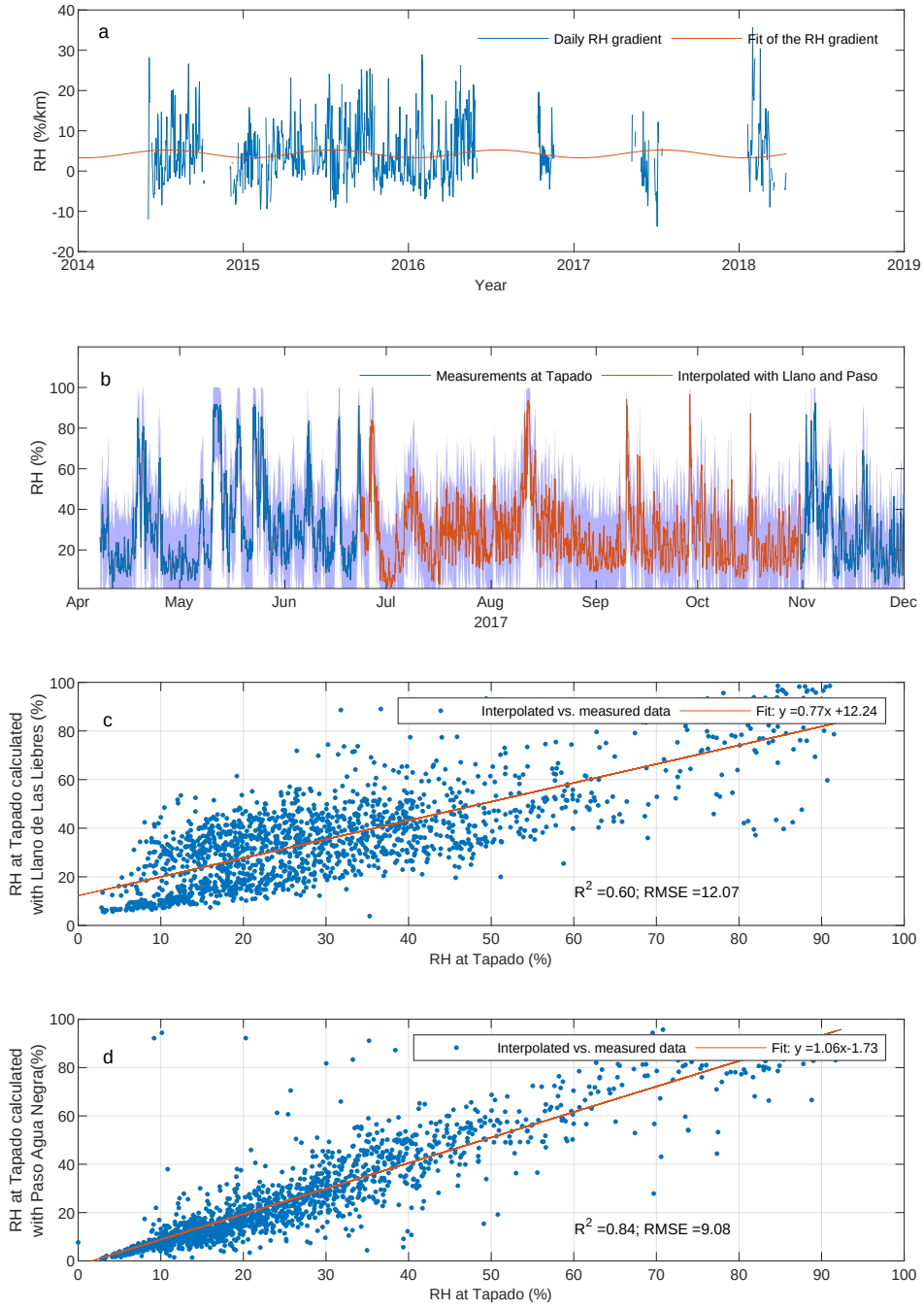

Figure 5.2: a) The daily RH gradient between AWS Paso Agua Negra and La Laguna (blue) and the seasonal fit of this daily temperature gradient (red). b) RH at Tapado that is calculated with data from Paso Agua Negra and Llano de Las Liebres (red) and the measurements at Tapado (dark blue). The light blue area around the line represents the 95% interval of confidence. c) Linear regression analysis of the interpolated RH data with Llano de Las Liebres. d) Linear regression analysis of the interpolated RH data with Paso Agua Negra.

the relative humidity data, it is relevant to use the high uncertainty of 12.83% in Equation 4.9. The final RH uncertainty is 13.02%. The light blue shade in Figure 5.2b gives the 95% interval of confidence calculated with $1.96\sigma_{RH}$.

Lastly, the linear regression analyses of the data from Llano de Las Liebres and Paso Agua Negra are given in Figure 5.2c and 5.2d respectively. The interpolated RH with Llano de Las Liebres and Paso Agua Negra are plotted against the measurements at Tapado and a linear trend is fitted through the data. The calculated trends are $y = 0.77x + 12.24$ for Llano de Las Liebres and $y = 1.06x - 1.73$ for Paso Agua Negra. The calculated relative humidity is better, when calculated with Paso Agua Negra, because the intercept of the trend is closer to zero and the slope is closer to one. Furthermore, the RMSE of Paso Agua Negra is 9.08% compared to 12.07% of Llano de Las Liebres and the R^2 of Paso Agua Negra is also better (0.84) in comparison to Llano de Las Liebres (0.60).

Table 5.2: Statistics of the relative humidity calculations with Paso Agua Negra and Llano de Las Liebres. The mean and standard deviation are calculated with the difference between the relative humidity at Tapado calculated with another station and the actual measurement at Tapado. The RMSE and R^2 are calculated with the calculated relative humidity and the relative humidity at Tapado, if this was available. The number of available data points are also given.

RH calculated with:	Llano de Las Liebres	Paso Agua Negra
# of observations	1638	1575
Mean	-5.14	0.11
Standard deviation	12.83	9.15
RMSE	12.07	9.08
R^2	0.60	0.84

5.1.3. Precipitation

The filtered measured precipitation and the possible corrections according to MacDonald and Pomeroy (2007), Smith (2007) and Wolff et al. (2015) for the precipitation are shown in Figure 5.3. The SWE data has also been plotted in this figure. The measured precipitation was about 40 mm or 33% lower than the SWE measurement. The number is not an exact number, because the measurement of the SWE is a measurement over 6 hours and it is hard to decide at which moment all the snow had settled in the precipitation gauge.

In agreement with these results, the first precipitation event corrected with the function of MacDonald and Pomeroy corresponds the best with the first SWE measurement peak. The formula that has been used with parameters a and b from Equation 4.11 is Equation 5.1.

$$CE_{Geonor} = 1.01 \exp(-0.09 WV) \tag{5.1}$$

Nevertheless, the sensor still seems to miss some precipitation events, such as on 3 June 2017. At this date, a clear increase in SWE and snow depth is visible, but the precipitation sensor did not register anything. Therefore it has been chosen to add some precipitation at 3 June, equal to the amount of snowfall between 00:00 and 10:00. The snow depth change in this time slot was 16.10 cm. A rule of thumb for the snow density is 1:10, so 1 meter of fresh snow is equal to 10 cm of water (e.q. Judson and Doesken (2000)). The precipitation has therefore been increased with 16 mm of water. This is noted as MacDonald & Pomeroy (adjusted) in Figure 5.3.

The precipitation that is derived from the SWE is given in Figure 5.3. The curve follows the curve of SWE (potassium) very well in the beginning of the season and simulates the maximum peak of the SWE. This data set of precipitation could be a better precipitation input for the model simulations, but as SWE is later used as validation data, the precipitation adjusted according to MacDonald and Pomeroy (2007) with the extra precipitation event is used as input for the models. Hereinafter this precipitation is referred to as reference precipitation.

The result of the distribution of precipitation with the first proposed method is visible in Figure 5.4a. The result are lines stacked above each other. Figure 5.4b shows the histogram of the accumulated precipitation at the end of the season for the 1000 runs. This distribution is approximately a normal distribution. The reference precipitation, which was corrected with the wind velocity, is encountered on the upper part of the distribution in May and June. Wind effects are not taken into account when the data is distributed between the measured precipitation and precipitation derived from SWE. Therefore the distributed precipitation is not distributed around the reference precipitation, but around the middle between the measurement and the precipitation calculated with the SWE.

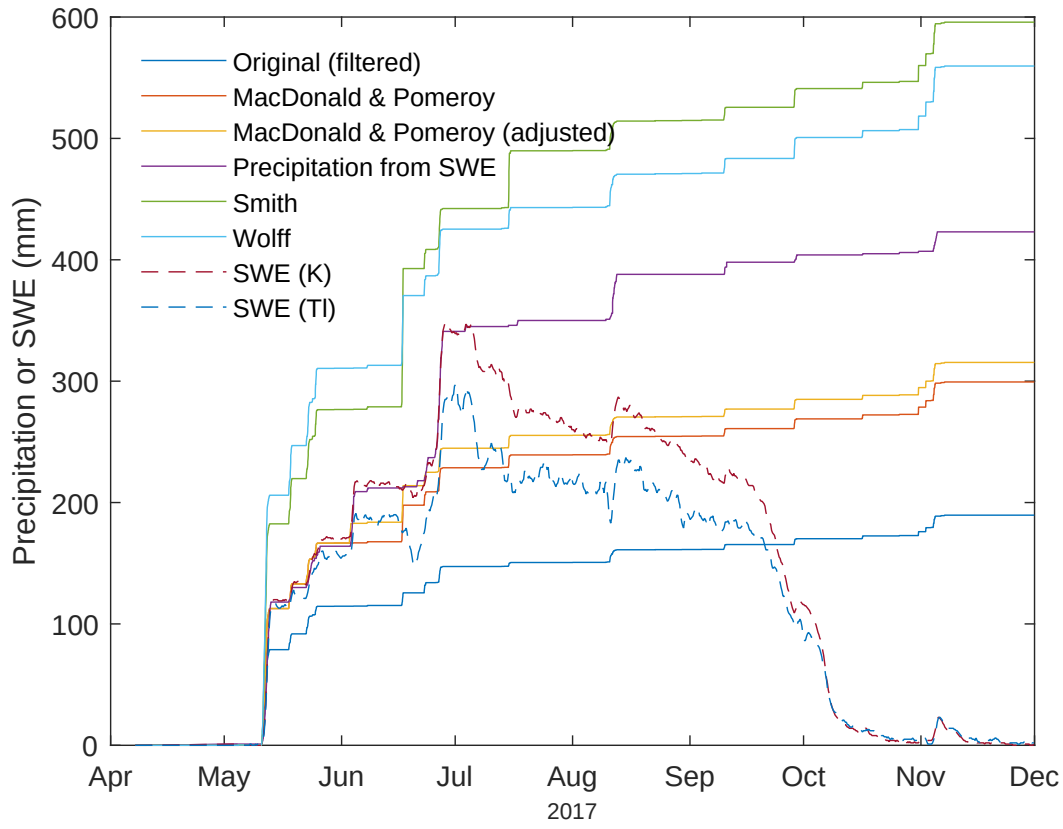

Figure 5.3: Acccumulated precipitation measurements with corrections according to MacDonald and Pomeroy (red), Smith (green), Wolff et al. (light blue). The filtered data from Figure 3.5 are plotted in blue and the SWE measurements are plotted in dark blue and red. The precipitation that has been derived from these SWE measurements is purple. One precipitation event has artificially been added to the correction of MacDonald and Pomeroy (yellow).

The distribution of precipitation for the second method with a random number per snow event is given in Figure 5.4c. The results are also sometimes outside the border of the measured precipitation and precipitation derived from SWE. The final distribution of the precipitation is less spread than in the first method (Figure 5.4d), because the alternating random number can be negative and positive and thus sometimes a lower precipitation rate is equalled out by a successive higher precipitation rate and vice versa. This makes it more likely that the final precipitation calculation ends closer to the middle of precipitation measurement and the precipitation derived from SWE.

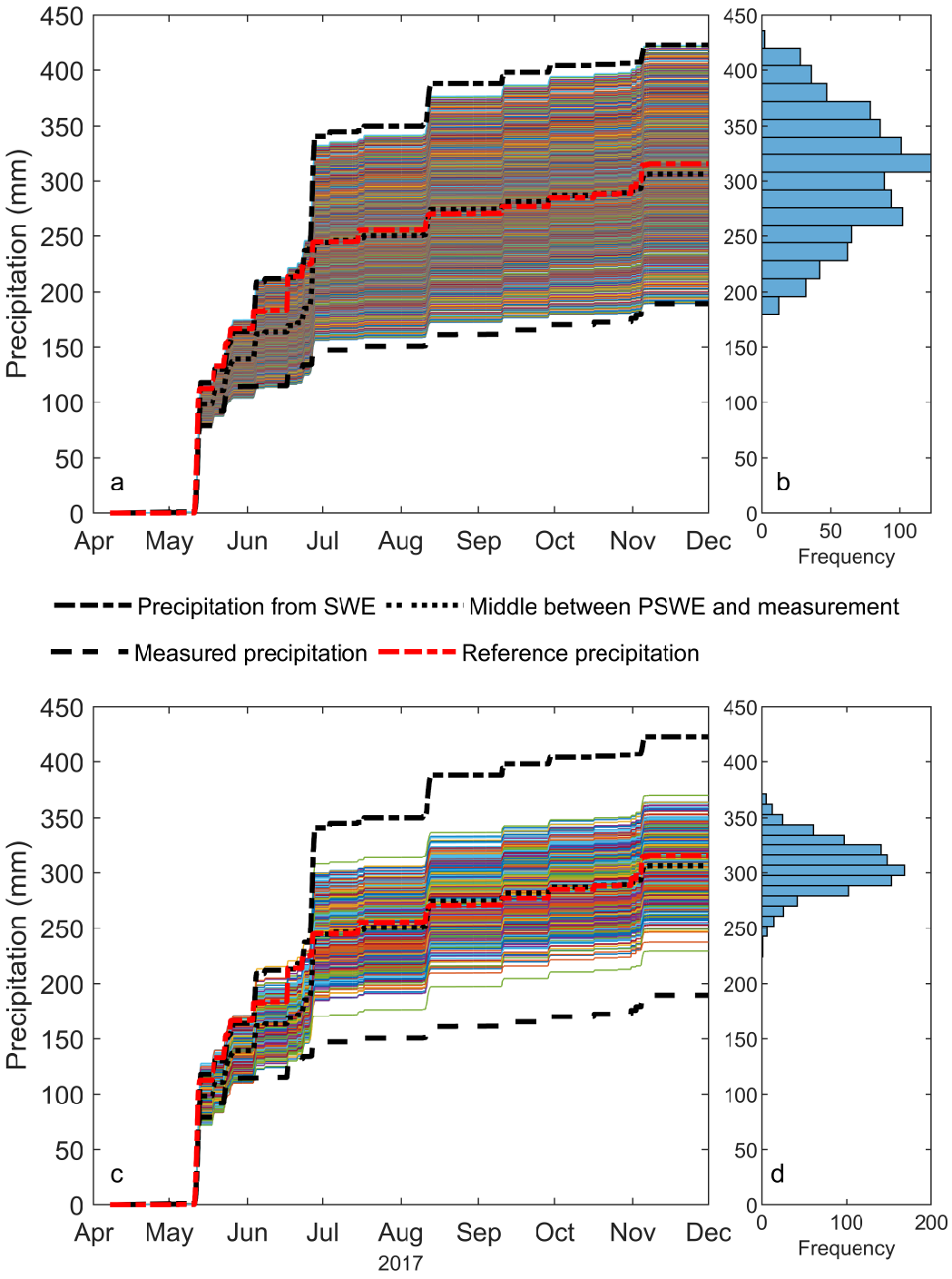

Figure 5.4: a) The first method for the uncertainties in precipitation. The random value that has been used to plot a possibility of the amount of precipitation stays constant for the entire year. The reference precipitation has also been given (red). c) The second method for the uncertainties in precipitation. An amount of precipitation has been added to the amount of precipitation that is between the measurement and the calculate precipitation from the SWE measurements. The amount that has been added has a different random number for every precipitation event. The reference precipitation has also been given (red). b) and d) The distribution of the accumulated precipitation for the 1000 runs at the end of the season for method 1 and 2 respectively.

5.2. SNOWPACK

5.2.1. Reference calibration

The results of the ensemble run are plotted in Figure 5.5. The simulated SWE until half September is lower than the measurement, but approaches the lower SWE measurement (thallium, dotted line) closely with a difference between 20 to 40 mm water equivalent in the middle of the season (July-August). The simulated snow depth is in accordance with the measured snow depth until half June. The rapid decrease (3-8 cm/day) of snow depth caused by compaction of the snow pack is simulate well by four out of five snow density parametrizations until July. Starting in July, the decrease is approximately 10 centimetres per 25 days, but the model still models a rapid decrease. The only density parametrization that simulates a more moderate decrease is LEHNING_OLD. The parametrizations only calculate the new snow densities, but this also influences the initial structure of the snowpack and thus the way it compacts after the snow event. The big decreases in snow depth at 15 July (-22 cm) and 29 August (-12 cm) are not simulated. These dates show wind velocities above 12 m/s and it is likely that snow erodes at such events, but snow erosion is not taken into account in the model. At the end of September, the air temperatures rise above 0°C and the snow melts with approximately 3 cm/day. The simulated snow depth decrease is between 1 and 1.8 cm/day.

In Section 4.3 it was stated that there are 20 possible calibrations for SNOWPACK, but four of the five calibrations that involved the albedo parametrization *Lehning_1* were aborted. The light blue line in Figure 5.5 that does not simulate the snow to be gone until December, is the *Lehning_1* run that worked. It is concluded that *Lehning_1* is not a suitable albedo parametrization for the study area.

The legend of Figure 5.5 shows that the most optimal calibration is the combination of the snow density parametrization *Lehning_old* and the albedo parametrization *Schmucki_GSZ* with a RMSE of 7.51 cm and R^2 of 0.91. The model has also been run with other roughness lengths and then slightly different statistics are found. The combination *Lehning_old* and *Schmucki_GSZ* is always one of the most favourable options according to its statistics and as literature also uses 1 mm as roughness length, it is the most relevant to use this combination as the reference calibration.

The results of step 2 to calibrate the roughness length (Figure 4.3) are plotted in Figure 5.6. Figure 5.7 shows that smaller roughness lengths improve the statistical results of the snow depth, but the RMSE and R^2 of the SWE are the lowest and highest respectively for a roughness value of 1 mm. It is chosen to use 1 mm as the reference roughness length.

5.2.2. Sensitivity to forcing data

The results of run 3.1 with variable forcing data is given in Figure 5.8. The quantile of the 2.5% and 97.5% has been calculated and this results in the 95% limits of the run. The maximum difference between the upper limit and the lower limit of the snow depth is 29.36 cm. This range is encountered during the first snowfall event. The median of this range is 5.7 cm. The maximum difference between the upper limit and the lower limit of SWE is 45.97 mm at 14 October and has a median of 13 mm. The maximum range of the surface temperature is 46°C at 16 September and the median difference between the upper and lower limit is 8°C.

The confidence interval of the SWE stays roughly constant between 11 and 15 mm after the first snow event and until the big melting starts at the end of the season.

The reference run of the snow depth lies on the lower border of the confidence interval starting from July. This is counter-intuitive, as the input data is normally distributed and thus also a normal distribution is expected around the reference run. However, the calculated relative humidity at Tapado is very low at the start of July. As relative humidity cannot be lower than 0%, a threshold is set while creating the .smet-input files that if a random number leads to values lower than 0% the RH value is set to 0%. As the relative humidity is already below 10% in July and the uncertainty of the relative humidity is more than 13%, the distribution of relative humidity in the Monte Carlo run is not normal and the measurement of the reference run is encountered on a lower quantile of the distribution. Once the reference run is outside the confidence interval, it can only get into the interval after a precipitation event.

Figure 5.9 demonstrates the Monte Carlo run with the precipitation uncertainty according to Figure 5.4c. The broad spread of precipitation input results into a broad distribution of the snow depth and SWE. The reference run is encountered in the upper part of the 95% confidence interval of both SWE and snow depth in May and June, because the reference precipitation is also in the upper part of the precipitation distribution in May and June. The maximum difference between the upper and lower limit of the snow depth is 63.81 cm on 19 September. The maximum range of SWE is 230.07 mm on 30 September and the maximum range of the surface temperature is 47°C at 16 September. The maximum range of the precipitation distribution was

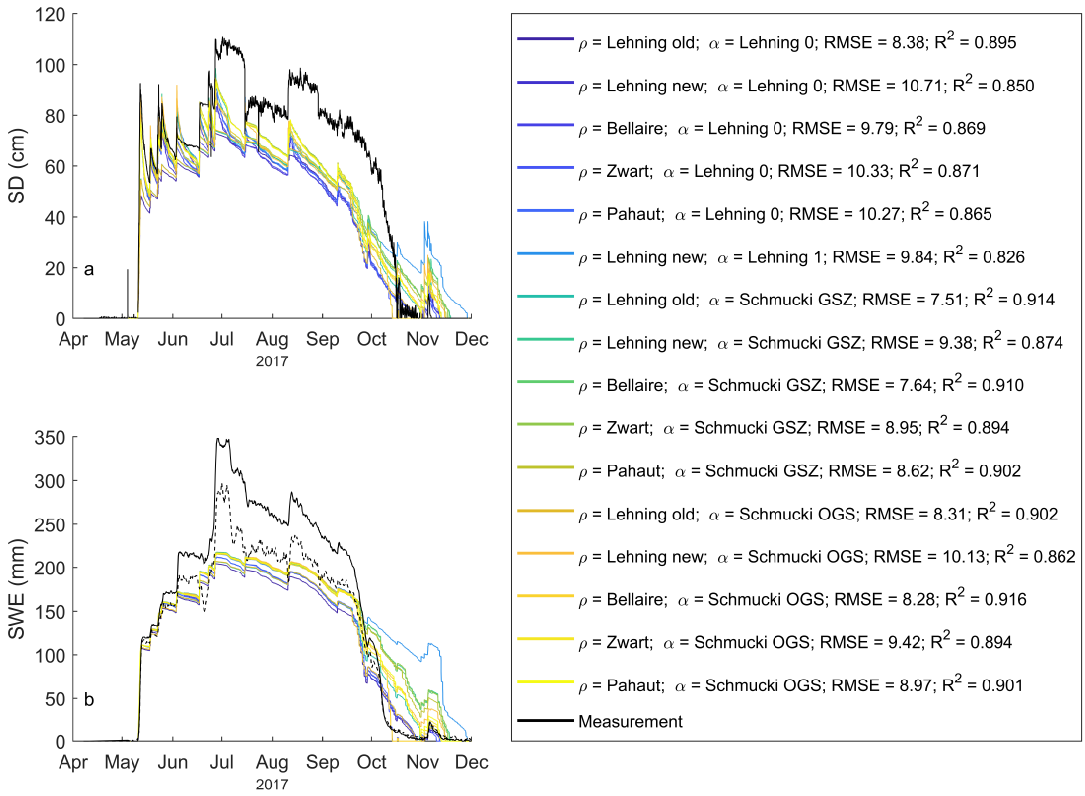

Figure 5.5: a) Snow depth and b) SWE observations and simulations of the different possible calibrations of SNOWPACK. The statistics of the ensembles are shown in the legend.

in the same order of magnitude as the maximum range of the SWE.

Figure 5.10 shows the Monte Carlo run with the precipitation distribution according to Figure 5.4c. The maximum range of snow depth is 35.60 cm on 27 June. On 12 October the maximum difference between the upper and lower limit of SWE of 138.52 mm is encountered and the maximum range of surface temperature is 46°C on 16 September. The distribution of the precipitation was not as broad as in Figure 5.4a and therefore the range of the simulated SWE and snow depth is not as broad as Figure 5.9. The surface temperature is barely influenced by the precipitation input, as the uncertainty range stays similar with different types of precipitation distribution. It is concluded that the simulated snow depth and SWE with SNOWPACK is very sensitive to the amount of precipitation used as input.

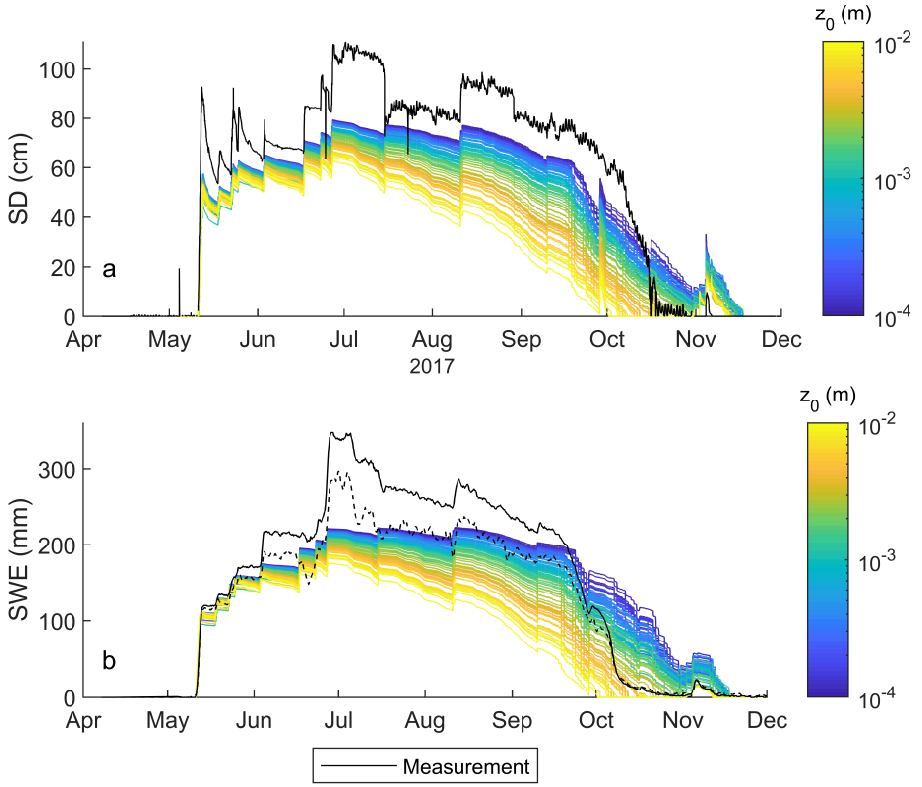

Figure 5.6: a) Simulated and measured snow depth and b) SWE with variable roughness lengths z_0 with SNOWPACK. The plot shows 100 randomly chosen roughness length on a logarithmic scale between 10^{-4} (blue) and 10^{-2} (yellow). The measurements are given in black.

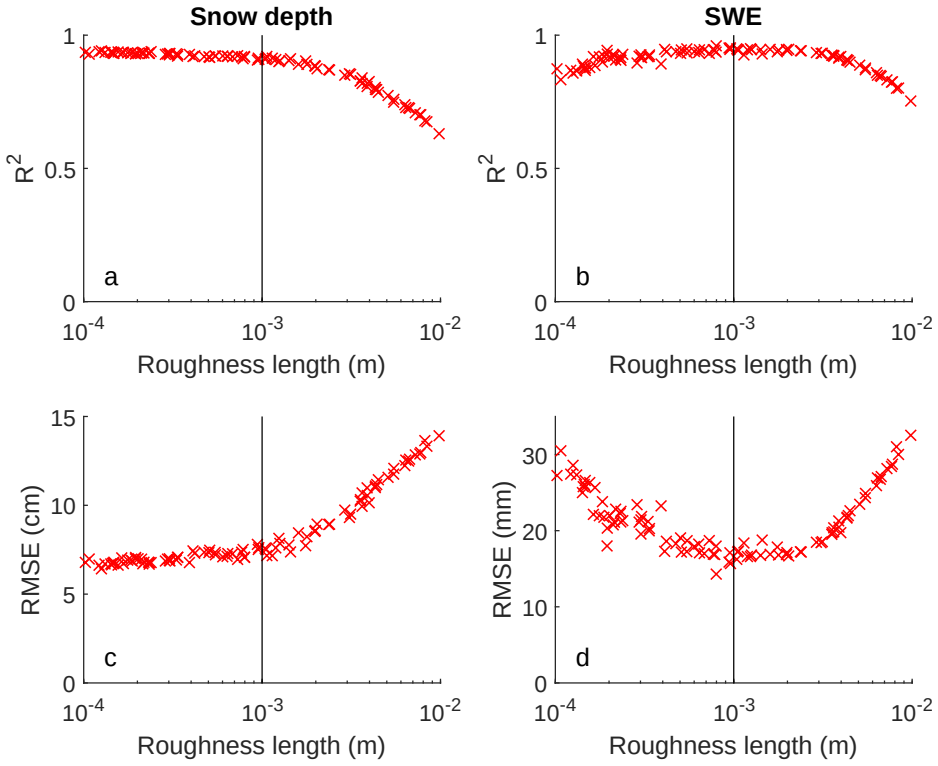

Figure 5.7: Roughness lengths plotted against the R^2 (a-b) and RMSE (c-d) of both snow depth (a-c) and SWE (b-d) of SNOWPACK.

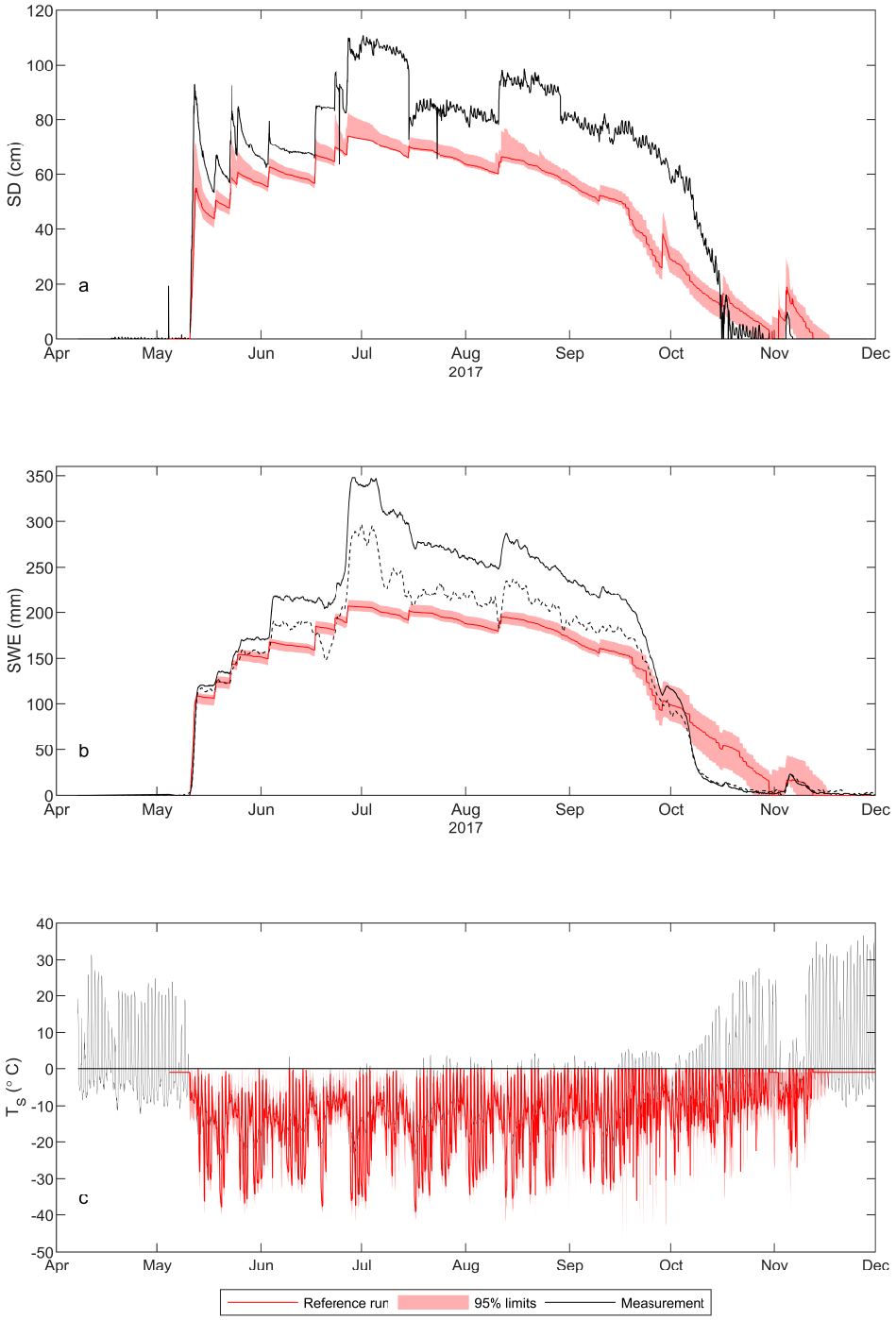

Figure 5.8: Simulated 95% confidence interval (red shade) of the a) snow depth and b) SWE of SNOWPACK with variable TA, RH, WV, WD, ISWR and ILWR. The reference run (red) and measurements (black) are also given.

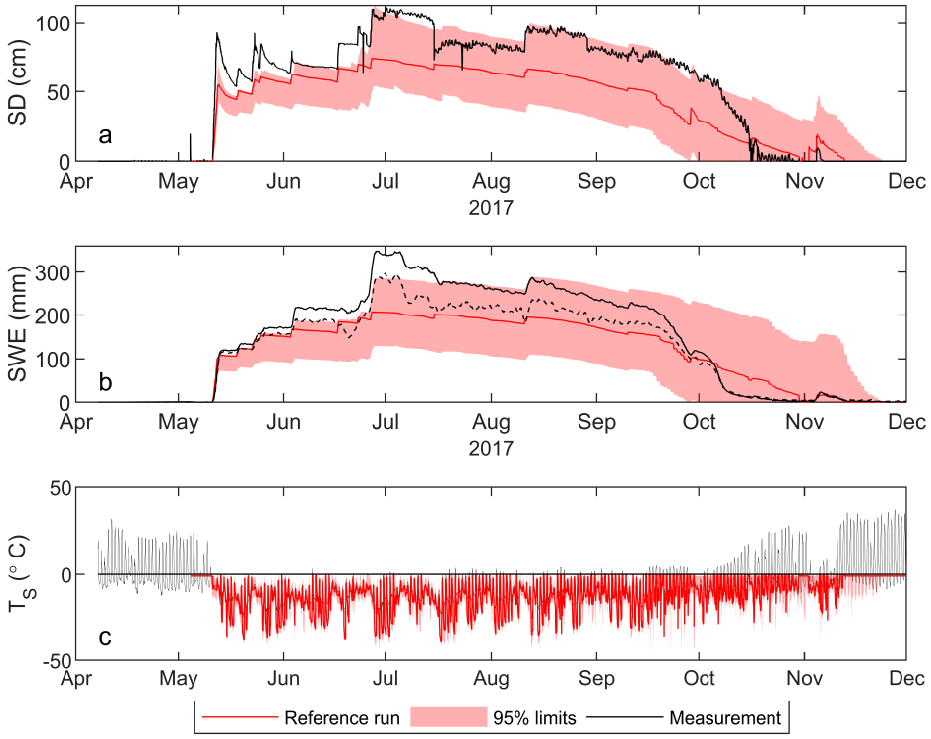

Figure 5.9: Simulated 95% confidence interval (red shade) of the a) snow depth and b) SWE of SNOWPACK with variable TA, RH, WV, WD, ISWR, ILWR and a precipitation distribution according to Figure 5.4a. The reference run (red) and measurements (black) are also given.

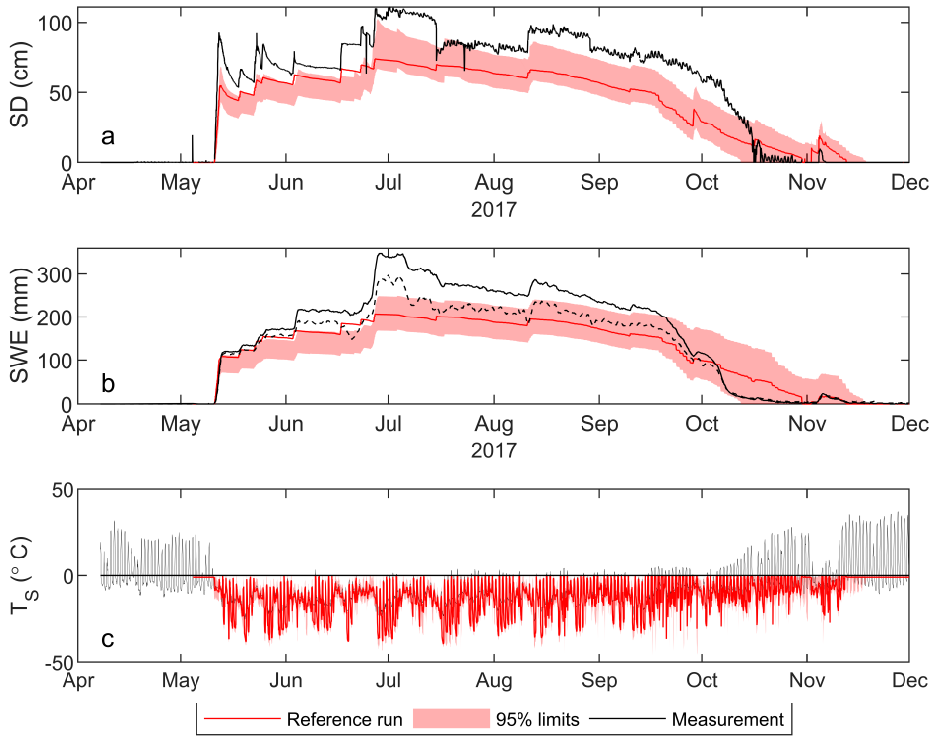

Figure 5.10: Simulated 95% confidence interval (red shade) of the a) snow depth and b) SWE of SNOWPACK with variable TA, RH, WV, WD, ISWR, ILWR and a precipitation distribution according to Figure 5.4c. The reference run (red) and measurements (black) are also given.

5.3. SnowModel

5.3.1. Reference calibration

The results of the two runs with different albedo parametrizations are displayed in Figure 5.11. Figure 5.11a displays the daily albedo. The albedo parametrization without time-evolution takes the air temperature into account and overestimates the albedo until October. The hourly albedo is set to 0.9 with air temperatures below freezing point. The air reaches temperatures above freezing point in the second half of September and correspondingly, the albedo is set to 0.6 on a hourly base. The albedo parametrization with time-evolution simulates the decay of the albedo over time. This result visually agrees better with the daily albedo measurements. The R^2 and RMSE of the albedo parametrization with time-evolution (0.770 and 0.13 respectively) are slightly better than without time-evolution (0.759 and 0.16 respectively). The albedo parametrization with time-evolution is chosen as reference parametrization because of those statistics and the visually more realistic simulation.

The statistical results for both snow depth and SWE are better for the parametrization without time-evolution than with time-evolution (Figure 5.11b and 5.11c). The overestimation of the albedo without time-evolution prevents the snow to melt quickly, because the net energy flux from shortwave radiation (Q_{SW}) from Equation 2.1 remains small with a high albedo. The simulations of the SWE model the measured SWE in May correctly, but after May the simulation is always lower than the measured SWE (potassium). This is due to the underestimation of the precipitation and thus the smaller amount of water that is available to establish a snowpack. The snow depth evolution of approximately 9 cm/day is modelled correctly at the first precipitation event, but after the measured decrease is approximately 10 centimetres per 25 days and the model still simulates decreases of 2-3 cm/day.

At first sight, the modelled surface temperature coincides pretty well with the measured data. The surface temperature is 0°C if the measured surface temperature is above 0°C and the surface temperature is modelled to be above 0°C if the snow is gone. The minima of the surface temperature disagree with the measurements, because the simulations are calculated sometimes almost 25°C lower than the measurements. This leads to low R^2 values of 0.108 and 0.070 and RMSEs of 10.54 and 11.09 of the surface temperature for the albedo without and with time-evolution respectively in Figure 5.11d.

The results of the second step (Figure 4.3) to evaluate SnowModel is plotted in Figure 5.12. The statistical results (Figure 5.13) reveal that a roughness length of approximately 1 mm gives the lowest RMSE (22 cm for the SD, 28 mm for the SWE) and the highest R^2 (0.60 for the SD, 0.89 for the SWE). Therefore, 1 mm is chosen as roughness length in the third step of the evaluation of SnowModel.

5.3.2. Sensitivity to forcing data

The resulting sensitivity range of the third step to evaluate SnowModel has been given in Figure 5.14. The reference run of the snow depth lies above the upper limit of the 95% confidence interval, whereas the simulated reference SWE falls within the interval of confidence. The difference between the SWE and snow depth is caused by a different rate of compaction of the snowpack. The reference run starts deviating from the confidence interval on 11 August 20:00. The maximum difference of the simulated snow depth is 14.9 cm during the first snow event on 12 May and a median range of 2.7 cm.

On the other hand, the SWE interval of confidence follows the reference run accurately until just before the half of September. The median difference between the upper and lower limit of the SWE is 1.3 mm and the maximum range is 27.7 mm at 22 September. This is during the rapid melt period at the end of the season.

The maximum range of uncertainty of the surface temperature is 20.5°C at 13 October. The lower limit of the surface temperature is on average 10°C lower than the measured surface temperature at moments when there is snow and the upper limit is on average 1.4°C lower than the measurement. This results into a higher outgoing longwave radiation (Equation 2.3), a lower net longwave radiation (Equation 2.1) and eventually a lower amount of energy available for melting.

The results of the first Monte Carlo run where also variable precipitation was used as input (step 3.2) is given in Figure 5.15. The reference run has been plotted and is also located in the upper half of the simulated interval of confidence. The maximum difference of the upper and lower limit of the snow depth is 93.92 cm on 27 June. The maximum range of SWE is 224.62 mm on 12 September and the maximum range of the surface temperature is 20.5°C at 13 October. The precipitation distribution is in the same order of magnitude as the maximum difference between the limits of the SWE. Thus, SnowModel is highly sensitive to the amount of precipitation input. The variations in the other variables are hardly visible, because of the uncertainty in precipitation.

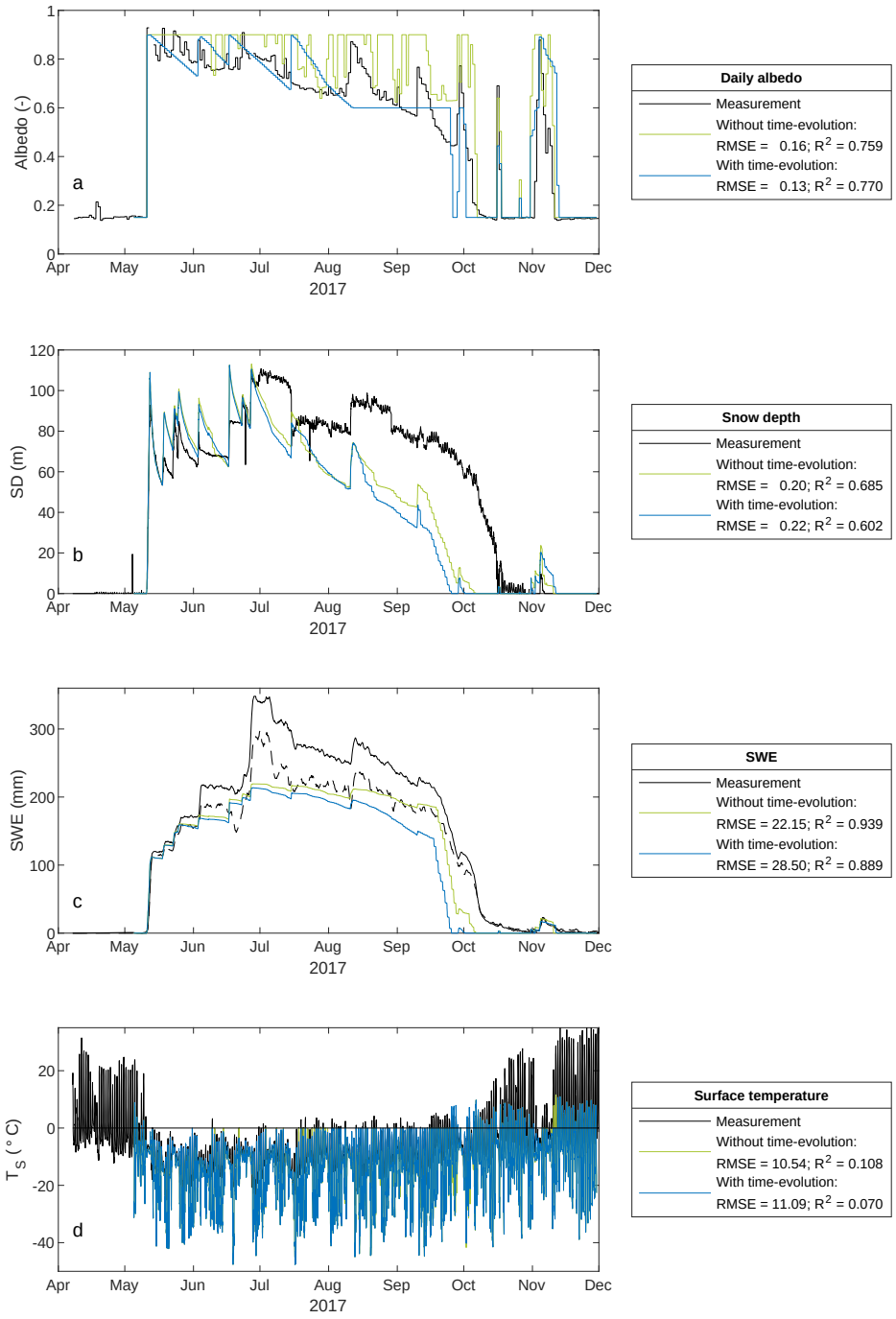

Figure 5.11: Simulated and measured a) albedo, b) snow depth, c) SWE and d) surface temperature without (green) and with (blue) time-evolution. The RMSE and R^2 per parameter are given in the tables next to the graphs.

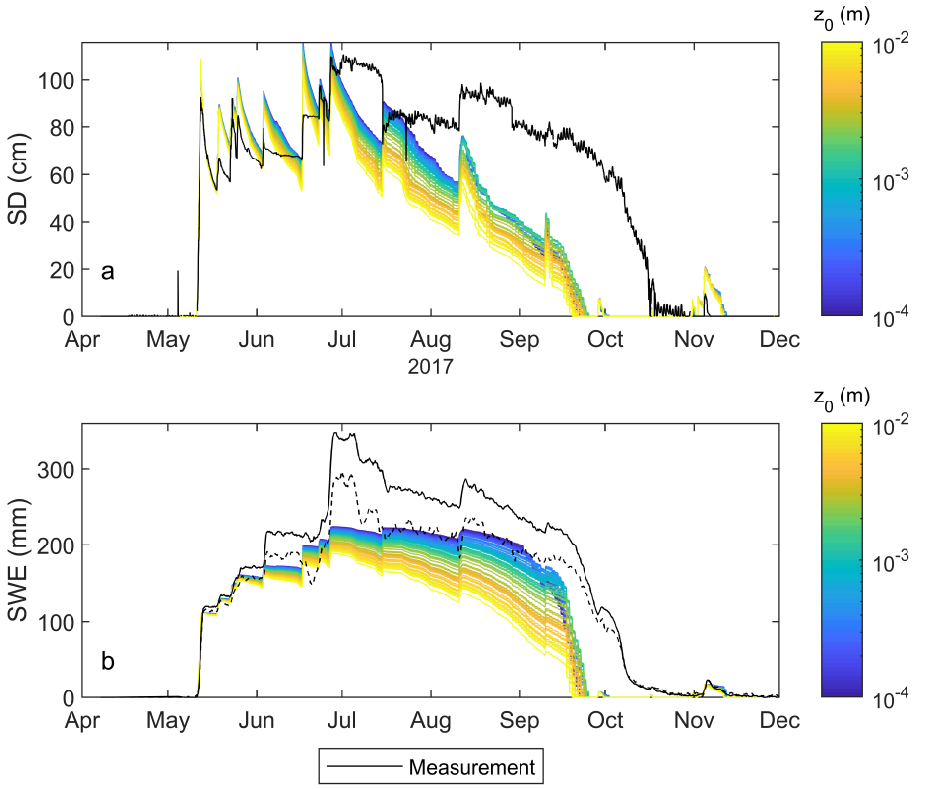

Figure 5.12: a) Simulated and measured snow depth and b) SWE with variable roughness lengths z_0 with SnowModel. The plot shows 100 randomly chosen roughness length on a logarithmic scale between 10^{-4} (blue) and 10^{-2} (yellow). The measurements are given in black.

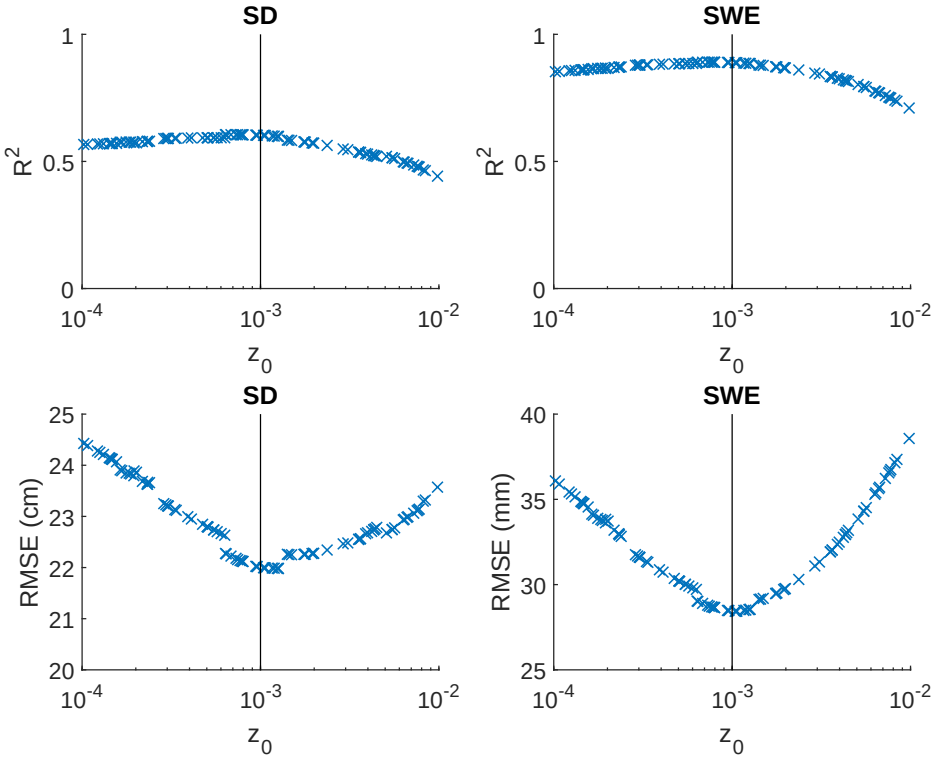

Figure 5.13: Roughness lengths plotted against the R^2 (a-b) and RMSE (c-d) of both snow depth (a-c) and SWE (b-d) of SnowModel.

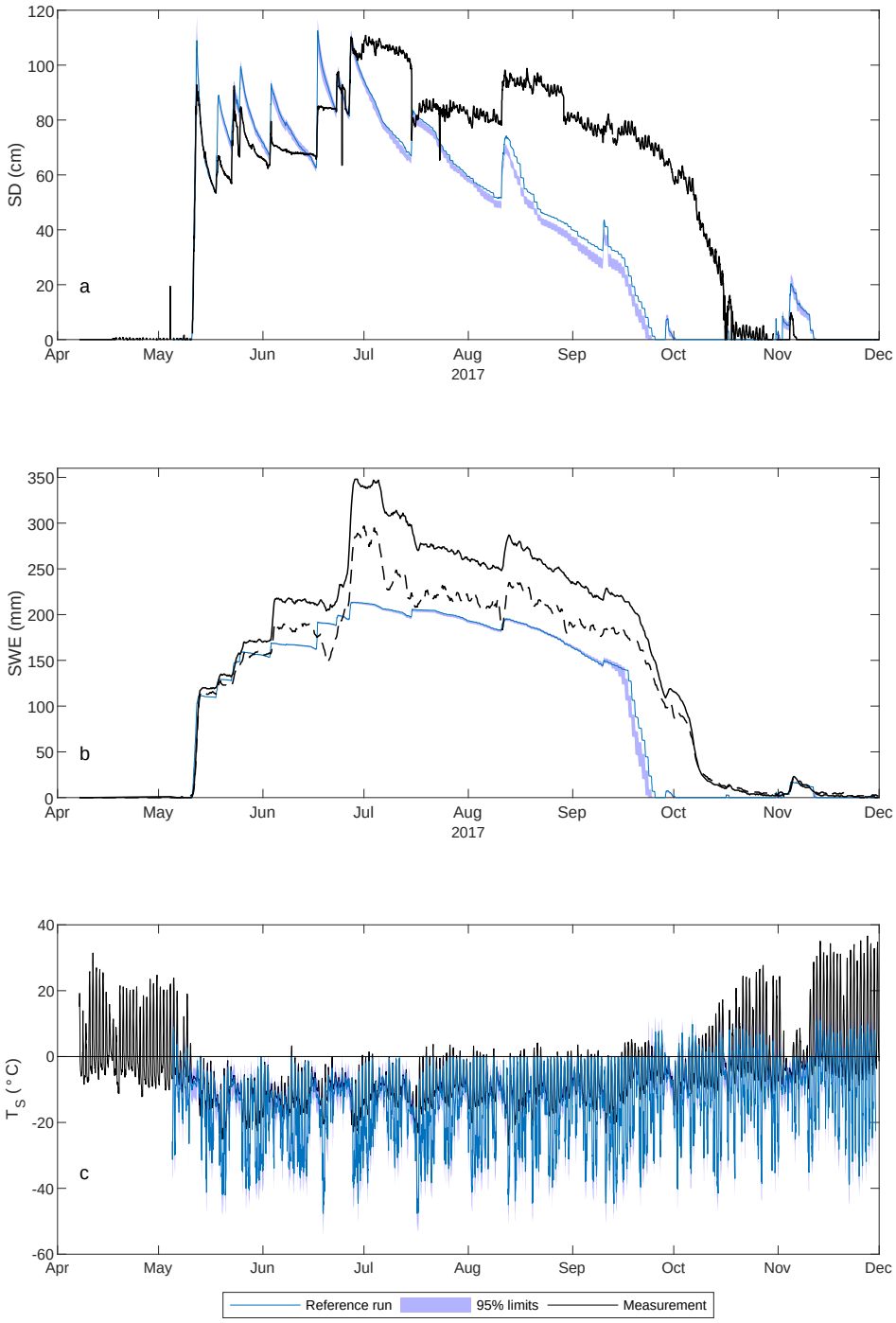

Figure 5.14: Simulated 95% confidence interval (blue shade) of the a) snow depth and b) SWE of SnowModel with variable TA, RH, WV, WD, ISWR and ILWR. The reference run (blue) and measurements (black) are also given.

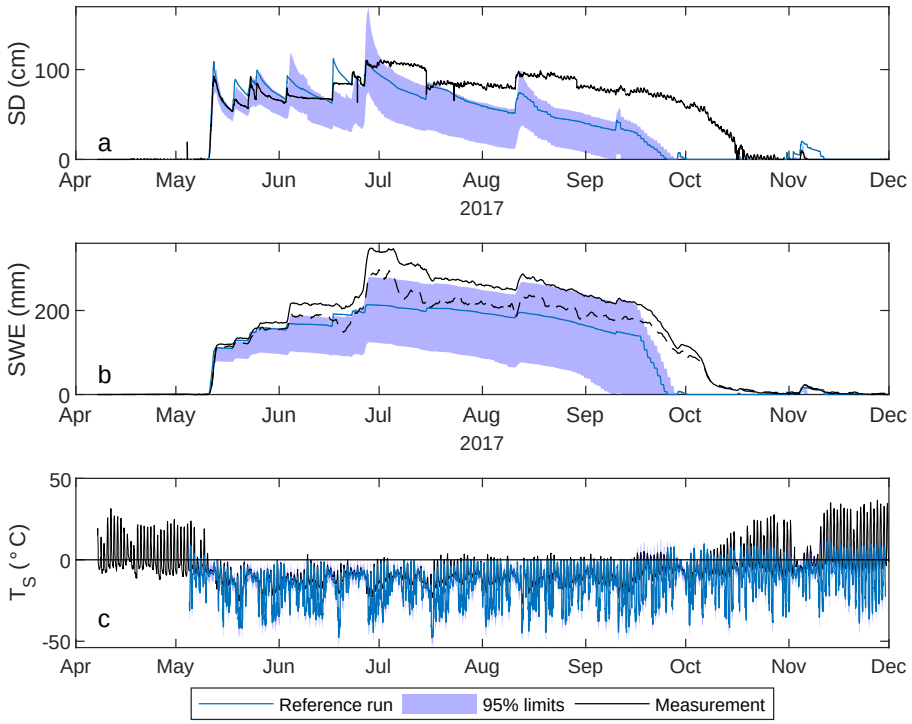

Figure 5.15: Simulated 95% confidence interval (blue shade) of the a) snow depth and b) SWE of SnowModel with variable TA, RH, WV, WD, ISWR, ILWR and a precipitation distribution according to Figure 5.4a. The reference run (blue) and measurements (black) are also given.

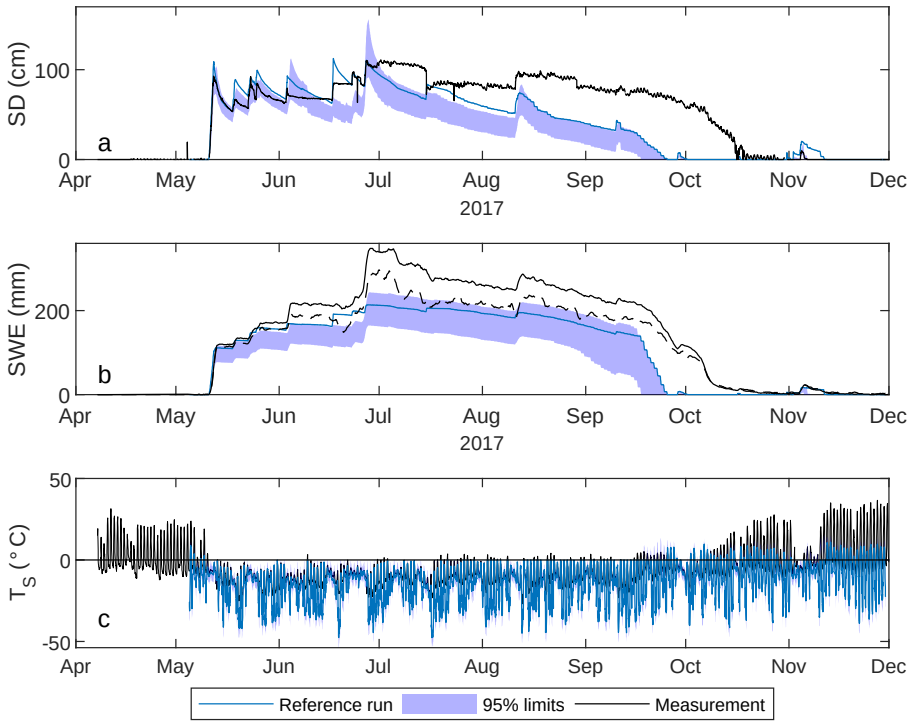

Figure 5.16: Simulated 95% confidence interval (blue shade) of the a) snow depth and b) SWE of SnowModel with variable TA, RH, WV, WD, ISWR, ILWR and a precipitation distribution according to Figure 5.4c. The reference run (blue) and measurements (black) are also given.

The results of step 3.3 (Figure 4.3) is given in Figure 5.16. The maximum range of the snow depth is 64.9 cm on 27 June. The maximum difference between the 95% limits of SWE is 127.9 mm on 17 September and the maximum range of the surface temperature is 24.3°C at 21 September. These results are expected, compared to the results of Figure 5.15. The distribution of the precipitation is smaller and thus the distribution of the SD and SWE of Figure 5.16 is smaller. The influence of the varying forcing variable TA, RH, wind, air pressure and incoming radiation terms is not visible any more.

5.4. Comparison between SNOWPACK and SnowModel

Figure 5.17 gives the results of the Monte Carlo run of step 3.1 for both SNOWPACK and SnowModel. Figure 5.17a shows the albedo of the reference runs. During the period with snow, the simulation of SNOWPACK comes closer to the measured albedo than the simulation of SnowModel. SnowModel simulates the albedo at the moment that the snow is gone at the start of October better than SNOWPACK. SNOWPACK overestimates the albedo after October, because it has not been given as input to the models that the albedo has decreased after a strong wind event. Hence, with the information that has been provided to the models, the albedo parametrization of SNOWPACK is considered better than the parametrization of SnowModel.

The reference run of SNOWPACK approaches the snow depth better than the reference run of SnowModel. The end of the snow season is also simulated better by SNOWPACK, especially if it is taken into account that the snow got covered with dust at the start of October and the measured melt rate is thus higher than what can be modelled, because of the decrease in albedo. This more accurate melt simulation is a result of the better albedo simulation of SNOWPACK. SnowModel decreases the albedo to 0.6, whereas SNOWPACK models a more gradual decay of the albedo at the end of the season, that corresponds better to the measured albedo.

The SWE simulated with SnowModel is maximal 7 mm higher in the reference run than the reference SWE of SNOWPACK. The simulated SWE of the models is almost the same until the melting starts in September. The melt rate at the end of the season of SnowModel is faster than SNOWPACK. The reference run of the snow depth simulated with SNOWPACK is found in the confidence interval, whereas the reference run with SnowModel is outside the confidence interval. Hence, the snow depth simulations of SnowModel are less reliable than the simulations with SNOWPACK, even though the confidence interval of SnowModel is smaller.

The surface temperature is simulated well with SNOWPACK and SnowModel, but the simulations of SnowModel look more noisy and the confidence interval is larger. Accordingly, the simulations of the surface temperature of SNOWPACK are considered better than the simulations of SnowModel.

Figures 5.18 and 5.19 show the combined results of step 3.2 and 3.3 respectively. The confidence intervals in both figures strongly depend on the precipitation distribution. The 95% confidence intervals for both SWE and snow depth of SnowModel and SNOWPACK have a similar broadness. The melt at the end of the season is simulated better with SNOWPACK, because the snow melts away too rapidly in the simulations of SnowModel, independently of the precipitation distribution.

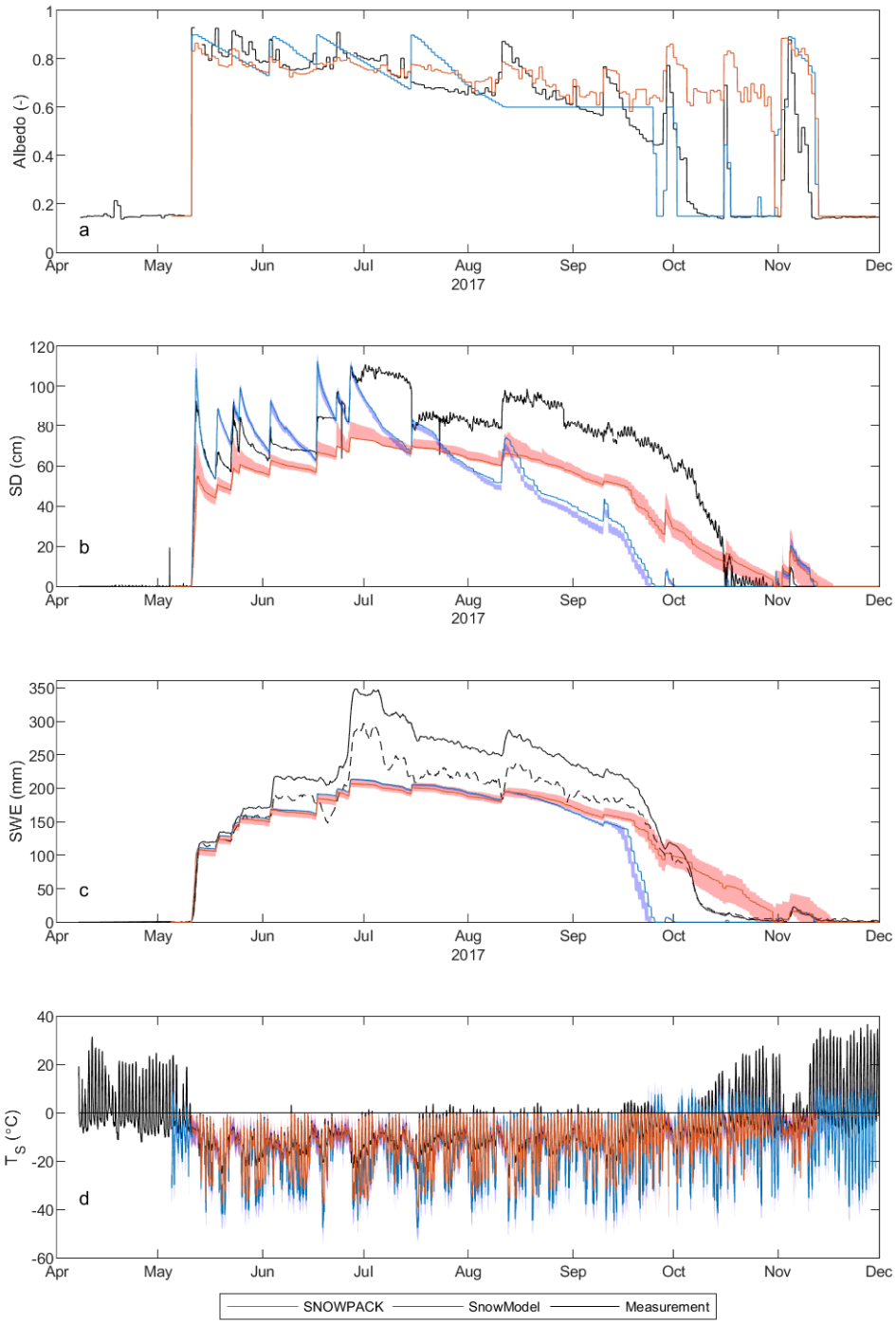

Figure 5.17: Comparison between the 95% confidence intervals the of a) albedo, b) snow depth, c) SWE and d) surface temperature of SNOWPACK (red) and SnowModel (blue) for the Monte Carlo run of step 3.1. The reference run of both models is the bold coloured curve and the measurements are given in black.

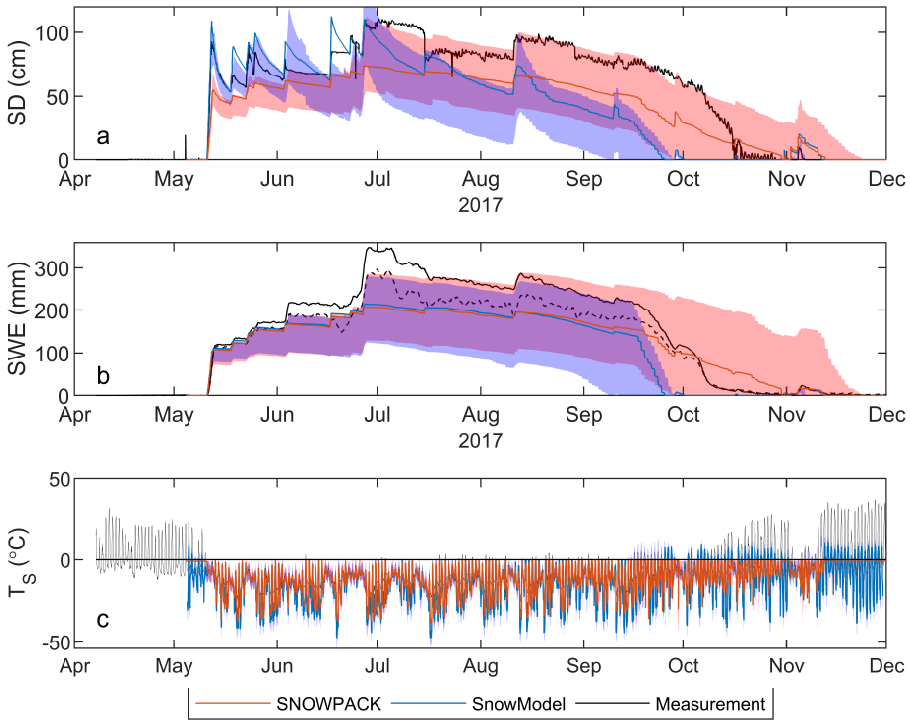

Figure 5.18: Comparison between the 95% confidence intervals the of a) snow depth, b) SWE and c) surface temperature of SNOWPACK (red) and SnowModel (blue) for the Monte Carlo run of step 3.2. The reference run of both models is the bold coloured curve and the measurements are given in black.

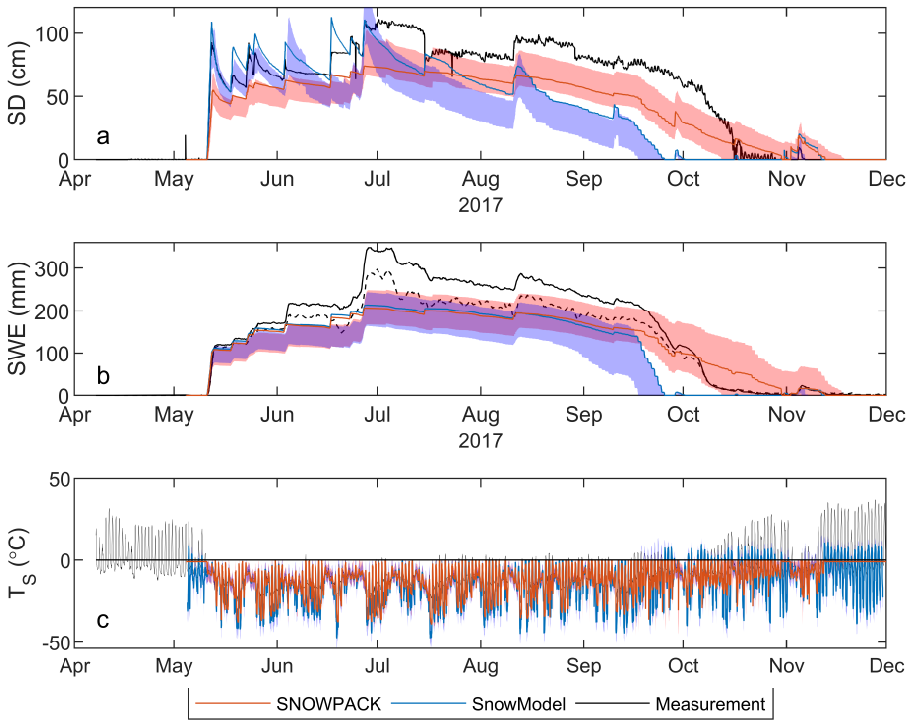

Figure 5.19: Comparison between the 95% confidence intervals the of a) snow depth, b) SWE and c) surface temperature of SNOWPACK (red) and SnowModel (blue) for the Monte Carlo run of step 3.3. The reference run of both models is the bold coloured curve and the measurements are given in black.

6

Discussion

The discussion is divided in 4 sections. Firstly, the interpolated temperature and relative humidity and the precipitation corrections are discussed. Secondly, the different calibrations of SNOWPACK and SnowModel are deliberated, because other parametrizations could have been chosen as well. Thirdly, the cause of the remarkable courses of the confidence intervals and reference runs of both models are explained. Lastly, two domains are distinguished from the the simulations of SNOWPACK and SnowModel, namely the period where the snowpack is mainly influenced by sublimation and the period of melt. These are examined and compared.

6.1. Uncertainty in forcing data

6.1.1. Temperature interpolation

The statistical results of the temperature interpolation with data of Paso Agua Negra are better than with Llano de Las Liebres with a mean closer to 0, a higher R^2 and a smaller standard deviation and RMSE (Table 5.1). This is caused by the smaller altitude difference between Paso Agua Negra and Tapado, because a small error in the lapse rate is propagated less with a smaller difference in elevation in Equation 4.5. The missing period could also partly be filled with the calculation from Paso Agua Negra, but it is nevertheless chosen to use the calculation with Llano de Las Liebres. The entire missing period can be filled with the data from this station and the use of only data from Llano de Las Liebres keeps the final temperature calculation more continuous, which means that if there is a bias in the data from Llano de Las Liebres, the bias remains the same for the entire period of sensor failure at Tapado.

6.1.2. Relative humidity interpolation

The data from Llano de Las Liebres and Paso Agua Negra are both used to interpolate the relative humidity data. Paso Agua Negra is preferred to be used, because its RMSE is smaller than from Llano de Las Liebres and the R^2 is bigger (Table 5.2). But the data of Paso Agua Negra is not available during the entire period of sensor failure at Tapado and thus also the RH calculated with Llano de las Liebres is used. The reason for the better statistical results of the calculation between Paso Agua Negra and Tapado than between Llano the las Liebres and Tapado is the smaller altitude difference between Tapado and Paso Agua Negra. Small errors in the gradient are propagated less in the final calculation than with a bigger difference in elevation. Whereas the temperature interpolation has been done with only data from Llano de Las Liebres to keep the bias the same throughout the entire period of malfunction of the sensor at Tapado, it is chosen to use Paso Agua Negra too, because the R^2 of Llano de Las Liebres is low (0.60), compared to Paso Agua Negra (0.84). Only 390 time slots are filled with data from Paso Agua Negra and the other 2733 missing blanks were filled with data calculated with Llano de Las Liebres. Furthermore, the assumption that the relative humidity shows a linear gradient is too simplistic. The sub-model MicroMet in SnowModel uses an interpolation which calculates the dew point temperature first (Liston and Elder, 2006a). This approach was done at a very late stage in the creation of this thesis and is visible in Appendix B. The dew point temperatures of Paso Agua Negra and La Laguna are calculated and a dew point lapse rate has been calculated between those stations. The dew point temperature at Tapado is interpolated and converted into RH data. The relative humidity interpolation would have been better if this routine was used with a RMSE of 9.66% instead of 12.07% and a R^2 of 0.79 instead of 0.60 with Llano de Las Liebres. The models were not run with this interpolation because of a lack of time.

6.1.3. Precipitation corrections and uncertainty

The correction of the precipitation according to the wind velocity is verified with the first precipitation event of the SWE. The first precipitation event is the only possibility to verify which correction corresponds the best to the real amount of precipitation, because after this event other processes, such as sublimation and erosion by wind take place in the snow pack and the water equivalent is not equal to the precipitation any more. It is more favourable to base the validation on more than one event, but 2017 is the only year that SWE data is available at Tapado, so other validations are not possible.

Secondly, the measured SWE also has large uncertainties, because the output of potassium gamma rays is supposed to be the same as the output of thallium gamma rays. It was stated in personal communication with John W. Pomeroy that the output of this sensor is not very adequate and that more users experience problems with it. It is therefore not very reliable to correct the precipitation completely with SWE measurements.

Additionally, the position of the precipitation gauge and the main tower of Tapado should be considered. The wind velocity at the precipitation gauge is different than at the main station, because the wind is restrained by the small hill behind the main station. The main tower is also located in a concave area and as the hill close to the main tower decelerates the wind, it is likely that more snow collects around the main tower than at the precipitation gauge.

The correction of the precipitation for the reference run only depends on the wind velocity, whereas the uncertainties of the precipitation depend on the measured precipitation and SWE. When the precipitation uncertainties are assessed, the precipitation sometimes lies below the border of measured precipitation or above the precipitation derived from the SWE data. This is caused by the procedure of calculating the uncertainties of the precipitation. For example, during the first snow event the measured precipitation rates in the precipitation gauge are sometimes larger than the rates derived from the SWE measurement, whereas the accumulated precipitation derived from the SWE is always larger than the measured precipitation. The absolute difference between the precipitation rates is used to calculate the standard deviation of the precipitation rate at each time slot. If this standard deviation is multiplied by a normally distributed random number larger than 1 or smaller than -1, the cumulative precipitation for the event can be respectively larger or smaller than the borders. The absolute difference must be taken, because otherwise a time slot might lead to a negative precipitation rate, which is not possible as the precipitation is cumulative. The difference in precipitation rates might be caused by the time it takes for snow to settle in the precipitation gauge. So if the snow falls, it takes some time for the snow to melt in the gauge and to be registered. Furthermore, wind effects during snow storms might influence those differences.

Lastly, this thesis has proposed two different ways to calculate the uncertainties of precipitation. Other distributions are also possible. For example, the data might be adjusted for the settling of the snow in the precipitation sensor, so the distribution stays within the borders of the measurement and the precipitation derived from the SWE. This has not been done in this case, because it is hard to distinguish the end of a precipitation event. The cause of this mainly comes from the SWE sensor, which provides six-hourly data, whereas the precipitation gauge gives hourly output.

In the end, another distribution would have been interesting to test, but the results already reveal that the models are highly sensitive to the amount of precipitation. The best thing to improve the precipitation input is to move the main tower closer to the precipitation gauge to cancel out the influence of the location of the main tower. In that case, the precipitation can be corrected with the wind velocity only. If SWE data is available for some consecutive years, it is also easier to calibrate Equation 4.11 to the conditions of the semi-arid Andes and the study area in particular.

6.2. Calibrations of the models

6.2.1. Reference calibration of SNOWPACK

Even though SNOWPACK has several options to calibrate the model, this study only considers the roughness value, snow density and albedo parametrization. The roughness value is important to calculate the turbulent fluxes (MacDonell et al., 2013a). The snow density is the parameter that provides the conversion from SWE to snow depth (Equation 2.15) and the albedo is a main quantity in the energy balance equation (Equation 2.1).

SNOWPACK provides six options for the atmospheric stability correction, but only the correction based on the Richardson number has been used. A study over Brewster Glacier in New-Zealand by Conway and Cullen (2013) shows that the use of parameterizations based on the Richardson number or the Monin-Obukhov Similarity theory underestimate the sensible heat flux by –4.1 to –8.3 Wm^{-2}, especially with wind velocities lower than 3 m/s. The wind velocity is generally higher than 3 m/s and thus the parameterization based on

the Richardson number is still usable at the Tapado glacier. Conway and Cullen (2013) also found that the turbulent latent heat flux was not influenced by the choice of atmospheric stability correction model and as this is the big contributor to sublimation in the region (MacDonell et al., 2013a), it is thought that it is reasonable to use the atmospheric stability correction model based on the Richardson number for SNOWPACK. The other five options have been tested on the reference run (results not shown), but no significant differences were found between them. Nevertheless, it might be interesting to take the atmospheric stability correction models into account into the ensemble run. This has not been done in this study, because with six different correction models, the computational time would be six times as long and by using the Richardson-parametrization, the conditions are similar to the atmospheric stability correction applied by SnowModel.

It is known from literature (MacDonell et al., 2013a; Pellicciotti et al., 2005) that the roughness length changes when the snow ages. SNOWPACK uses an estimate of the roughness length and calculates the friction velocity and roughness length iteratively (Lehning et al., 2000). The implemented roughness length is an average roughness length during the season and the iterative scheme calculates a roughness length close to the implemented value, and so the roughness value does not change as described in literature.

It is also possible to adjust the threshold temperatures for the rain and hoar layers, the grain size of the fresh snow and several other parameters, but as no good information was available for these parameters, the default has been used. Additionally, the provided snow density and albedo parametrizations are calibrated with measurements which have mainly been done at the Weisfluhjoch test site in Switzerland. The empirical parameters in these parametrizations should be calibrated for the conditions in the semi-arid Andes, but these adjustments have not been done, because there were no density measurements available and the aim of the thesis was to compare the base settings of the two models, without adjusting empirical parameters.

SNOWPACK can also consider wind erosion, but this is only possible if the snow depth also has been implemented. This is not done, because snow depth is used as validation data. Furthermore, it is not expected that this implementation would lead to better results, because the snow depth sensor is located such that it is more likely that snow will be deposited instead of eroded.

In further work, it would be interesting to test the influence of parameters such as the atmospheric stability correction model, threshold temperatures, etcetera and to adjust the empirical parameters within the density and albedo parametrizations with measurements from the semi-arid Andes.

6.2.2. Reference calibration of SnowModel

Whereas SNOWPACK needs the snow depth to take wind erosion into account, this is not needed for SnowModel. Nevertheless, the part of the code that distributes the wind velocity over the topography has been disabled and the SnowTran3D subroutine has not been used. The distribution of the wind velocity has been removed, because the model interpolates the measured wind speed to the height of the topography and by removing it, the model was forced to use the exact measurement of the station. This made it possible to compare the models in a proper way on a point scale. In addition, the DEM that has been used, has a spatial resolution of 100 metres. The problem with the concave location of the main tower is not taken into account, as the spatial extent of this site is smaller than 100 metres.

On the other hand, this calibration does not take full advantage of the properties of SnowModel. The model is especially designed for wind transport of snow. It is interesting to take the wind transport into account on a later stage, but then it is also needed to use a finer DEM, such as a 30 metre DEM and use the distribution of the wind velocity over the topography.

Secondly, the subroutine MicroMet uses thresholds for the wind speed and RH. The wind velocity is set to a minimum of 0.1 m/s and this is also used in the Monte Carlo simulation. If a wind velocity lower than 0.1 has been produced by adding a random number, the value is set to 0.1 m/s in the Matlab script to make the forcing file. The relative humidity is set to a minimum of 10% by SnowModel and the forcing file sets the minimum to 0%. The threshold for the wind is considered realistic, because it is known from fieldwork trips that there is always some wind at the weather station, but the threshold for the RH is not reasonable, because the measured RH is sometimes lower than 10%. Nevertheless, this threshold has not been disabled in SnowModel, because the RH data is interpolated and uncertain and thus the default of the model is kept. These thresholds should be considered in future research, because the effect on the output has not been tested and SNOWPACK also does not apply these thresholds. This makes the conditions between SnowModel and SNOWPACK not perfectly comparable.

The albedo parametrizations of SnowModel are simplistic, compared to SNOWPACK. The empirical parameters for the change of albedo over time could easily be adjusted and therefore this has extensively been tested, but they are not changed, because the models are tested on there basic settings.

6.3. Sensitivity to forcing data

6.3.1. SNOWPACK

The confidence interval of the SWE of Figure 5.8 stays roughly constant with a median width of 13 mm after the first precipitation event and until the big melting starts at the end of the season. Hence the variation of the forcing data influences the amount of SWE at the first precipitation event, but not a lot after this event. SNOWPACK only accepts new precipitation if the relative humidity at the corresponding time slot is higher than 50%, the difference between the air temperature and surface temperature is smaller than 3°C and there are clouds, which is derived from the ISWR. The uncertainty in RH causes some precipitation events to be rejected, but this also works the other way around. Some precipitation events were rejected in the reference run and are accepted when adding a certain amount of RH and TA in the Monte Carlo run. Figure 6.1 gives a clarification of this matter. The first 100 Monte Carlo runs are plotted for May 2017. It is clearly visible that the SWE already deviates from the reference run after the first precipitation event, but the lines remain stacked above each other afterwards. The order of the different runs slightly changes at new precipitation events, but these variations are smaller as the amount of new precipitation is smaller than at the first precipitation event. The calculation of the fresh snow density is more affected by the variations in forcing data and therefore the confidence interval of the snow depth is larger.

The sensitivity of SNOWPACK to the forced precipitation in Figure 5.9 and 5.10 is reasonable, because the SWE is formed by the precipitation without the influence of sublimation and melt and if not enough water is put into the model, the model will never be able to calculate more water equivalent then what has been used as input. The decrease of the SWE and snow depth goes too slowly starting from the end of September. The albedo is estimated higher than the measurement. The cause of this was already described in Section 3.2.5. The snow got covered with dust and the model can not take events like this into account, because it is not provided with the reflected shortwave radiation data.

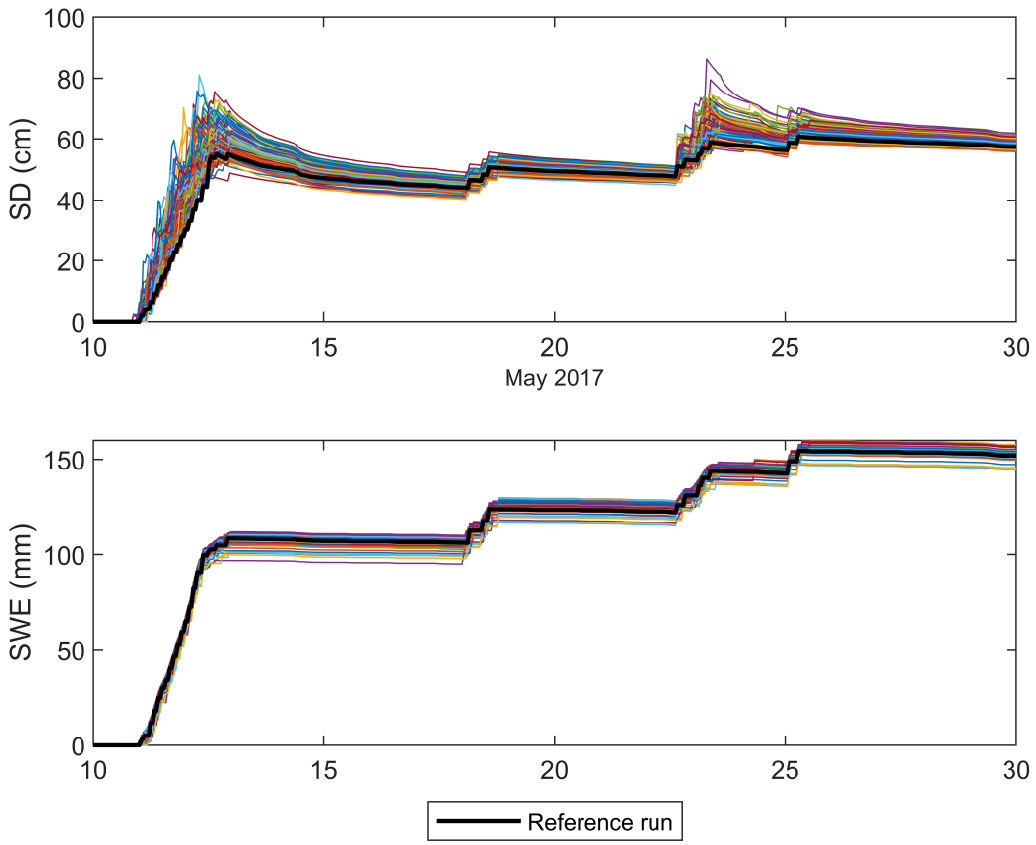

Figure 6.1: The simulated a) snow depth and b) SWE of the first 100 runs of the Monte Carlo simulation of step 3.1 of SNOWPACK during May 2017. The reference run has been plotted in black and the 100 runs have been plotted individually in color.

6.3.2. SnowModel

The reference run of SnowModel is outside the confidence interval in Figure 5.14. This is explained with a closer look on the measured RH and TA. The wet bulb temperature T_{wb} depends on the RH and TA and is solved iteratively with Equation (29) from Liston and Hall (1995). The new snow density ρ_{ns} in SnowModel is calculated with Equation 6.1 and shows that the density of fresh snow has a threshold for the wet bulb temperature at 258.16K. The RH and TA between 11 August 20:00 and 13 August 10:00 while precipitation was falling are plotted against each other in Figure 6.2. The boundary in this plot has been calculated with setting the T_{wb} to 258.16K and calculating the corresponding RH and TA. All ten precipitation events in this time slot lead to a new snow density of 50 $\mathrm{kg\,m^{-3}}$. When the random numbers are added to the measurements, it is always found that at least one of the measurements ends in the region of a higher fresh snow density. The snowpack is more dense at that moment and thus the resulting snow depth is lower. This also happens in Figure 5.14 and therefore the reference run is outside the interval of confidence.

$$\rho_{ns} = \begin{cases} 50 + 1.7(T_{wb} - 258.16)^{1.5}, & \text{if } T_{wb} \geq 258.16 \\ 50, & \text{if } T_{wb} < 258.16 \end{cases} \tag{6.1}$$

Secondly, it is very remarkable that the median 95% confidence interval of the SWE is only 1.3 mm, but as there is no threshold for precipitation events to be rejected, all the precipitation is added to the snowpack. The SWE can be influenced by sublimation and melt. The variations applied to the wind speed are rather small and as the roughness length of the snow is not adjusted in SnowModel, the sublimation does not change a lot during the season compared to the sublimation of the reference run. Furthermore, the influence of varying forcing after snow events is small, because as the variations are added on an hourly basis, the variations cancel each other out.

6.4. Comparison of SNOWPACK and SnowModel

6.4.1. Ablation processes

The comparison of SNOWPACK and SnowModel is incomplete without determining the main drivers of ablation of the models. Snow erosion or deposition caused by the wind has not been considered in this study and thus the change in SWE must come from other processes. Figure 6.3a reveals that the change of the SWE develops in the same way until 15 September with a minimum rate of -3 mm/day for the reference runs of both models. Figure 6.3b shows that the main driver of this SWE development is sublimation. Sublimation refers to the latent heat flux (Cuffey and Paterson, 2010, Chapter 5) and can be adjusted with the atmospheric stability correction model and the implemented roughness length. The atmospheric stability correction is based on the Richardson number and the roughness length is 1 mm for both models and thus the resulting sublimation of SNOWPACK and SnowModel agree with each other. The physics behind the atmospheric stability correction are the same, except that SNOWPACK slightly adjusts the roughness value over time, whereas this has not been done in SnowModel.

Whereas the change of SWE is the same for the utmost extent for SNOWPACK and SnowModel until 15 September, this changes when the air temperatures rise and the snow starts to melt. Figure 6.3a shows that the SWE of SnowModel decreases with up to 20 mm/day, while the SWE of SNOWPACK only decreases with a maximum of 12 mm/day. Figure 6.3d shows the cumulative run-off for both models. This is not exactly the melt, but the amount of water that percolates the soil after it has melted. Melting already occurs before that moment and the melt water is kept within the snowpack for a period of time and possibly refreezes. SnowModel simulates a steep run-off starting at 15 September. The run-off of SNOWPACK is more gradual and starts at 19 September. SNOWPACK accounts for refreezing in the snowpack if the air temperatures are below freezing point at night again and SNOWPACK preserves the melt water within the snowpack for a longer period of time. SnowModel also takes some refreezing into account with the multi-layer approach, but this is more simplistic than in SNOWPACK and the run-off is too imprecise and rough. The final cumulative run-off of SnowModel is 33.7 mm higher than the run-off of SNOWPACK and this is caused by evaporation, which is also driven by the latent heat flux (Cuffey and Paterson, 2010, Chapter 5). The evaporation is only considered by SNOWPACK and not by SnowModel (Figure 6.3c).

The measured snow depth starts to decrease at 19 September with a rate of approximately 3 cm/day. This rate amplifies at 3 October when wind velocities above 10 m/s were detected, the snow got covered with dust and the albedo decreased. The models were not provided with information about this decrease in albedo, because only the incoming shortwave radiation was given as input. The albedo simulation of SnowModel is defined by the air temperature. The air temperatures are above the freezing point at the moment the rapid

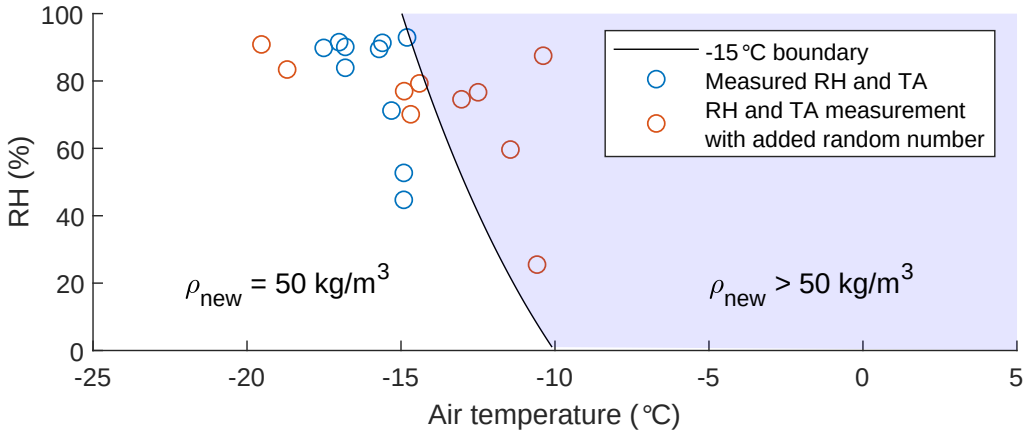

Figure 6.2: The black line gives the -15°C boundary where the fresh snow density is 50 kgm^{-3} (light blue) or higher than 50 kgm^{-3} (white). The blue circles indicate the measured RH and TA between 11 August 20:00 and 13 August 10:00 while precipitation was falling. The red circles are the measurements with a random number added according to the standard deviation of TA and RH.

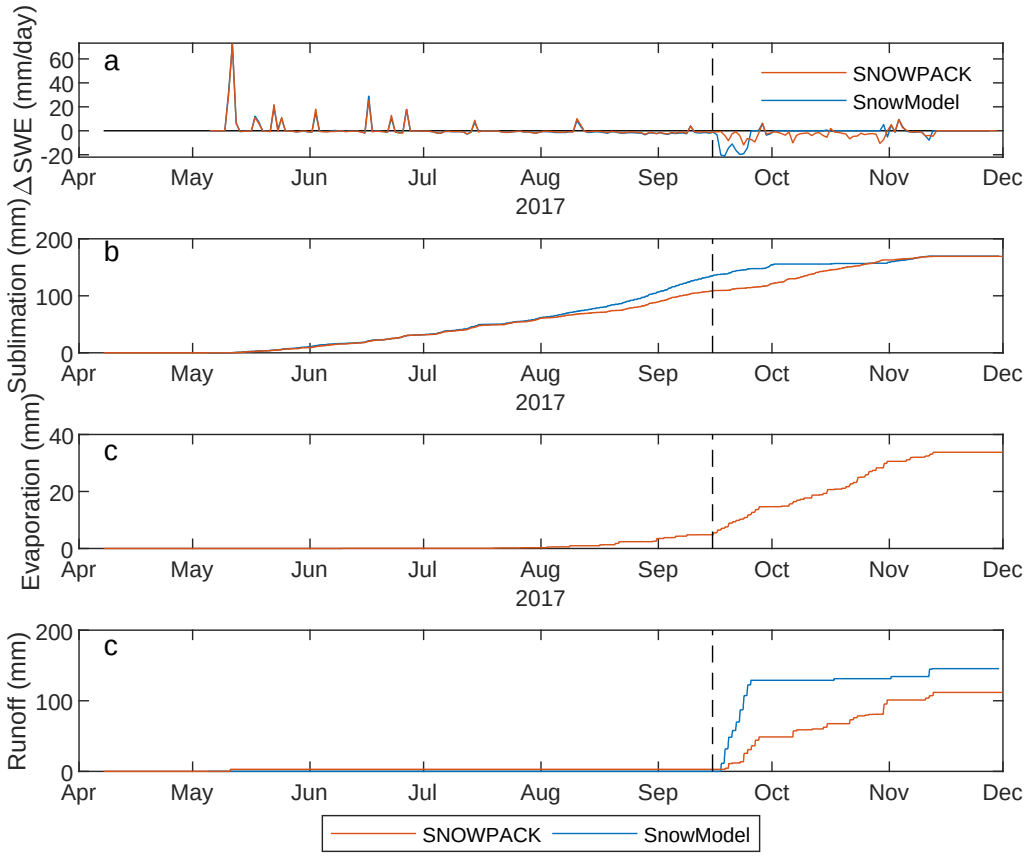

Figure 6.3: a) The change of SWE per day, b) the modelled cumulative sublimation, c) modelled cumulative evaporation and d) modelled cumulative run-off for the reference runs of SNOWPACK (red) and SnowModel (blue). The vertical dashed line indicates 15 September at 7:00.

decrease of the snowpack starts in SnowModel and thus an albedo of 0.15 is simulated. This causes the simulated melt to start earlier than measured, but with a similar rate of change as the measurement. SNOWPACK simulates a more moderate decrease of the albedo and if the snow would not have been covered with dust, it is very likely that this is an accurate way to model the albedo and thus the melt of the snow at the end of the season. In other words, the melt of SnowModel is predominantly defined by the air temperature, because

SnowModel already starts to subtract amounts of water from the total SWE if the air temperature is above zero. The melt simulated by SNOWPACK is defined by the energy available for melt within the snowpack and SNOWPACK preserves the melt water for a longer period of time within the snowpack.

Both models simulate the sublimation in the same manner, but only SNOWPACK simulates the start of the melt of the snowpack at the right moment. Even though the melt is modelled more gradual than what has been measured, SNOWPACK is considered the best model to simulate the snowpack evolution. This is concluded, because the snowpack was strongly influenced by the decrease of albedo and with the information provided to the models, it was impossible to model this.

6.4.2. Differences and similarities in sensitivity

The big difference in the width of the confidence interval for SWE and snow depth in Figure 5.17 results from the threshold that has been applied by SNOWPACK to reject precipitation if it is not cloudy, the RH is too low, or the surface is not cold enough, compared to the air temperature. This threshold is not applied in SnowModel and therefore the SWE is not sensitive to variable forcing in this model.

SnowModel does not have this response to precipitation events. Both models are not significantly sensitive to the parameters TA, RH, WV, WD, ISWR, ILWR and P when it is not snowing or raining. It is likely that they do not react immediately to a variation in the forcing and that the consecutive hour equalizes the variation of the previous hour. The same process occurs with the SWE of SNOWPACK, because the SWE does not vary any more after a precipitation event (Figure 6.1).

The sensitivity of both models to variations in the precipitation is similar. If the distribution of the precipitation at the end of the season is broader, so is the interval of confidence of the Monte Carlo runs. These 95% confidence intervals follow the run-off rates of the reference runs and hardly show the influence of the TA, RH, WV, WD, ISWR, ILWR and P.

6.4.3. Comparison to previous work

The undergraduate thesis of Mengual Henríquez (2017) also compares the results of SNOWPACK with measured snow depth of the AWS Tascadero (-31° 15', -70° 32'), which is close to Tapado. The aim of this study was to characterize differences and similarities between the snow in different regions of Chile. Mengual Henríquez (2017) also found large differences between the measurements and simulations of the different regions, but did not assess the sensitivity of the model to the forcing data and the precipitation is not corrected for high wind velocities, which are likely for the region. He also concluded that good input data is needed for the model and that the empirical parameters of SNOWPACK were not adjusted to the meteorological conditions of Chile. Furthermore, the results of Mengual Henríquez (2017) are not comparable to this study, because data of another location was used and different corrections and interpolations were applied to the data of Tascadero.

According to results of Bartelt and Lehning (2002), better agreement has been found between measured and modelled snow depth with SNOWPACK, but this is only possible of the measured snow depth is also used as input for the models. Moreover, SNOWPACK has been calibrated with data from the Swiss Alps so it was predictable that the simulations are better when the model has been applied to the Alps than to the Andes. As stated before, it is interesting to adjust the internal parameters in SNOWPACK with measurements from the semi-arid Andes.

SnowModel has been used by Gascoin et al. (2013), but the focus of this research was on the wind transport of snow in the semi-arid Andes on a 3D-scale. The agreement on a point scale between measured and modelled snow depth is also poor in this study, but this was mainly related to wind events and not to the forced temperature, relative humidity or precipitation.

Ginot et al. (2001) found a sublimation rate of 1.9 mm/day at the Tapado glacier. This is in agreement of the sublimation that has been found in Figure 6.3b. The difference between the study of Ginot et al. (2001) is that the rate of 1.9 mm/day was measured at the glacier, whereas this study models the sublimation of a snowpack on soil close to the glacier in similar the meteorological conditions.

7

Conclusion and recommendations

The sensitivity of the snow models SNOWPACK and SnowModel in the semi-arid Andes to its input parameters and parametrizations is assessed by answering five subquestions. Those subquestions are answered before the final conclusion of this thesis is given. Consequently, some recommendations and an outlook on further research is given.

7.1. Conclusion

- *What data handling and processing steps are necessary to constitute a consistent set of forcing data for the models?*

The temperature and relative humidity sensor were not working during 5 months in 2017. The data has been interpolated by assuming that there is a linear gradient between altitude and temperature and altitude and relative humidity. Daily lapse rates of temperature and RH have been calculated between an automatic weather station lower in elevation (Laguna) and one higher in elevation than Tapado (Paso Agua Negra). The data of another nearby station (Llano de Las Liebres) and these lapse rates are used to interpolate the temperature and RH at Tapado.

The location of the precipitation sensor and wind events lead to an underestimation of the precipitation measurements. The accumulated precipitation has been corrected with the wind velocity by the empirical, exponential formula by MacDonald and Pomeroy (2007). An extra precipitation dataset has been derived from the SWE measurements. The uncertainty of the precipitation measurement is assessed by the proposal of two types of distributions between the measured data from the precipitation gauge and the precipitation derived from the SWE measurements. These distributions are not influenced by the wind velocity.

The other forcing data consist of the air pressure, incoming shortwave and longwave radiation and wind velocity and direction. These measurements only miss measurements during timeslots of one or a few hours. This is interpolated by taking the average of adjacent measurements of the same sensor.

- *What is the effect of different parametrizations of each model? Which parametrization is the most appropriate one?*

SNOWPACK has more than 100 parameters that can be adjusted. SnowModel is less extensive, but this model also has possibilities to run extra subroutines and to use or neglect several physical parameters. The focus of this study is on the parametrizations of the snow albedo and fresh snow density and on the roughness value. The snow albedo is a good measure for snow melt, because a high albedo leads to a higher amount of reflected shortwave radiation and eventually less available energy for melt. The snow density provides the conversion between the snow water equivalent and the snow depth and controls the way of compaction of the snowpack. The roughness value influences the sublimation rate of the snowpack.

SNOWPACK has several parametrizations for the snow albedo and density. 20 combinations of these parametrizations were tested. The statistical albedo model Schmucki_GSZ in combination with the snow density parametrization Lehning_old gives the best result compared to the measured SWE and snow depth. The snowpack evolution is modelled the best compared to the other combinations, because the simulation of the compaction of the snowpack and the melt comes the closest to the measurements.

SnowModel provides only one option for the snow density calculation and two options for the albedo parametrization. It has been found that the model works the most optimal if the evolution of albedo over time is taken into account.

The possibility of wind transport of snow is neglected in both models. Therefore, only sublimation, melt and precipitation influence the evolution of the snow water equivalent of the snowpack. The simulations of the SWE and snow depth show the best results if a roughness length of 1 mm has been used.

- *What is the influence of variations in the input parameters in each of the models?*

The relative humidity, air temperature and incoming shortwave radiation form thresholds for the acceptance or rejection of precipitation events in SNOWPACK. This leads to variations in the height of the SWE after a precipitation event. After a snowfall event, the variations in the forced TA, RH, ISWR, ILWR, P and wind cancel each other out and the variations do not influence the SWE. The forcing data also influences the modelled evolution of the snow depth with SNOWPACK, but this evolution strongly depends on the density of the fresh snow at a snow event.

SnowModel has two options for the fresh snow density. The density can be 50 $\mathrm{kg\,m^{-3}}$ or higher than 50 $\mathrm{kg\,m^{-3}}$. The threshold for this is set by a combination of the relative humidity and air temperature and thus variations in these parameters influence the snowpack.

The variations in the incoming shortwave and longwave radiation, wind and air pressure were so small, that those variations did not result in a significant response of the snow depth, SWE or surface temperature.

The only forcing parameter that strongly influences the snowpack evolution is the precipitation. The more precipitation is given as input to the models, the more snow can be simulated. This response is the same for SNOWPACK and SnowModel.

- *What are the physical differences between simulations of snow depth, snow water equivalent and surface temperature on a point scale of SNOWPACK and SnowModel?*

SNOWPACK and SnowModel use the energy balance equation to simulate snow depth, SWE and surface temperature. SNOWPACK is especially designed to model the evolution of the snowpack to forecast avalanches. The physics behind the model takes the evolution of grains and layers within the snowpack into account. SnowModel is principally made to simulate wind transport of snow over a topography, but wind transport is not considered in this study.

The evolution of the SWE is simulated similarly for both models if the snowpack is only influenced by sublimation. SNOWPACK sometimes rejects precipitation events and thus the reference run of SNOWPACK is maximally 7 mm smaller if no melt takes place. The SWE simulations deviate from each other at the moment that the air temperatures reach above the freezing point and the snowpack starts to melt. The simulation of melt is done differently in the models, where SNOWPACK models a more gradual melt, because the refreezing of melt water within in the snowpack is simulated more correctly, whereas the melt simulated by SnowModel is dominantly influenced by air temperatures above 0°.

The snow depth is calculated with the snow density and SWE in both models. Another big physical difference between the models arises in the calculation of this snow density. There is only one density parametrization possible in SnowModel and this parametrization calculates compaction rates of the snowpack that are too high. The calibration of SNOWPACK lead to a density parametrizations that simulates a snow depth evolution comparable to the measurement. The most optimal density parametrization of SNOWPACK depends on the surface and air temperature, relative humidity, wind velocity and several empirical parameters, whereas the density of SnowModel only depends on the wet bulb temperature, which is calculated with the relative humidity and air temperature.

The surface temperature is solved iteratively in SnowModel and SNOWPACK. If the snow surface temperature is estimated correctly, the energy balance is correct. The surface temperature in SnowModel is computed iteratively with a Newton-Raphson method and SNOWPACK also solves iteratively using Neumann boundary conditions at the snow surface.

- *Which model is the most appropriate for understanding snowpack processes, and model snow depth evolution in arid settings?*

The most appropriate model for understanding snowpack processes and model snow depth evolution is SNOWPACK, because this model also evaluates the internal evolution of the snowpack and parametrizes the albedo better than SnowModel. Nevertheless, improvements can be made to the empirical parameters in the model to adjust it for semi-arid settings.

- **What is the sensitivity of the snow models SNOWPACK and SnowModel to its input parameters and parametrizations.**

The conclusion of this thesis is that SNOWPACK and SnowModel are sensitive to a correct albedo and snow density parametrization. The snow density parametrization only influences the snow depth and not the SWE. The albedo is a good measure for the snow melt.

The models are predominantly sensitive to the input of precipitation. The simulated SWE is formed by the amount of precipitation minus the sublimation and melt. The precipitation measurements are lower than the precipitation that was derived from the SWE measurements, because of the location of the SWE sensor and the undercatch in the precipitation gauge. This makes it impossible to compare the SWE measurements with the simulation, because the amount of water used as input for the model never equals the amount of water without sublimation and melt measured by the SWE sensor.

Furthermore, the models are significantly sensitive for the forced relative humidity and air temperature. This influences the melt, acceptance of precipitation events (SNOWPACK) and the snow density (SnowModel). The influence of air pressure, incoming longwave and shortwave radiation and wind velocity and direction is inconsiderable.

7.2. Recommendations

7.2.1. Improvements of the forcing data

Firstly, the interpolation of the relative humidity data according to a dew point temperature gradient should be used in the models. The assumption of an linear gradient of the relative humidity in this study is not correct and the uncertainty of the relative humidity decreases when a dew point lapse rate is assumed. The interpolation has been given in Appendix B, but not used in the models.

Secondly, the precipitation measurements must be improved. It is not a very practical solution, but the main tower of Tapado must be moved closer to the precipitation gauge. Another option would be to correct the precipitation measurements with the wind velocity and SWE measurements of adjacent years. The precipitation correction based on the wind velocity is only validated with the first snowfall, but with a validation over several years, the empirical parameters in this correction can improve.

7.2.2. Development of SnowModel

SnowModel only provides one density parametrization. It is recommended to add a parametrization similar to Lehning_old, which uses the air and surface temperature, relative humidity and wind velocity. It is expected that this improves the results of the snow depth simulations.

7.2.3. Development of SNOWPACK

The threshold that has been applied by SNOWPACK whether precipitation is rejected or approved should be updated. In the semi-arid Andes, the incoming shortwave radiation is always strong and even with more clouds and during snowfall, the shortwave radiation is likely to be higher than the applied threshold. The threshold for the relative humidity of 50% is discussable, because the interpolated relative humidity is very uncertain and thus likely to be lower than 50%. If the relative humidity interpolation is improved, the threshold for the acceptance of new snow is more consistent.

7.3. Outlook on further research

The study executed for this thesis was only on a point scale, but both models offer options to spatially distribute the snowpack simulations. Actually, SnowModel was designed as a three-dimensional model and SNOWPACK can be extended to the model Alpine3D. The performances of these models must be tested. In this case, the wind transport of snow can also be taken into account. It is likely that this improves the results of SnowModel, because the model is specialized in this feature.

A

Available measurements

Table A.1: Available sensors, sensor height and its manufacturers at AWS Laguna.

Measurement	Unit	Height (m)	Brand/type
Accumulated precipitation	mm	0	NA/NA
Air temperature	°C	1.5	NA/NA
Incoming shortwave radiation	W/m^2	2	NA/NA
Relative Humidity	%	1.5	NA/NA
Wind velocity	m/s	10	RM Young/5103
Wind direction	°	10	RM Young/5103
Snow depth	cm	0	NA/NA
Water equivalent	cm	0	NA/NA

Table A.2: Available sensors, sensor height and its manufacturers at AWS Llano de Las Liebres.

Measurement	Unit	Height (m)	Brand/type
Air temperature	°C	2	Vaisala/HMP155
Relative Humidity	%	2	Vaisala/HMP155
Wind velocity	m/s	3	RM Young/5103
Wind direction	°	3	RM Young/5103
Snow depth	m	3	Campbell/SR50A

Table A.3: Available sensors, sensor height and its manufacturers at AWS Paso Agua Negra

Measurement	Unit	Height (m)	Brand/type
Air pressure	hPa	2	Vaisala/PTB110
Air temperature	°C	1.5	NA/NA
Incoming shortwave radiation	W/m^2	2	Middleton Solar/EQ16
Reflected shortwave radiation	W/m^2	2	Middleton Solar/EQ16
Relative Humidity	%	1.5	NA/NA
Wind velocity	m/s	2	NA/NA
Wind direction	°	2	NA/NA
Snow depth (at 3.5 m)	m	2	Campbell/SR50A

B

Second method for relative humidity interpolation

This appendix proposes a second method for the interpolation of the relative humidity. Whereas the interpolated relative humidity as proposed in Section 4.1.2 has been used as input for the models, it was later found that the interpolation of the relative humidity is more accurate with the interpolation according to the Equations (4)-(7) of Liston and Elder (2006a). This interpolation has not been used as input for the models, because time did not allow to run the models again with this interpolation.

Firstly, Liston and Elder (2006a) calculate the saturation vapour pressure, e_s (Pa), at temperature T with Equation B.1.

$$e_s = a \exp\left(\frac{bT}{c+T}\right) \tag{B.1}$$

a is 611.21 Pa, b is 17.502, and c is 240.97°C for water. With this saturation vapour pressure and the measured relative humidity, the actual vapour pressure e (Equation B.2) and the dew point temperature T_d (Equation B.3) have been calculated at La Laguna and Paso Agua Negra.

$$RH = 100\frac{e}{e_s} \tag{B.2}$$

$$T_d = \frac{c\ln(e/a)}{b-\ln(e/a)} \tag{B.3}$$

A dew point temperature gradient has been calculated between La Laguna and Paso Agua Negra according to Equation 4.1 and a fit of this lapse rate Γ_d has been calculated (Equations 4.2-4.5). The dew point lapse rate and fit is given in Figure B.1a. Liston and Elder (2006a) use a vapour pressure coefficient λ (Equation B.4) according to Kunkel (1989), but that is not used, because the dew point temperature lapse rate is calculated between La Laguna and Paso Agua Negra.

$$\Gamma_d = \lambda\frac{c}{b} \tag{B.4}$$

The minimum and maximum Γ_d with the coefficients from Kunkel (1989) are -5.8 and -4.5°C/km and calculated with La Laguna and Paso Agua Negra are -5.7 and -4.5 °C/km respectively. The dew point temperature at Tapado is interpolated with Equation 4.5 and the dew point temperature at Llano de Las Liebres. The actual vapour pressure and the corresponding RH at Tapado is calculated with the dew point temperature at Tapado. This leads to Figure B.1b.

The validation of this relative humidity calculation is also done by calculating the mean and standard deviation between the differences of the RH at Tapado when measurements were available with the RH at Tapado calculated with data from Llano de Las Liebres. These results are given in Table B.1, together with the R^2 and RMSE.

The standard deviation of the calculation with the dew point temperature of Llano de Las Liebres $\sigma_{calculation}$ is 9.69% instead of 12.81% with the method in Section 4.1.2. The final RH uncertainty σ_{RH} is 9.97% instead of 13.02%. The light blue shade in Figure B.1b gives the 95% interval of confidence calculated with $1.96\sigma_{RH}$. This interval is smaller than the interval used in the Monte Carlo runs.

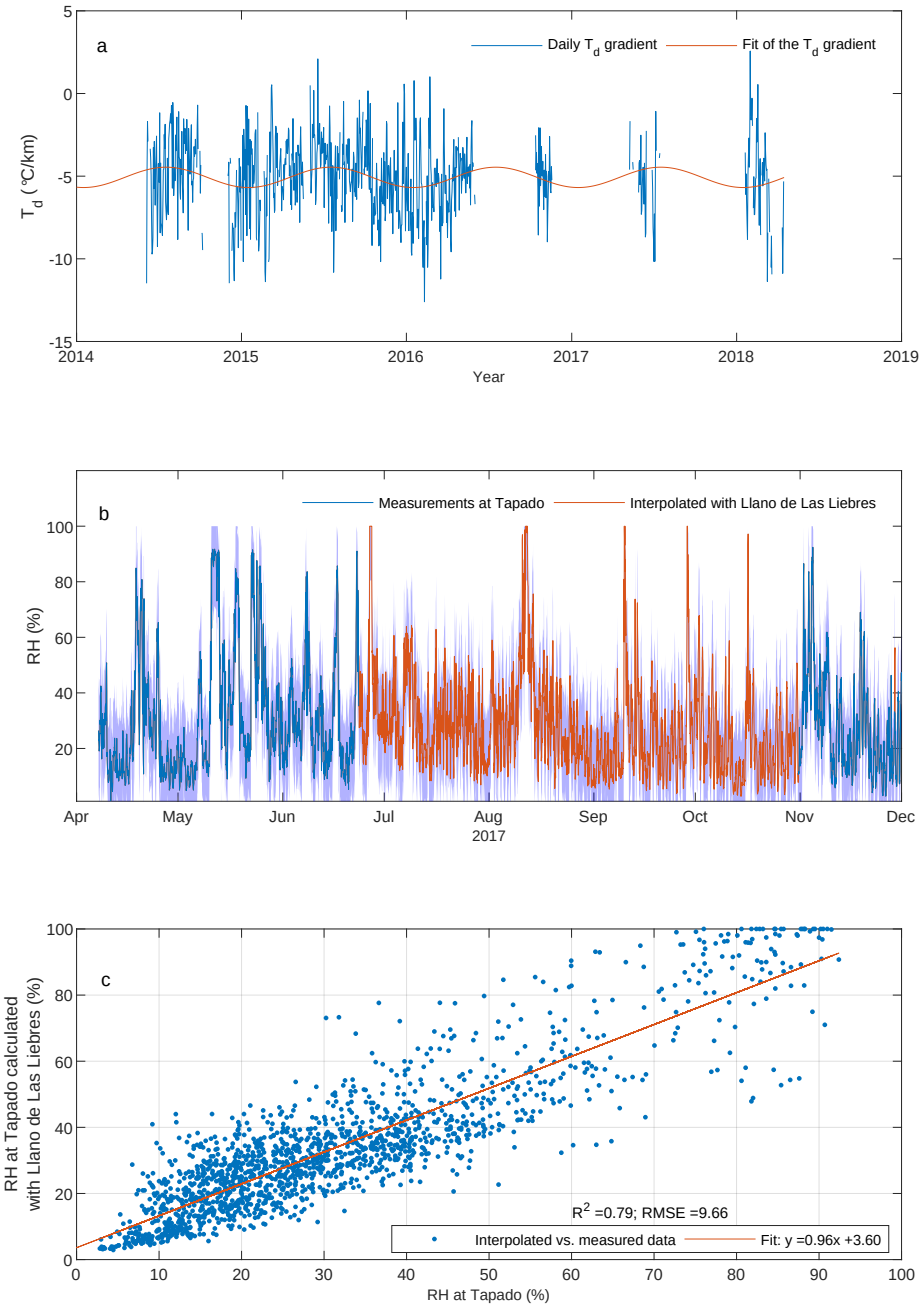

Figure B.1: a) The dew point temperature gradient between AWS Paso Agua Negra and La Laguna (blue) and the seasonal fit of this gradient (red). b) RH at Tapado that is calculated with data from Llano de Las Liebres (red) and the measurements at Tapado (dark blue). The light blue area around the line represents the 95% interval of confidence. c) Linear regression analysis of the interpolated RH data with Llano de Las Liebres.

Table B.1: Statistics of the relative humidity calculations with the dew point temperatures and Llano de Las Liebres. The mean and standard deviation are calculated with the difference between the relative humidity at Tapado calculated with another station and the actual measurement at Tapado. The RMSE and R^2 are calculated with the calculated relative humidity and the relative humidity at Tapado, if this was available. The number of available data points are also given.

RH calculated with:	Llano de Las Liebres
# of observations	1637
Mean	-2.48
Standard deviation	9.69
RMSE	9.66
R^2	0.79

Lastly, the linear regression analysis of the data from Llano de Las Liebres is given in Figure B.1c. The interpolated RH with the dew point temperature of Llano de Las Liebres is plotted against the measurements at Tapado and a linear trend is fitted through the data. The calculated trend is $y = 0.96x + 3.6$. The calculated relative humidity is better if the dew point temperature is used than when a simple linear interpolation is used. The dew point temperature is a linear gradient over altitude, but the conversion to the actual vapour pressure is exponential. This is taken into account with the equations according to Liston and Elder (2006a) and hence the statistics of this interpolation (Table B.1) are better than Table 5.2. Table B.1 shows that this interpolation method uses 1637 instead of 1638 observations. One of the measurements is exactly zero and thus the calculated actual vapour pressure is zero and the dew point temperature is infinitely small. This measurement is rejected.

Bibliography

E. Anderson. *A point energy and mass balance model of a snow cover*. NOAA technical report. U.S. Department of Commerce, National Oceanic and Atmospheric Administration, National Weather Service, Office of Hydrology, 1976.

E. L. Andreas, R. E. Jordan, P. S. Guest, O. G. Persson, A. A. Grachev, and C. W. Fairall. Roughness lengths over snow. In *18th Conference on Hydrology of the American Meteorological Society, Seattle, WA, 11–15 January 2004*, 2004.

C. D. Q. Antonissen. The effectiveness of a snow fence in the dry Andes region of Chile. Master's thesis, University of Technology Delft, 2017.

S. L. Barnes. A technique for maximizing details in numerical weather map analysis. *Journal of Applied Meteorology*, 3(4):396–409, 1964.

S. L. Barnes. Mesoscale objective map analysis using weighted time series observations. *NOAA. Tech. Memo.*, 60, 1973.

P. Bartelt and M. Lehning. A physical SNOWPACK model for the Swiss avalanche warning: Part I: Numerical model. *Cold Regions Science and Technology*, 35(3):123–145, November 2002. doi: 10.1016/s0165-232x(02)00074-5.

M. Bavay. Format specication for the SMET Weather Station Meteorological Data Format. Technical Report 1.1, SLF, 2017. URL `https://models.slf.ch/docserver/meteoio/SMET_specifications.pdf`.

S. Bellaire, M. Proksch, M. Schneebeli, M. Niwano, and K. Steffen. Measured and modeled snow cover properties across the Greenland Ice Sheet. *The Cryosphere Discussions*, pages 1–22, may 2017. doi: 10.5194/tc-2017-55.

B. W. Brock, I. C. Willis, and M. J. Sharp. Measurement and parameterization of albedo variations at Haut Glacier d'Arolla, Switzerland. *Journal of Glaciology*, 46(155):675–688, 2000. doi: 10.3189/172756500781832675.

O. Bruland, G. E. Liston, J. Vonk, K. Sand, and Å. Killingtveit. Modelling the snow distribution at two high arctic sites at Svalbard, Norway, and at an alpine site in central Norway. *Hydrology Research*, 35(3):191–208, 2004.

E. Brun, E. Martin, V. Simon, C. Gendre, and C. Coleou. An energy and mass model of snow cover suitable for operational avalanche forecasting. *Journal of Glaciology*, 35(121):333–342, 1989. doi: 10.3189/s0022143000009254.

D. Brunt. Notes on radiation in the atmosphere. *Quarterly Journal of the Royal Meteorological Society*, 58(247):389–420, September 1932. doi: 10.1002/qj.49705824704.

W. Brutsaert. On a derivable formula for long-wave radiation from clear skies. *Water Resources Research*, 11(5):742–744, October 1975. doi: 10.1029/wr011i005p00742.

Campbell Scientific. HMP45C, temperature and relative humidity probe, 1998. URL `https://www.campbellsci.com/hmp45c-l`.

Campbell Scientific. SR50A-L Sonic Distance Sensor, 2018. URL `https://s.campbellsci.com/documents/us/product-brochures/b_sr50a-l.pdf`.

CEAZAmet. Estación El Tapado. URL `http://www.ceazamet.cl/index.php?pag=mod_estacion&e_cod=TPF`.

J. P. Conway and N. J. Cullen. Constraining turbulent heat flux parameterization over a temperate maritime glacier in New-Zealand. *Annals of Glaciology*, 54(63):41–51, 2013. doi: 10.3189/2013aog63a604.

K. M. Cuffey and W. S. B. Paterson. *The Physics of Glaciers*. Elsevier LTD, Oxford, 2010. ISBN 0123694612. URL https://www.ebook.de/de/product/10550595/kurt_m_cuffey_w_s_b_paterson_the_physics_of_glaciers.html.

A. Dilley and D. O'Brien. Estimating downward clear sky long-wave irradiance at the surface from screen temperature and precipitable water. *Quarterly Journal of the Royal Meteorological Society*, 124(549):1391–1401, July 1998. doi: 10.1002/qj.49712454903.

R. Essery. A factorial snowpack model (FSM 1.0). *Geoscientific Model Development*, 8(12):3867–3876, December 2015. doi: 10.5194/gmd-8-3867-2015.

V. Favier, M. Falvey, A. Rabatel, E. Praderio, and D. López. Interpreting discrepancies between discharge and precipitation in high-altitude area of Chile's Norte Chico region (26-32°s). *Water Resources Research*, 45(2), February 2009. doi: 10.1029/2008wr006802.

R. Garreaud, J. Rutllant, and H. Fuenzalida. Coastal lows along the subtropical west coast of South America: Mean structure and evolution. *Monthly Weather Review*, 130(1):75–88, 2002.

S. Gascoin, S. Lhermitte, C. Kinnard, K. Bortels, and G. E. Liston. Wind effects on snow cover in Pascua-Lama, Dry Andes of Chile. *Advances in Water Resources*, 55:25–39, May 2013. doi: 10.1016/j.advwatres.2012.11.013.

Geonor. Geonor T-200B series; all-weather precipitation gauges; 600 mm - 1000 mm - 1500 mm, 2010. URL http://www.geonor.com/brochures/t-200b-series-all-weather.pdf.

P. Ginot, C. Kull, M. Schwikowski, U. Schotterer, and H. W. Gäggeler. Effects of postdepositional processes on snow composition of a subtropical glacier (Cerro Tapado, Chilean Andes). *Journal of Geophysical Research: Atmospheres*, 106(D23):32375–32386, December 2001. doi: 10.1029/2000jd000071.

B. Hasholt, G. Liston, and N. Knudsen. Snow-distribution modelling in the Ammassalik Region, South East Greenland. *Hydrology Research*, 34(1-2):1–16, February 2003. doi: 10.2166/nh.2003.0025.

P. Hublart, D. Ruelland, I. G. de Cortázar-Atauri, S. Gascoin, S. Lhermitte, and A. Ibacache. Reliability of lumped hydrological modeling in a semi-arid mountainous catchment facing water-use changes. *Hydrology and Earth System Sciences*, 20(9):3691–3717, September 2016. doi: 10.5194/hess-20-3691-2016.

Instituto Nacional de Estadísticas - Chile, I. N. de Estadísticas Chile. País y regiones. población total e indicadores, 2014. URL http://www.ine.cl/estadisticas/demograficas-y-vitales.

A. Judson and N. Doesken. Density of freshly fallen snow in the Central Rocky Mountains. *Bulletin of the American Meteorological Society*, 81(7):1577–1587, July 2000. doi: 10.1175/1520-0477(2000)081<1577:doffsi>2.3.co;2.

S.-T. Khu and M. G. F. Werner. Reduction of Monte-Carlo simulation runs for uncertainty estimation in hydrological modelling. *Hydrology and Earth System Sciences*, 7(5):680–692, 2003. doi: 10.5194/hess-7-680-2003.

Kipp and Zonen. CNR 4 Net Radiometer; Instruction Manual, 2014. URL http://www.kippzonen.com/Product/85/CNR4-Net-Radiometer#.W4KpGOhKhPY.

E. J. Klok and J. Oerlemans. Modelled climate sensitivity of the mass balance of Morteratschgletscher and its dependence on albedo parameterization. *International Journal of Climatology*, 24(2):231–245, February 2004. doi: 10.1002/joc.994.

S. E. Koch, M. DesJardins, and P. J. Kocin. An interactive Barnes objective map analysis scheme for use with satellite and conventional data. *Journal of Climate and Applied Meteorology*, 22(9):1487–1503, 1983.

G. Kuczera and E. Parent. Monte Carlo assessment of parameter uncertainty in conceptual catchment models: the Metropolis algorithm. *Journal of Hydrology*, 211(1-4):69–85, November 1998. doi: 10.1016/s0022-1694(98)00198-x.

C. Kull, M. Grosjean, and H. Veit. Modeling Modern and Late Pleistocene Glacio-Climatological Conditions in the North Chilean Andes (29–30°). *Climatic Change*, 52(3):359–381, 2002. doi: 10.1023/a:1013746917257.

K. E. Kunkel. Simple procedures for extrapolation of humidity variables in the mountainous western United States. *Journal of Climate*, 2(7):656–670, July 1989. doi: 10.1175/1520-0442(1989)002<0656:spfeoh>2.0.co;2.

M. G. Lawrence. The relationship between relative humidity and the dewpoint temperature in moist air: A simple conversion and applications. *Bulletin of the American Meteorological Society*, 86(2):225–234, February 2005. doi: 10.1175/bams-86-2-225.

M. Lehning, P. Bartelt, B. Brown, T. Russi, U. Stöckli, and M. Zimmerli. SNOWPACK model calculations for avalanche warning based upon a new network of weather and snow stations. *Cold Regions Science and Technology*, 30(1-3):145–157, December 1999. doi: 10.1016/s0165-232x(99)00022-1.

M. Lehning, J. Doorschot, and P. Bartelt. A snowdrift index based on SNOWPACK model calculations. *Annals of Glaciology*, 31:382–386, 2000. doi: 10.3189/172756400781819770.

M. Lehning, P. Bartelt, B. Brown, and C. Fierz. a physical SNOWPACK model for the Swiss avalanche warning: Part III: Meteorological forcing, thin layer formation and evaluation. *Cold Regions Science and Technology*, 35(3):169–184, November 2002a. doi: 10.1016/s0165-232x(02)00072-1.

M. Lehning, P. Bartelt, B. Brown, C. Fierz, and P. Satyawali. a physical SNOWPACK model for the Swiss avalanche warning: Part II: Snow microstructure. *Cold Regions Science and Technology*, 35(3):147–167, November 2002b. doi: 10.1016/s0165-232x(02)00073-3.

G. E. Liston and K. Elder. A meteorological distribution system for high-resolution terrestrial modeling (MicroMet). *Journal of Hydrometeorology*, 7(2):217–234, April 2006a. doi: 10.1175/jhm486.1.

G. E. Liston and K. Elder. A distributed snow-evolution modeling system (SnowModel). *Journal of Hydrometeorology*, 7(6):1259–1276, December 2006b. doi: 10.1175/jhm548.1.

G. E. Liston and D. K. Hall. An energy-balance model of lake-ice evolution. *Journal of Glaciology*, 41(138):373–382, 1995. doi: 10.3189/s0022143000016245.

G. E. Liston and S. H. Mernild. Greenland freshwater runoff. Part I: A runoff routing model for glaciated and nonglaciated landscapes (HydroFlow). *Journal of Climate*, 25(17):5997–6014, 2012.

G. E. Liston and M. Sturm. Winter precipitation patterns in arctic Alaska determined from a blowing-snow model and snow-depth observations. *Journal of hydrometeorology*, 3(6):646–659, 2002.

J. MacDonald and J. Pomeroy. Gauge undercatch of two common snowfall gauges in a prairie environment. In *Proceedings of the 64th Eastern Snow Conference*, volume 29, pages 119–126, 2007.

S. MacDonell, C. Kinnard, T. Mölg, L. Nicholson, and J. Abermann. Meteorological drivers of ablation processes on a cold glacier in the semi-arid Andes of Chile. *The Cryosphere*, 7(5):1513–1526, September 2013a. doi: 10.5194/tc-7-1513-2013.

S. MacDonell, L. Nicholson, and C. Kinnard. Parameterisation of incoming longwave radiation over glacier surfaces in the semi-arid Andes of Chile. *Theoretical and Applied Climatology*, 111(3-4):513–528, June 2013b. doi: 10.1007/s00704-012-0675-1.

C. Magono and T. Nakamura. Aerodynamic studies of falling snowflakes. *Journal of the Meteorological Society of Japan. Ser. II*, 43(3):139–147, 1965.

S. A. Mengual Henríquez. Caracterización de la nieve de distintas localidades de Chile mediante el uso del modelo SNOWPACK. Master's thesis, Universidad de Chile, 2017.

S. H. Mernild, G. E. Liston, B. Hasholt, and N. T. Knudsen. Snow distribution and melt modeling for Mittivakkat Glacier, Ammassalik Island, Southeast Greenland. *Journal of Hydrometeorology*, 7(4):808–824, August 2006. doi: 10.1175/jhm522.1.

T. Mölg. Ablation and associated energy balance of a horizontal glacier surface on Kilimanjaro. *Journal of Geophysical Research*, 109(D16), 2004. doi: 10.1029/2003jd004338.

T. Mölg, N. J. Cullen, D. R. Hardy, G. Kaser, and L. Klok. Mass balance of a slope glacier on Kilimanjaro and its sensitivity to climate. *International Journal of Climatology*, 28(7):881–892, 2008. doi: 10.1002/joc.1589.

A. Monin and A. Obukhov. Basic laws of turbulent mixing in the surface layer of the atmosphere. *Contrib. Geophys. Inst. Acad. Sci. USSR*, 151(163):e187, 1954.

F. Obleitner and M. Lehning. Measurement and simulation of snow and superimposed ice at the Kongsvegen glacier, Svalbard (Spitzbergen). *Journal of Geophysical Research: Atmospheres*, 109(D4):n/a–n/a, February 2004. doi: 10.1029/2003jd003945.

T. Oke. The urban energy balance. *Progress in Physical Geography*, 12(4):471–508, December 1988. doi: 10.1177/030913338801200401.

F. Pellicciotti, B. Brock, U. Strasser, P. Burlando, M. Funk, and J. Corripio. An enhanced temperature-index glacier melt model including the shortwave radiation balance: development and testing for Haut Glacier d'Arolla, Switzerland. *Journal of Glaciology*, 51(175):573–587, 2005. doi: 10.3189/172756505781829124.

K. L. Randall. Campbell scientific web request (case:83574). Personal communication, 2018.

A. Rango and J. Martinec. Revisiting the degree-day method for snowmelt computations. *Journal of the American Water Resources Association*, 31(4):657–669, August 1995. doi: 10.1111/j.1752-1688.1995.tb03392.x.

R.M. Young Company. Wind monitor model 05103, 2005. URL `http://www.youngusa.com/Brochures/05103(0106).pdf`.

C. Rolland. Spatial and seasonal variations of air temperature lapse rates in Alpine regions. *Journal of Climate*, 16(7):1032–1046, April 2003. doi: 10.1175/1520-0442(2003)016<1032:sasvoa>2.0.co;2.

T. Sauter and F. Obleitner. Assessing the uncertainty of glacier mass-balance simulations in the European Arctic based on variance decomposition. *Geoscientific Model Development*, 8(12):3911–3928, December 2015. doi: 10.5194/gmd-8-3911-2015.

L. Scaff, J. A. Rutllant, D. Rahn, S. Gascoin, and R. Rondanelli. Meteorological interpretation of orographic precipitation gradients along an Andes west slope basin at 30°s (Elqui Valley, Chile). *Journal of Hydrometeorology*, 18(3):713–727, March 2017. doi: 10.1175/jhm-d-16-0073.1.

C. Shea and B. Jamieson. Some fundamentals of handheld snow surface thermography. *The Cryosphere*, 5(1):55–66, February 2011. doi: 10.5194/tc-5-55-2011.

SLF. Snowpack-3.4.5: Snlaws class reference, 2017a. URL `https://models.slf.ch/docserver/snowpack/html/classSnLaws.html`.

SLF. Snowpack-3.4.5: Programming with libsnowpack, 2017b. URL `https://models.slf.ch/docserver/snowpack/html/libsnowpack_basics.html`.

C. D. Smith. Correcting the wind bias in snowfall measurements made with a Geonor T-200B precipitation gauge and alter wind shield. In *87th American Meteorological Society Annual Meeting, San Antonio, TX*, 2007.

F. A. Squeo, N. Olivares, S. Olivares, A. Pollastri, E. Aguirre, R. Aravena, C. Jorquera, and J. R. Ehleringer. Grupos funcionales en arbustos desérticos definidos en base a las fuentes de agua utilizadas. *Gayana Bot*, 56(1):1–15, 1999.

C. R. Steger, C. H. Reijmer, M. R. van den Broeke, N. Wever, R. R. Forster, L. S. Koenig, P. K. Munneke, M. Lehning, S. Lhermitte, S. R. M. Ligtenberg, C. Miège, and B. P. Y. Noël. Firn meltwater retention on the Greenland Ice Sheet: A model comparison. *Frontiers in Earth Science*, 5, January 2017. doi: 10.3389/feart.2017.00003.

J. E. Strack, G. E. Liston, and R. A. Pielke Sr. Modeling snow depth for improved simulation of snow-vegetation-atmosphere interactions. *Journal of Hydrometeorology*, 5(5):723–734, 2004.

L. Urkidi. A glocal environmental movement against gold mining: Pascua–Lama in Chile. *Ecological Economics*, 70(2):219–227, December 2010. doi: 10.1016/j.ecolecon.2010.05.004.

Vaisala. Vaisala BAROCAP®Barometer PTB110, 2018. URL https://www.vaisala.com/sites/default/files/documents/PTB110-Datasheet-B210681EN.pdf.

M. van den Broeke, D. van As, C. Reijmer, and R. van de Wal. Assessing and improving the quality of unattended radiation observations in Antarctica. *Journal of Atmospheric and Oceanic Technology*, 21(9):1417–1431, September 2004. doi: 10.1175/1520-0426(2004)021<1417:aaitqo>2.0.co;2.

M. van den Broeke, D. van As, C. Reijmer, and R. van de Wal. Sensible heat exchange at the Antarctic snow surface: a study with automatic weather stations. *International Journal of Climatology*, 25(8):1081–1101, 2005. doi: 10.1002/joc.1152.

M. Vuille and J.-P. Milana. High-latitude forcing of regional aridification along the subtropical west coast of South America. *Geophysical Research Letters*, 34(23):n/a–n/a, December 2007. doi: 10.1029/2007gl031899.

P. Wagnon. Wintertime high-altitude surface energy balance of a Bolivian glacier, Illimani, 6340 m above sea level. *Journal of Geophysical Research*, 108(D6), 2003. doi: 10.1029/2002jd002088.

M. A. Wolff, K. Isaksen, A. Petersen-Øverleir, K. Ødemark, T. Reitan, and R. Brækkan. Derivation of a new continuous adjustment function for correcting wind-induced loss of solid precipitation: results of a Norwegian field study. *Hydrology and Earth System Sciences*, 19(2):951–967, February 2015. doi: 10.5194/hess-19-951-2015.

M. Wright. Performance analysis of CS725 snow water equivalent sensor. Technical report, Campbell Scientific, 2011.

S. Yamaguchi, A. Sato, and M. Lehning. Application of the numerical snowpack model (SNOWPACK) to the wet-snow region in Japan. *Annals of Glaciology*, 38:266–272, 2004. doi: 10.3189/172756404781815239.

L. Zhang, L. Zhao, C. Xie, G. Liu, L. Gao, Y. Xiao, J. Shi, and Y. Qiao. Intercomparison of solid precipitation derived from the weighting rain gauge and optical instruments in the interior Qinghai-Tibetan Plateau. *Advances in Meteorology*, 2015:1–11, 2015. doi: 10.1155/2015/936724.